

For Reference

NOT TO BE TAKEN FROM THIS ROOM

For Reference

NOT TO BE TAKEN FROM THIS ROOM

Ex LIBRIS
UNIVERSITATIS
ALBERTAENSIS





Digitized by the Internet Archive
in 2019 with funding from
University of Alberta Libraries

<https://archive.org/details/Mason1964>

Thesis
1964 (F)
#14 D

THE UNIVERSITY OF ALBERTA

A NEUTRON POLARIMETER
AND ITS USE FOR THE REACTION $B^{11}(D,N)C^{12}$

by

GRENVILLE ROBERT MASON

A THESIS

SUBMITTED TO THE FACULTY OF GRADUATE STUDIES
IN PARTIAL FULFILMENT OF THE REQUIREMENTS FOR THE DEGREE
OF DOCTOR OF PHILOSOPHY

DEPARTMENT OF PHYSICS

EDMONTON, ALBERTA

AUGUST, 1964

UNIVERSITY OF ALBERTA
FACULTY OF GRADUATE STUDIES

The undersigned certify that they have read, and recommend to the Faculty of Graduate Studies for acceptance, a thesis entitled A NEUTRON POLARIMETER AND ITS USE FOR THE REACTION $B^{11}(D,N)C^{12}$, submitted by Grenville Robert Mason in partial fulfilment of the requirements for the degree of Doctor of Philosophy.

ABSTRACT

This thesis describes the development of a neutron polarimeter which can be used to measure the polarization of incident neutrons with energy from three to twenty million electron volts. The polarimeter consists basically of an array of nine helium-filled proportional counters. Groups of three counters are separated by collimating vanes which permit He^{++} recoils to pass from a central group to left or right side groups of counters. Sum-coincidence techniques yield the left-right scattering asymmetry from which the polarization may be determined for neutron groups well separated in energy.

Angular distributions of neutron polarizations were measured for the reactions $\text{D}(\text{d},\text{n})\text{He}^3$, $\text{T}(\text{d},\text{n})\text{He}^4$, $\text{B}^{11}(\text{d},\text{n})\text{C}^{12}_{\text{g.s.}}$, and $\text{B}^{11}(\text{d},\text{n})\text{C}^{12}_{4.43}$ using a 2 Mev van de Graaff accelerator. Measurements for the first two reactions served primarily as checks on the operation of the polarimeter, and yielded values in agreement with those of previous workers.

Polarizations for both neutron groups from $\text{B}^{11}(\text{d},\text{n})\text{C}^{12}$ were found generally to be positive (using the Basel convention) and small (less than thirty percent). Angular distributions of the products of polarization values and differential cross sections were fitted with associated Legendre functions, a reasonable fit being obtained with a linear combination of the first, second and third functions.

ACKNOWLEDGEMENTS

I am very grateful to Dr. J. T. Sample for suggesting the project and for his advice and encouragement during the course of the work. I would also like to thank Dr. W. K. Dawson, and my supervisor, Dr. G. C. Neilson, for many helpful suggestions.

My thanks are due to Messrs. Jock Elliott, Conrad Green, and Lars Holm of the Nuclear Research Center for technical assistance.

Although many other people have helped in different ways it is impractical to try to list all their contributions. I should mention, however, that I am particularly grateful to my wife for typing this thesis and for her forbearance throughout a rather long term of graduate studies.

TABLE OF CONTENTS

	<u>Page</u>
Title Page	i
Approval Sheet	ii
Abstract	iii
Acknowledgements	iv
Table of Contents	v
List of Tables	vi
List of Illustrations	vii
Chapter 1 Introduction	1
Chapter 2 Theoretical Outline and Principles of Measurements	9
Chapter 3 Review of Previous and Contemporary Experimental Work	18
Chapter 4 Neutron Polarimeter Design	24
4-1 Proportional Counters	24
4-2 Mechanical Design	41
Chapter 5 Electronics	63
Chapter 6 Experimental Procedure, Uncertainties, and Corrections	71
Chapter 7 Experimental Results	80
Chapter 8 Discussion and Conclusions	94
References	99
Appendix A Polarimeter Drawings	102
Appendix B Computer Program for Geometric corrections to data	114

LIST OF TABLES

<u>Table</u>		<u>Page</u>
7-1	Neutron polarizations for $D(d,n)He^3$	81
7-2	Neutron polarizations for $T(d,n)He^4$	81
7-3	Neutron polarizations for $B^{11}(d,n)C^{12}_{g.s.}$	86
7-4	Neutron polarizations for $B^{11}(d,n)C^{12}_{4.43}$	87
B-1	Alphabetical list of definitions and symbols	135
B-2	Fortran II statements for program to determine the geometric average value of the analyzing power, $P_2 \cos\varphi$, for the neutron polarimeter	138

LIST OF ILLUSTRATIONS

<u>Figure</u>		<u>Page</u>
1-1	The basic neutron polarimeter	4
2-1	Geometry for fast neutron polarization measurements	10
2-2	Neutron-Helium 4 phase shifts	13
2-3	Polarization produced in neutrons scattered from helium	13
4-1	Normalized pulse size due to the movement of positive ions	26
4-2	Typical proportional counter pulse shapes for various clipping times	27
4-3	Equipotential lines for symmetric sections of central and side counters	35
4-4	Fractional voltages in central counters as function of radial distance	36
4-5	Fractional voltages in side counters as function of radial distances	37
4-6	Electron drift velocities	39
4-7	Electron collection times for proportional counters	40
4-8	Pulse shapes for various distances from horizontal axial plane	40
4-9	Collimating hole	45
4-10	Collimating strips	45
4-11	Frame for holding collimating vanes	46
4-12	Counter volumes and angles defined by vanes and target	47
4-13	Alpha particle ranges in mixtures of helium plus CO ₂ at 15°C, 76 cm Hg	49
4-14	Pressures required for recoil alpha range of 10 cm at 25°C	51
4-15	Total n - α scattering cross section and normalized count rate as function of neutron energy	53

<u>Figure</u>		<u>Page</u>
4-16	Laboratory differential scattering cross section for alpha recoil at $22\frac{1}{2}^\circ$, and normalized coincidence rate as function of incident neutron energy	53
4-17	Pulse height variation across counters	59
4-18	Gas handling system	60
4-19	Polarimeter mount and collimating shield	62
5-1	General schematic diagram of the electronics for the neutron polarimeter	64
5-2	High voltage adjustment and filter for each counter	66
5-3	Pre-amplifier for vertical set of three counters	67
5-4	Adding circuits	68
5-5	Anti-coincidence gating circuit	69
6-1	Some experimental data for $B^{11}(d,n)C^{12}$	79
7-1	Measured neutron polarizations for $D(d,n)He^3$ for mean energy of 1.1 Mev	83
7-2	Measured neutron polarizations for $D(d,n)He^3$ for mean energy of 1.5 Mev	83
7-3	$\sum a_\ell P'_\ell(\theta)$ fitted to $P \cdot \sigma$ data for $D(d,n)He^3$ at 1.1 Mev	84
7-4	$\sum a_\ell P'_\ell(\theta)$ fitted to $P \cdot \sigma$ data for $D(d,n)He^3$ at 1.5 Mev	84
7-5	Neutron polarizations for $B^{11}(d,n)C^{12}$ ground state, for mean deuteron energies of 1.35, 1.65, and 1.85 Mev	88
7-6	Neutron polarizations for $B^{11}(d,n)C^{12}$ first excited state for mean deuteron energies of 1.35, 1.65, and 1.85 Mev	89
7-7	Neutron polarizations for $B^{11}(d,n)C^{12}$, ground state, for mean deuteron energy of 1.45 Mev	90
7-8	Neutron polarizations for $B^{11}(d,n)C^{12}$, first excited state, for mean deuteron energy of 1.45 Mev	91

<u>Figure</u>		<u>Page</u>
7-9	$\sum a_\ell P'_\ell(\theta)$ fitted to $P \cdot \sigma$ data for ground state neutrons from $B^{11}(d,n)C^{12}$ at 1.45 Mev	92
7-10	$\sum a_\ell P'_\ell(\theta)$ fitted to $P \cdot \sigma$ data for first excited state neutrons from $B^{11}(d,n)C^{12}$ at 1.45 Mev	93
A-1	Polarimeter tank assembly drawing	103
A-2	Polarimeter tank end flange	104
A-3	Polarimeter tank back end plate	105
A-4	Polarimeter tank front end plate	106
A-5	Counter frame assembly	107
A-6	Counter support discs and front plate	108
A-7	Horizontal support rods	109
A-8	Counters-in-frame assembly	110
A-9	Center counter wall outlines	111
A-10	Side counter wall outlines	112
A-11	Front end insulators and supports, kovar seals, and counter wire	113
B-1	Schematic diagram of polarimeter, showing lab angles and distances	115
B-2	Relation between coordinate systems 2 and 1	117
B-3	Relation between coordinate systems 3 and 1	118
B-4	Relation between coordinate systems 3 and 4	118
B-5	Relation between coordinate systems 4 and 5	119
B-6	Relation between coordinate systems 1 and 6	119
B-7	Relation between coordinate systems 6 and 7	120
B-8	Reaction neutron direction	123
B-9	Recoil alpha direction in the polarimeter system, 2	126
B-10	Recoil alpha direction in the reaction-neutron system, 4	126
B-11	Flow diagram	134

CHAPTER 1

INTRODUCTION

In order to explain many physical phenomena, it is necessary to attribute to electrons, protons and neutrons an inherent angular momentum, or spin. In spite of other, quite different characteristics of these three basic constituents of atoms, their spins all have the same measurable component $\frac{1}{2}(h/2\pi)$, where h is Planck's constant. Because of this intrinsic angular momentum, one can associate with each of these particles a definite direction in space.

The term 'polarization' is used to refer to the average direction of the spins of a group of identical particles. The polarization of such a group is defined as a vector quantity having the average direction of the spins; its magnitude is usually normalized to unity through the equation

$$P = \frac{N_+ - N_-}{N_+ + N_-} \quad \text{--- 1-1}$$

where N_+ is the number of particles with spin component in the direction of polarization, while N_- is the number in the opposite direction. Clearly, P can have values between the limits $+1$ and -1 , describing groups completely polarized (in opposite directions). An unpolarized group has P equal to zero, corresponding to spins randomly oriented in space.

A device which can measure the polarization of a group of identical particles is called a polarimeter. This thesis is concerned with the design and construction of a neutron

polarimeter and its use in measuring the polarization of neutrons coming from some specific nuclear stripping reactions.

The fact that intrinsic angular momentum can be detected indicates that its effects are present to some extent in all nuclear interactions. Indeed, even in simple elastic scattering spin effects can produce appreciable polarization. One can compute the polarization produced in scattering from a knowledge of the phase shifts for the scattering; and the phase shifts can, in turn, be obtained from experimental scattering data. This is done with least difficulty for nuclei with zero spin, such as He^4 and C^{12} , and it is these nuclei which are used as analyzers in polarization measurements.

If an unpolarized beam of particles is incident upon a scattering medium the particles will be scattered symmetrically about the incident direction, and although the scattered particles may be polarized as a result of the scattering process such polarization would not be detected in conventional detectors since they are not sensitive to polarization. However, the scattering of an already polarized beam will depend upon the azimuthal angle of scattering.

For a given scattering angle, θ , and for a beam with polarization P_1 incident on an unpolarized target, the dependence of the differential cross section on the azimuthal angle, ϕ , is given by

$$\sigma(\theta, \phi) = \sigma(\theta) (1 + P_1 \cdot P_2 \cos \phi) \quad - - - \quad 1-2$$

where P_2 is the polarization which would have been produced

in an initially unpolarized beam, and $\sigma(\theta)$ is the ordinary differential cross section for an unpolarized beam. The azimuthal angle, ϕ , is defined, in accordance with the Basel convention (Basel, 1961) by (see also figure 2-1):

$$\cos \phi = \frac{\bar{k}_2 \times \bar{k}_2'}{|\bar{k}_2 \times \bar{k}_2'|} \cdot \bar{n}_1 \quad - - - \quad 1-3$$

where \bar{k}_2 and \bar{k}_2' are the initial and final momenta, while \bar{n}_1 is a unit vector defining the direction of the initial polarization \bar{P}_1 .

The left-right scattering asymmetry, ϵ , is defined by

$$\epsilon = \frac{\sigma(\theta, \phi) - \sigma(\theta, \phi')}{\sigma(\theta, \phi) + \sigma(\theta, \phi')} , \quad - - - \quad 1-4$$

where $\phi' = \pi - \phi$. On substituting equation 1-2 in 1-4, we see that

$$\epsilon = P_1 P_2 \cos \phi \quad - - - \quad 1-5$$

By measuring ϵ for an incident neutron beam, and knowing both P_2 and ϕ , then the polarization P_1 for the incident beam can be calculated.

The neutron polarimeter described in this thesis is based upon the result expressed by equation 1-5. The scatterer is helium 4 gas for which phase shifts are well known, (Austin, 1962), so that P_2 can be calculated; the left-right scatterings are detected by proportional counters operating with the helium gas through the ionization produced by the recoiling helium nuclei, or alpha particles.

There are nine of these proportional counters placed

horizontally side by side in a three-by-three array. Collimating vanes separate the central column of three counters from side columns of three counters on either side of the central column. The vanes permit helium nuclei, recoiling from scattering events, to pass through only if they recoil within a well-defined solid angle prescribed by the vanes.

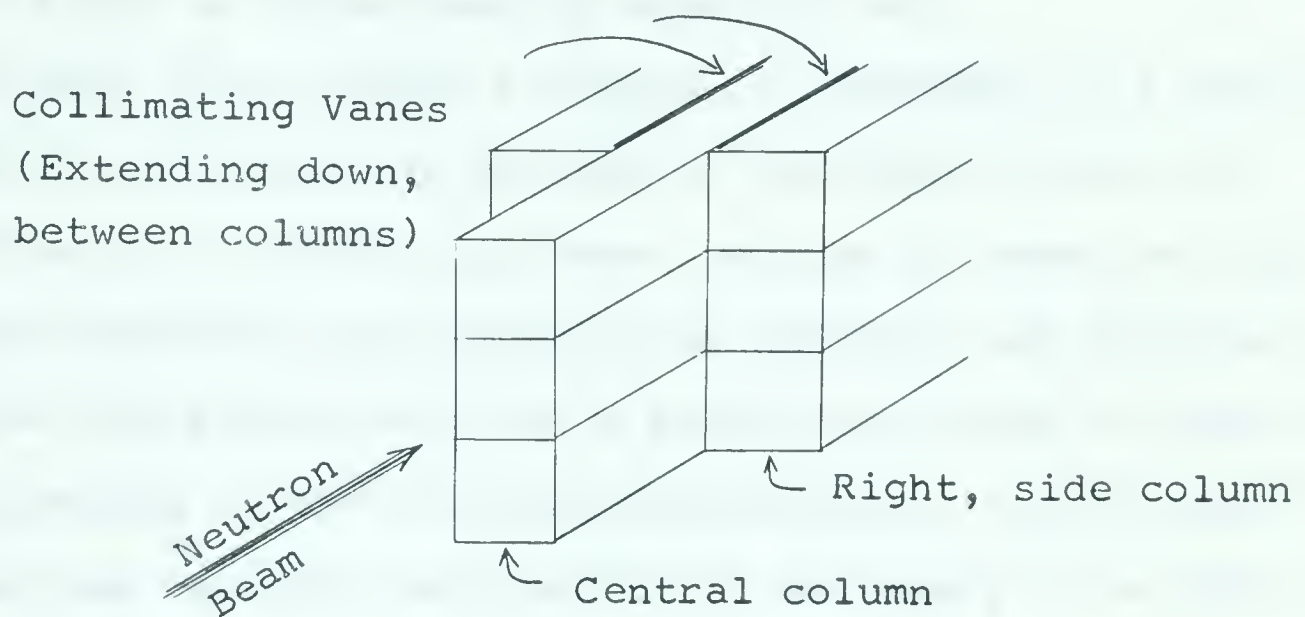


Figure 1-1 The Basic Neutron Polarimeter, Showing the Nine Proportional Counters and the Collimating Vanes.

The polarimeter functions in the following way. The neutron beam, whose polarization is to be measured, is allowed to pass into the central column of counters; a small fraction of this beam is scattered by the helium nuclei. When a neutron is scattered in one direction, the helium nucleus, or alpha particle, recoils in the opposite direction (in the center-of-mass system). If the scattering direction is within the limits prescribed by the collimating vanes then the recoiling alpha particle passes from a central counter into

one of the side counters. These particular scattering events are selected electronically by requiring that a pulse from the central counters be in coincidence with a pulse from a side counter. The relative number of coincidences for one set of side counters as compared to the number for the other set provides a measure of the polarization of the incident neutron beam, as determined by equation 1-5.

In many cases, where a target is bombarded by a beam of particles, reactions can proceed to different states of excitation of a residual nucleus. Groups of neutrons with different energies may therefore be emitted, and in order to determine the polarization of a particular group of neutrons (corresponding to the reaction proceeding to a particular state of the residual nucleus) it is necessary to be able to distinguish between neutrons of different energies. For this reason, apparatus is desirable which not only measures neutron polarization but also selects neutron groups with a given energy.

Since proportional counters are used, then the sum of the pulse heights for the two coincident pulses is proportional to the energy of the recoiling alpha particle. For the chosen recoil angle there is a proportional relationship between the energies of the recoil alpha particle and the incident neutron, and therefore the pulse height is proportional to the energy of the incident neutron. Although the resolution obtainable in practice is only about eighteen percent, the apparatus does permit selection of neutron

groups, widely separated in energy, for polarization analysis.

Perhaps the most imposing problem in polarization measurements is one of low counting rates. Since the measurement itself involves a scattering process, detection efficiency is greatly reduced. The combination of two scattering processes, or else of a reaction followed by a scattering process results in low counting rates which make experiments borderline in feasibility; statistics generally are poor.

While a neutron polarimeter can be used to measure the polarization of neutrons from any source, the polarimeter described in this thesis was used specifically to study the polarization of neutrons produced through stripping reactions. A stripping reaction is perhaps the best known of a general classification of reactions called 'direct reactions', in which there is presumed to be a direct passage from an initial nuclear state to the final state. This is in contrast to the compound nucleus theory initiated by Bohr which assumes that in a nuclear reaction the colliding nuclear particles coalesce into one compound nucleus for a comparatively long time before breaking up again into reaction products. Such a model has provided information concerning properties of nuclear matter in general, with particular success in explaining the occurrence of sharp resonances in total cross sections. Direct reactions provide information concerning specific properties of nuclei, such as spin and parity.

The deuteron is composed of just two nucleons, a neutron and a proton, which are very loosely held together with a binding energy of only 2.3 Mev; these two nucleons are separated by relatively large distances for much of the time. Consequently, when a deuteron approaches a nucleus it is quite possible that only one nucleon will be strongly influenced by the nucleus. In stripping reactions, one of the nucleons is actually captured by the nucleus while the other continues on some slightly deviated path. The deviation of the non-captured particle is typically small and stripping cross sections are normally peaked in the forward direction. The shape of the stripping cross section indicates the angular momentum with which the captured particle was taken into a nucleus. Such information dictates usually only one or two possible spin values for the final nucleus, assuming the initial nuclear state spin was known. Parities of states can also be deduced and the absolute magnitude of the stripping cross section provides clues to the actual structure of the nuclei involved in the reaction.

According to the simplest stripping theory the outgoing, uncaptured particle will be unpolarized. Hence, any observed polarization of the uncaptured particle indicates the extent to which the simple stripping theory is valid. The more advanced distorted-wave-Born (DWB) approximation allows some polarization, but predicts that the magnitude should always be less than one-third.

Neutron polarizations were measured for the reactions

$D(d,n)He^3$, $T(d,n)He^4$, and $B^{11}(d,n)C^{12}$. Polarization measurements for the first two reactions have been made by many workers, so that the measurements were done here mainly to check the operation of the apparatus. The measurement of the polarization of the neutrons from the reaction $B^{11}(d,n)C^{12}$ yielded results well within the limits indicated by the distorted wave theory.

CHAPTER 2

THEORETICAL OUTLINE AND PRINCIPLES OF MEASUREMENTS

The purpose of this chapter is not to give detailed developments of polarization and stripping theories -- numerous excellent accounts are available (Wolfenstein, 1956; Tobocman, 1961; Welton, 1963; Haeberli, 1963) -- but rather to give a general outline of some theoretical results and of pertinent information for use in this thesis.

Since polarization is a vector quantity, it is necessary to define unambiguously a direction in space. By the Basel convention (Basel, 1961), the positive direction is defined by the cross product of the momentum vectors:

$$\bar{n} = \frac{\bar{k} \times \bar{k}'}{|\bar{k} \times \bar{k}'|} \quad - - - \quad 2-1$$

where \bar{n} is a unit vector in the positive direction,

\bar{k} is the initial momentum vector,

and \bar{k}' is the final momentum vector.

Figure 2-1 shows typical momentum vectors and unit normals for neutron polarization measurements. Whenever an unpolarized beam or target is involved the polarization is perpendicular to the reaction or the scattering plane, as is required by parity conservation (Wolfenstein, 1956). The magnitude, P , of polarization is defined by equation 1-1, while 2-1 gives the direction, so that the complete description of a polarization vector is given by

$$\bar{P} = P \cdot \bar{n} \quad - - - \quad 2-2$$

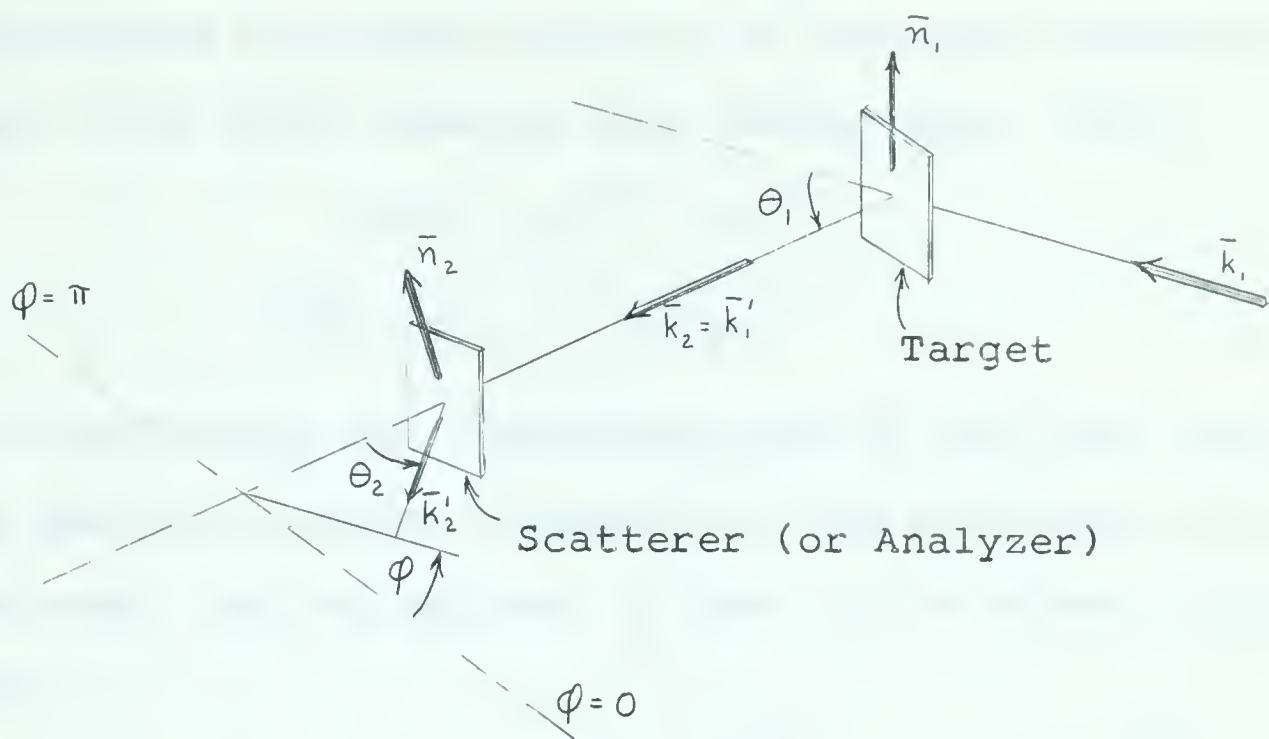


Figure 2-1 Geometry for Fast Neutron Polarization Measurements

If the neutron beam from the target is polarized, then the differential scattering cross section depends on the azimuthal angle ϕ as well as on the scattering angle θ_2 . The differential scattering cross section is given by

$$\sigma(\theta_2, \phi) = \sigma(\theta_2) \left[1 + \bar{P}_1 \cdot \bar{P}_2 \right], \quad \text{--- 2-3}$$

or, since $\bar{n}_1 \cdot \bar{n}_2 = \cos \phi$, --- 2-4

by $\sigma(\theta_2, \phi) = \sigma(\theta_2) \left[1 + P_1 P_2 \cos \phi \right].$ --- 2-5

In these equations, $\sigma(\theta_2)$ is the differential scattering cross section for an unpolarized neutron beam, and P_2 is the polarization which would have been produced in an unpolarized incident beam by the scattering. Sometimes P_2 is called 'the analyzing power' and the scatterer is called the 'analyzer'.

Both differential cross sections and polarizations can be calculated from phase shifts, if these are known well enough. The usual formulae are (Baumgartner, 1953):

$$\sigma(\theta) = |g|^2 + |h|^2, \quad - - - \quad 2-6$$

$$P(\theta) \cdot \sigma(\theta) = - 2 \operatorname{Im}(g^* h). \quad - - - \quad 2-7$$

where 'Im' stands for 'imaginary part of' and the asterisk means that the complex conjugate of the preceding symbol is to be used. We can express 'g' and 'h' in terms of phase shifts:

$$g = \frac{1}{k} \sum_{\ell} P_{\ell} \left[(\ell + 1) \sin \delta_{\ell}^{+} e^{i\delta_{\ell}^{+}} + \ell \sin \delta_{\ell}^{-} e^{i\delta_{\ell}^{-}} \right] - - \quad 2-8$$

$$\text{and } h = \frac{1}{k} \sum_{\ell} P_{\ell}^1 \sin(\delta_{\ell}^{+} - \delta_{\ell}^{-}) e^{i(\delta_{\ell}^{+} + \delta_{\ell}^{-})} \quad - - - \quad 2-9$$

where the coefficients P_{ℓ} are the Legendre polynomials

$$\left[P_0 = 1; P_1 = \cos \theta; P_2 = \frac{1}{2}(3 \cos^2 \theta - 1); \text{ etc } \right],$$

P_{ℓ}^1 are the associated Legendre polynomials

$$\left[P_0^1 = 0; P_1^1 = \sin \theta; P_2^1 = \frac{3}{2} \sin 2\theta; \text{ etc } \right],$$

ℓ refers to the orbital angular momentum in units of $h/2\pi$ (h is Planck's constant),

δ_{ℓ}^{+} are phase shifts for $J = \ell + \frac{1}{2}$,

δ_{ℓ}^{-} are phase shifts for $J = \ell - \frac{1}{2}$,

J is the total angular momentum,

and k is the momentum of the incident particle (neutron) in units of $h/2\pi$.

Scattering data usually is not sufficiently accurate that phase-shift analysis is possible; however, the scattering of

nucleons from helium has been studied well enough that phase shifts for such scattering can be used with confidence. The most reliable data (Burke, 1960) seems to be that of Seagrave (1953), and more recently that of Austin et. al. (1962). A summary of the phase shift variation with incident neutron energy is shown in figure 2-2.

Polarization produced in the scattered neutron beam is shown in figure 2-3 as a function of neutron energy for an unpolarized beam and target. It is noted that the polarization is close to unity for a scattering angle of 135 degrees in the center of mass system over the wide range of neutron energies from about 3 to 20 Mev. Scattering at this angle is excellent for analysis of the polarization of fast neutrons.

In general, the angular dependence of the polarization of the neutrons from a reaction can be expressed in the form

$$P(\theta) \cdot \sigma(\theta) = \sum_{\ell=1}^{\ell_{\max}} a_{\ell} P_{\ell}'(\theta) \quad - - - \quad 2-10$$

where the symbols are as defined above; a_{ℓ} are coefficients which depend upon the matrix elements of the reaction (Haeberli, 1963). Since the dependence is complicated, a number of simple rules, which are frequently useful, are given below (Simon, 1953; Blin-Stoyle, 1957).

(i) If the largest effective values of the incident orbital angular momentum, final orbital angular momentum, and total angular momentum are ℓ , ℓ' , and J respectively, then ℓ_{\max} in equation 2-10 above must be less than or equal to 2ℓ , $2\ell'$, and $2J$.

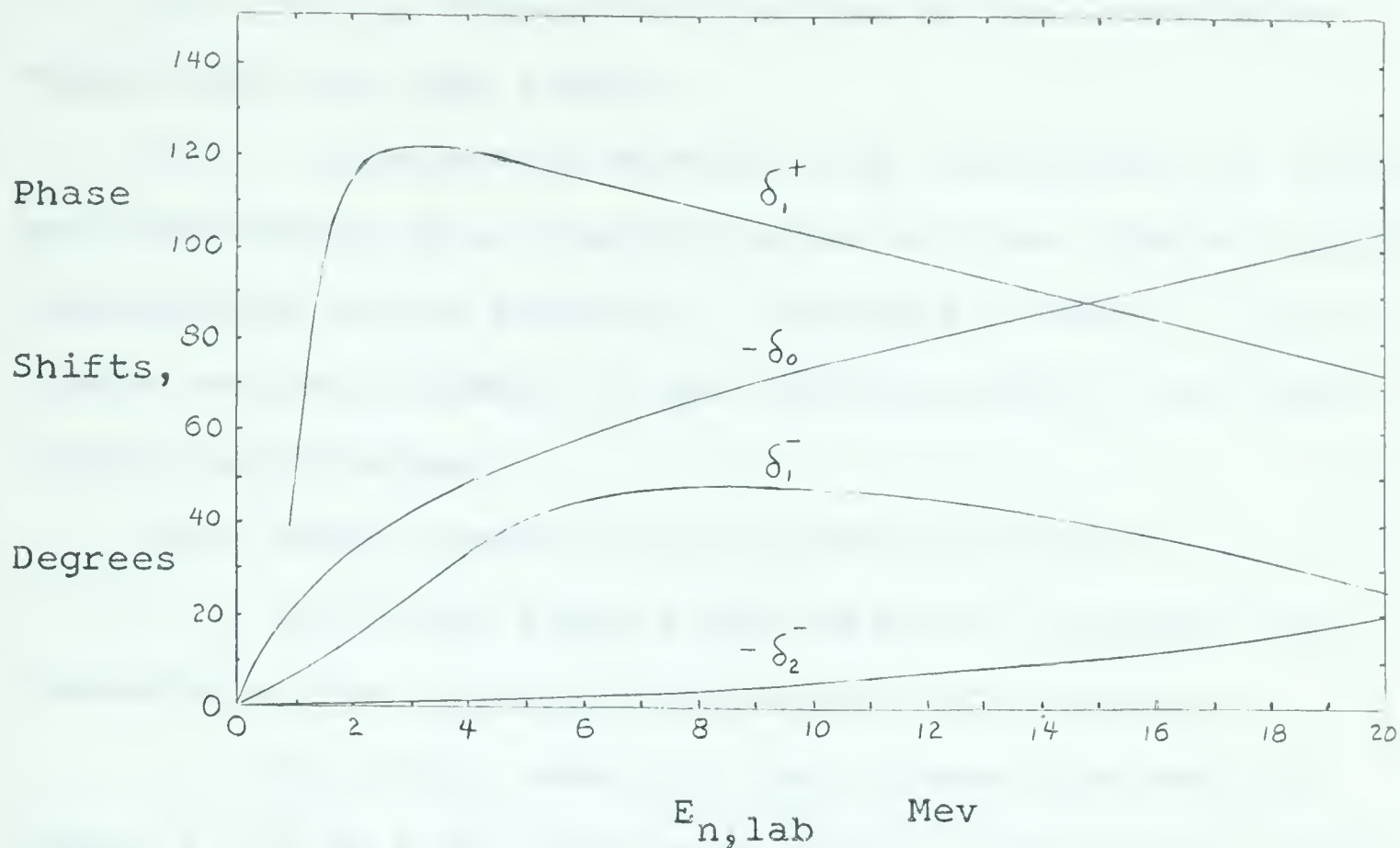


Figure 2-2 Neutron-Helium 4 Phase Shifts

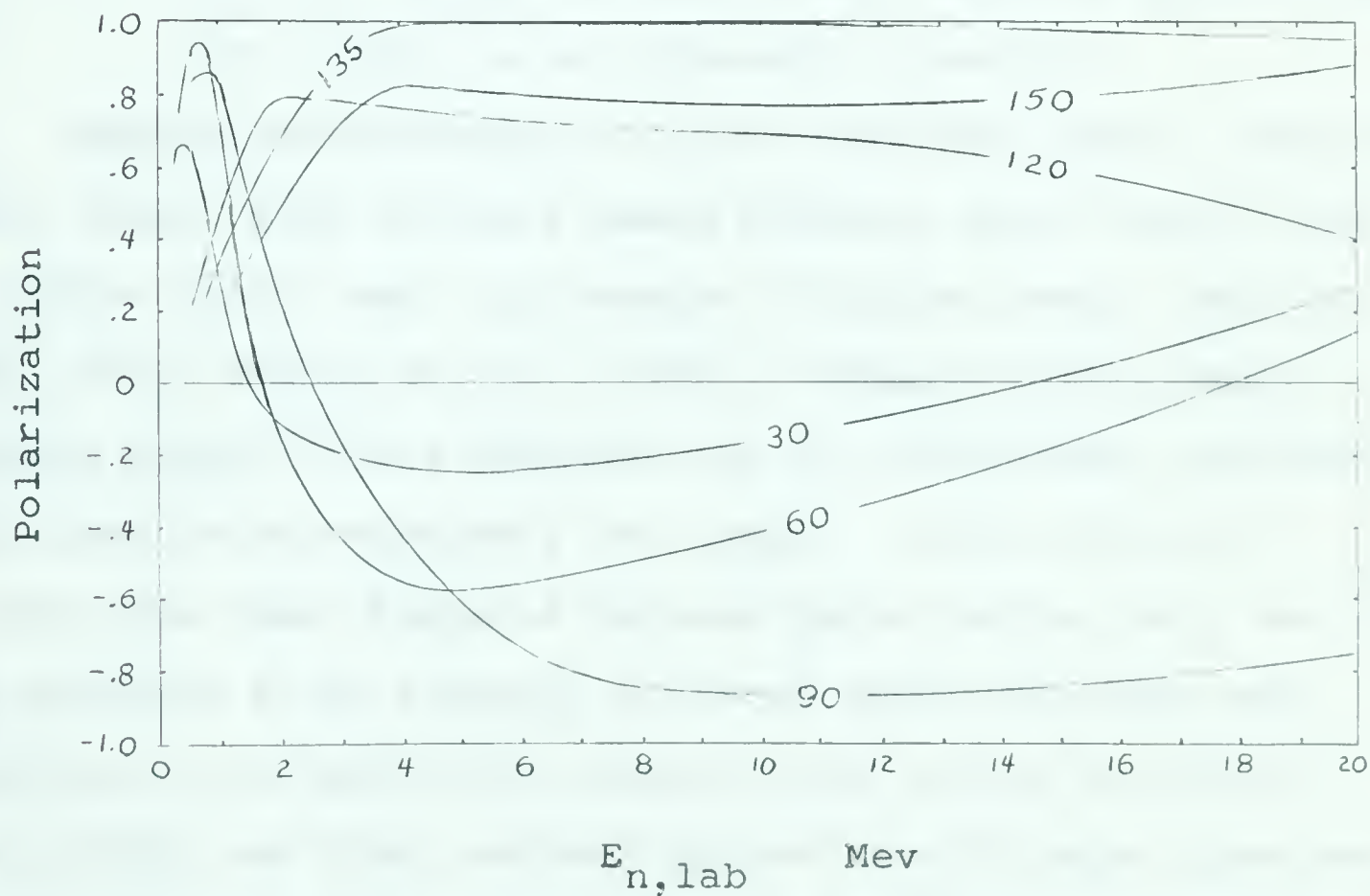


Figure 2-3 Polarization Produced in Neutrons Scattered from Helium (Angles are in Center-of-Mass).

(ii) All ℓ values must be even if the interfering states have the same parity.

(iii) Polarization results from interference of different subchannels (i.e., partial waves or final channel spins) contributing to the reaction. Therefore if there is only a single non-zero element of the reaction matrix, the polarization will vanish.

(iv) There cannot be any polarization if:

(a) only s-waves are effective in either the formation or the decay of the intermediate nucleus,

(b) only levels of the intermediate nucleus having $J = 0$ or $\frac{1}{2}$ are effective (unless interference arises between $J = \frac{1}{2}$ states of opposite parity),

(c) the only effective final channel spin is zero, or
(d) there is no spin-orbit coupling.

Angular distributions of (d,n) reactions have a characteristic shape, with strong forward peaking, which usually can be fitted fairly well by deuteron stripping theory (Butler, 1950, 1951; Bhatia et. al., 1952). Because of the small binding energy of the deuteron the two constituent nucleons will tend to be relatively far apart. In the field of a nucleus the short range of nuclear forces allows only one of the nucleons to be strongly affected while the other may continue on its path with comparatively little deviation. The initial and final nuclear states have definite spins and parities which place restrictions on the angular momentum transferred by the captured nucleon (the proton); there is,

in turn, a relationship between the angular distribution of the outgoing nucleon (the neutron) and the angular momentum transfer. This can be seen as follows. Let the momenta of the incident deuteron, the outgoing neutron, and the captured proton be $\hbar \bar{k}_d$, $\hbar \bar{k}_n$, and $\hbar \bar{k}_p$, respectively where $\hbar = h/2\pi$. Momentum conservation requires that $\bar{k}_p = \bar{k}_d - \bar{k}_n$. If the proton is captured into a state of orbital angular momentum $\ell \hbar$ and if the deuteron is broken up at some radial distance \bar{R} , then ℓ equals $\bar{R} \times \bar{k}_p$. Consequently,

$$|\bar{k}_d - \bar{k}_n| \cdot \bar{R} \geq \ell. \quad - - - \quad 2-11$$

This inequality can only be satisfied for scattering angles greater than some minimum value which depends on ℓ .

The differential cross section may be written in the form (Glendenning, 1963):

$$\frac{d\sigma}{d\Omega} = \frac{m_d^* m_n^*}{2(2\pi \hbar^2)^2} \frac{k_n}{k_d} \frac{2J_f + 1}{2J_i + 1} C^2 \sum_{\ell, m} S(\ell) |B_\ell^m|^2, \quad - - - \quad 2-12$$

where m_d^* , m_n^* are the reduced masses and k_d , k_n are the wave numbers for relative motion in the initial and final states, respectively:

$$k_d^2 = \frac{2m_d^* E_d}{\hbar^2}, \quad k_n^2 = \frac{2m_n^* E_n}{\hbar^2}. \quad - - - \quad 2-13$$

$$\text{Also,} \quad E_n = E_d + Q \quad - - - \quad 2-14$$

where Q is the energy release for the reaction, and E_n and E_d are center-of-mass energies of the neutron and deuteron, respectively. J_i and J_f are the total angular momenta of the initial and final states. C is the Clebsch-Gordan

coefficient for the isospin:

$$C = (T_i \ M_{T_i} \ , \ \frac{1}{2} \ m_t \ | \ T_f \ M_{T_f}) \quad - - - \quad 2-15$$

where T_i , T_f are the isospins for the initial and final states respectively; M_{T_i} , M_{T_f} are the corresponding z components; and m_t is the z component for the outgoing particle ($\frac{1}{2}$ for neutrons). The $S(\ell)$ are spectroscopic factors, or relative reduced widths (Macfarlane, 1960). And the B_ℓ^m are amplitude factors for the absorption of a proton with quantum numbers ℓ , m ; these amplitudes depend sensitively upon the value of ℓ -- which is the reason why the stripping reaction is of value as a source of spectroscopic information. Two methods are currently employed to evaluate the amplitudes B_ℓ^m ; these are known as the plane-wave and the distorted-wave calculations.

In the simpler plane-wave calculation there is assumed to be no interaction between the deuteron and the target nucleus nor between the neutron and the final nucleus. The wave functions for the incoming deuteron and the outgoing neutron are then approximated by plane waves, and the amplitude factors can be obtained, after considerable manipulation, in relatively simple analytical form.

However, the plane-wave theory does not yield a particularly detailed account of angular distributions, even though it does give reliable spectroscopic data for light nuclei within certain energy limits. To obtain more detailed agreement over a wide range it is necessary to take account of interactions in the entrance and exit channels, and when

this is done the distorted-wave method is being used. Distortion of the wave functions is caused by two interactions, the long-range repulsive Coulomb force and the short range attractive nuclear force. The effects of these two interactions tend to cancel each other. Distorted wave analysis is complex, involves numerical integrations and requires the use of high-speed digital computers.

Both the plane wave method and the distorted wave analysis result in stripping angular distributions which are characterized by the orbital angular momentum transfer, ℓ , but which do not depend upon which of the two spin-orbit states $j = \ell + \frac{1}{2}$ or $j = \ell - \frac{1}{2}$ is involved. Such information can be obtained from the angular correlation between the outgoing neutron and the de-excitation gamma ray for excited states, (Biedenharn, 1952; Gallagher, 1952; Satchler, 1952) or from the polarization of the outgoing neutron (Newns, 1953).

In the absence of any spin-dependent interaction in either the incident or outgoing channels, the possibility of polarization of the neutron spin is due to its correlation in the deuteron with the proton spin through $\bar{S}_n + \bar{S}_p = \bar{S}_d$. Through the proton spin it is correlated to the proton orbital angular momentum $\bar{\ell}$ because of spin-orbit interaction. If the proton is captured into a specific state $j = \ell + \frac{1}{2}$ or $\ell - \frac{1}{2}$, then any mechanism which tends to prefer a particular orientation of ℓ with respect to the reaction plane will cause the outgoing neutrons to be polarized.

CHAPTER 3

REVIEW OF PREVIOUS AND CONTEMPORARY EXPERIMENTAL WORK

Neutron polarimeters generally depend upon the use of a zero-spin scatterer, such as helium, carbon, or oxygen, as an analyzer. The analyzing power is more smoothly varying and is known better for the lighter nuclei and, at least partly for this reason, helium has been the commonly used analyzer, and then carbon, and to a lesser extent oxygen.

Willard et. al. (1954) were the first experimenters to report results using oxygen as an analyzer. They studied the $\text{Li}^7(p,n)\text{Be}^7$ reaction by scattering the neutrons from a sample of ordinary water and detecting the neutrons scattered at 90 degrees with a propane recoil counter placed alternately on opposite sides of the analyzing sample. Large paraffin wedges shielded the propane counters from the site of the p,n reaction. Adair et. al. (1954) in a similar experimental arrangement, used liquid oxygen as the scatterer and a hydrogen recoil counter, operated at seven atmospheres pressure for increased efficiency, for detecting scattered neutrons. Uncertainties and the considerable variation with energy in the analyzing power of oxygen have made its use unpopular.

Numerous experimenters have used carbon as the analyzer (Dubbeldam, et. al. 1960; Baumgartner and Huber, 1953; McCormac et. al. 1956; Ricamo, 1953). The solid analyzer results in greater analyzing efficiency than that obtained

with helium gas; however, one can only detect the scattered neutron, which means that shielding problems are severe. Carbon also suffers from the relatively rapid variation and reduction in analyzing power as compared with helium and generally is only useful for lower neutron energies.

Levintov et. al. (1957) used helium proportional counters in a method similar to that described in this thesis. Two long counters were used with their axes set at $\pm \theta_{\alpha}$ with respect to an incident neutron beam; the helium pressure and discriminators were set so that only helium nuclei (alpha particles) recoiling along the counter axis were counted. They measured neutron polarizations from $D(d,n)$ (Levintov, et. al., 1957a) and from $T(d,n)$ reactions (Levintov, et. al., 1958). The great advantage of using helium as an analyzer lies in the fact that for particular scattering angles it has an analyzing power close to one over the neutron energy range from about 3 to 20 Mev. The fact that helium is a gas except at extremely low temperatures is a disadvantage since the density of the gas is low; however, for the technique used by Levintov the fact that helium is a gas is an essential requirement.

Pasma (1958) determined the polarization of $D(d,n)$ and $T(d,n)$ neutrons using a helium gas scintillator as the scatterer and detector of recoil alphas, and liquid scintillators as the detectors of the scattered neutrons. The fast pulses obtained from scintillation counters, and the coincidence technique involved would seem to make this method

attractive. However, even with a large amount of bulky shielding and a resolving time of $0.2\mu\text{s}$, background corrections were necessary.

A less conventional technique was employed by Baicker and Jones (1960) who detected asymmetries in scattering from liquid helium by observing the scattered neutrons in a time-of-flight technique. While this technique reportedly gives good energy resolution and excellent signal to background ratios, alignment of the experimental equipment was so difficult that angular distributions were not attempted. A considerable amount of shielding was used.

Another technique employing liquid helium was developed by Simmons and Perkins (1961). Their method involved the use of the liquid helium both as an analyzer and as a scintillator. Coincidence was demanded between plastic scintillator neutron detectors for the scattered neutrons and the liquid helium scintillator for the recoiling alpha particles. Energy resolution was in the region of 25 to 30 percent, while a charge of helium could last 7 hours under experimental conditions. Shadow cones were used to shield the plastic scintillators from the target.

Generally, the use of helium as an analyzer for the measurement of polarization of neutrons with energy from about 3 to 20 Mev is best because of its large and relatively constant analyzing power over this range of energies. The use of liquid helium with the development of its function as a scintillator, or with the time-of-flight technique, approach

the ultimate in neutron polarimetry. However, the sophisticated and costly equipment required and the comparatively poor energy resolutions obtained would seem to leave room for alternative designs.

Because of the probability of introducing false asymmetries into measurements, precautions must be taken to avoid this. Generally one measures 'left' and 'right' scattering events simultaneously with two separate counters, and further, one repeats a measurement at the same angle on the other side of a beam or else rotates the polarimeter 180 degrees about its axis in order to reverse the role of the two counters and so to eliminate false instrumental asymmetries. An alternative technique was developed by Dubbeldam et. al. (1959) for neutrons of energy about 5 Mev, which involves the use of a solenoid for rotating the spin directions of neutrons moving along its axis. By this technique, the polarization vector of the neutrons is first rotated 90 degrees clockwise, for example, and a run made, and then 90 degrees counter-clockwise, and a second corresponding run made. In this way the parts of the polarimeter are effectively rotated by 180 degrees, even though in fact nothing is changed except the direction of the current in the solenoid. The technique reduces the possibility of introducing instrumental asymmetries. It has the disadvantages that the required solenoid is 78 cm long and may not be compatible with a given experimental set-up; and also the strong magnetic field may affect surrounding equipment. For example, Jonker (1961)

reports that a correction of three percent had to be applied to some results because of the influence of the magnetic field on the pulse height of photomultipliers.

Barschall (1956) suggested a method for measuring the polarization of nuclear reaction products in which the reverse reaction is used for analysis. The resulting asymmetry depends only on the square of the polarization and no knowledge of resonance parameters is needed. Although the technique is interesting, special geometric requirements must be met and experiments are only feasible in a few cases for restricted ranges of energy and of angle.

Because of low counting rates in polarization measurements, Brinkman (1960) proposed a ring geometry for the scatterer in order to increase efficiency. In this method two detectors would be placed on the axial line of the accelerated particle which initiates the reaction, with the scatterer forming a complete ring coaxial with the line of the accelerated particle. The method is unorthodox in that intensities are measured for the same azimuthal scattering angles but different polar angles. While efficiency may be increased by this method, analysis is complex and it would be difficult to check any inherent asymmetries in the apparatus. Although the apparatus was to be used at the Groningen Physical Institute, no results have been reported.

Polarization might also be measured using small-angle scattering from heavy nuclei. For example, Sample (1955) has estimated an asymmetry ratio of 14.5 for the scattering

of completely polarized 3.1 Mev neutrons from lead at an angle of 0.5 degrees. Problems in collimation, however, make this method impractical at present.

CHAPTER 4

NEUTRON POLARIMETER DESIGN

4-1 Proportional Counters

A gas counter is a chamber containing a gas and a central electrode (usually a fine wire) maintained at a high positive voltage relative to the walls of the chamber. Whenever ionizing radiation passes through the gas, the voltage difference between the electrodes drops momentarily as the separated electrons and ions are swept by the electric field to opposite electrodes. This momentary reduction in voltage constitutes a voltage pulse and serves as an indication of the particle which caused the ionization.

In a proportional counter the applied voltage is sufficiently high that secondary ionization is produced in the region of the central wire, where the electric field is large. The ratio of the total number of ion pairs collected to the number of primary ion pairs is defined as the gas gain. Gas gain begins whenever the electric field strength is sufficient to give free electrons enough energy between collisions with gas molecules to cause additional ionization. An actual calculation of gas multiplication is not practical since it depends upon cross sections, which are not well known, and also is very sensitive to the presence of impurities. One normally depends upon empirical results obtained from actual counter operation. As a rough indication, however, of the voltage at which one can expect gas

gain to become significant, Wilkinson (1950) has given the expression

$$V \sim 10 p a \ln (b/a) \quad - - - \quad 4-1$$

where V is the applied voltage,

p is the gas pressure, in mm Hg,

a is the wire radius, in cm,

and b is the outer radius of the chamber, in cm.

For normal gas gains, primary electron collection contributes only a small fraction to the output pulse height with the major part coming from secondary ionization. Half the secondary ion pairs are formed within a mean free path of the wire, and ninety-nine percent within seven mean free paths. Since the mean free path of an electron normally is small compared with the radius of the central wire one may consider that essentially all of the ionization is created at the wire surface. The major portion of the pulse is then due to the motion of the positive ions created in the secondary ionization. Wilkinson (1950) shows that the voltage, V , induced on the central wire due to the motion of a single positive ion from the wire surface to an outer cylindrical wall varies with time, t , according to:

$$V(t) = (e/C) \ln \left[1 + (b^2/a^2 - 1)t/t_m \right] / (2 \ln b/a) \quad - - - \quad 4-2$$

where
$$t_m = (b^2 - a^2) \ln(b/a) / (2KV) \quad - - - \quad 4-3$$

When $t = t_m$ the positive ion reaches the cathode and the voltage change equals its maximum value e/C . In these equations, C is the total capacitance between the two electrodes, e is the electron charge, and K is the mobility of

the positive ion.

Figure 4-1 is a normalized plot of $V(t)$ for a positive ion collected in unit time and for a counter with a ratio of $b/a = 250$. Typical total collection times are of the order of $100 \mu\text{sec}$, but they vary considerably with counter gas and pressure. The pulse rises rapidly to half amplitude while the second half is relatively slow. For the collection of positive ions, as shown in figure 4-1, half amplitude is reached in about .005 of the total collection time.

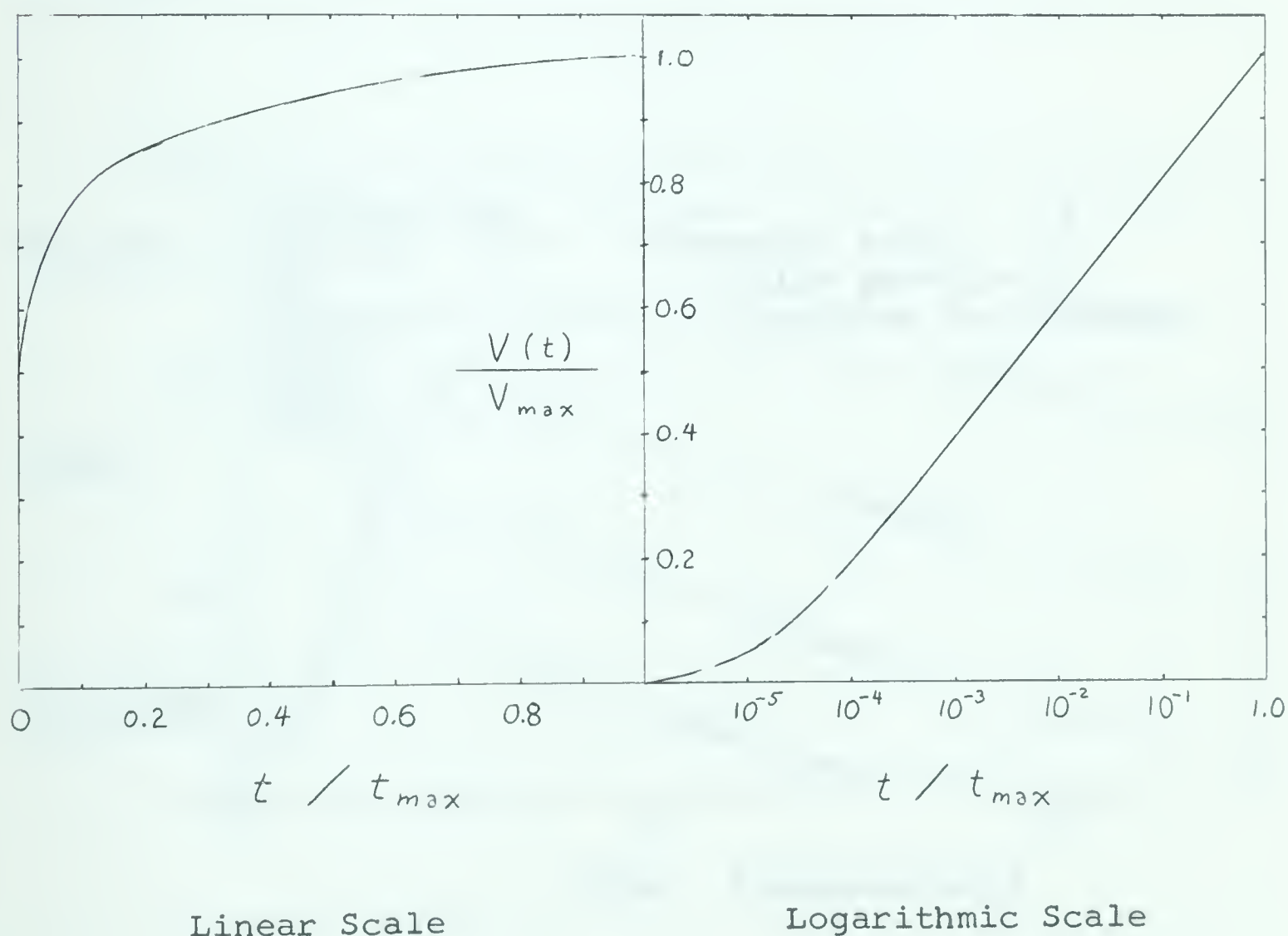


Figure 4-1 Normalized Pulse Size Due to the Movement of Positive Ions

When the initial ionization has an appreciable radial distribution in the counter, then the overall pulse will be a composite of curves like figure 4-1 each starting at a different time corresponding to the time at which various primary electrons drift into the multiplication region. When the primary ionization is radially distributed then the initial rise of a pulse will be representative of electron drift velocities in the counter. Such a composite pulse is shown in figure 4-2. Normally the slow part of the pulse is 'clipped off' electronically, and resultant pulse shapes for various clipping speeds are also shown in figure 4-2.

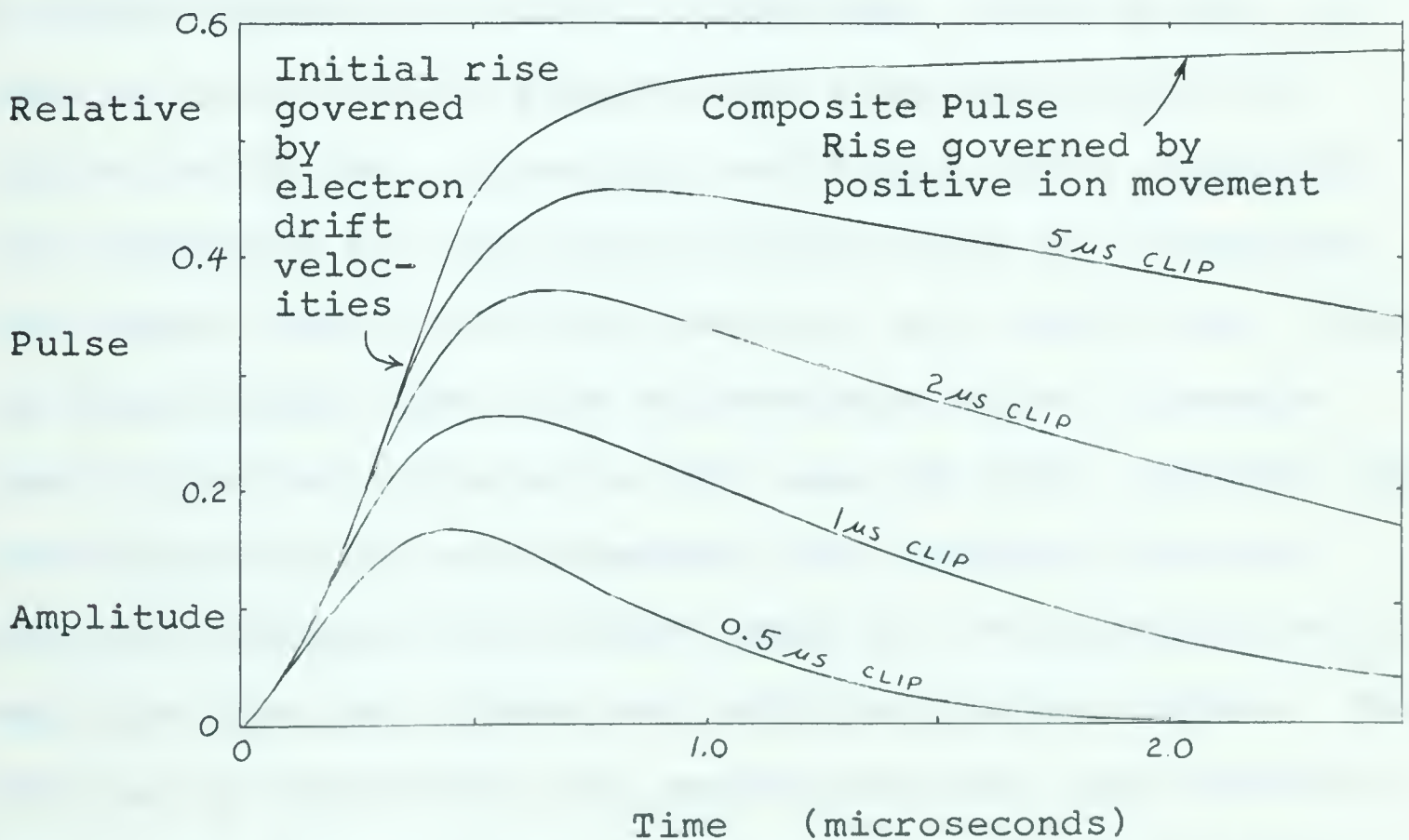


Figure 4-2 Typical Proportional Counter Pulse Shapes for Various Clipping Times

For normal proportional counters pulse rise times are typically of the order of $0.5\mu\text{sec}$, and may be as low as $0.1\mu\text{sec}$ in low pressure counters. While these times are slow compared with scintillation detectors, proportional counters are more nearly linear for heavily ionizing particles (Williams, 1961) provided the gas gain is not too high. The reasons for using gas proportional counters here, however, lie mainly in the nature of the experiment --- in the requirements that the detection medium consist of helium for polarization analysis and that the recoiling alpha particles be able to travel appreciable distances so that they can get from one counter to another, non-interacting, counter. Unfortunately, pure helium by itself is a notoriously poor counter gas with a marked tendency for erratic behaviour. This is due, in part at least, to the formation of long-lived metastable states in the gas. Generally, noble gases have relatively low thresholds for gas multiplication since the mechanisms for energy loss of drifting electrons are inefficient. This in itself might seem to be an advantage since it permits lower operating voltages for the same gas gain. However, the multiplication is very dependent upon voltage, and also energetic photons from excited atoms may cause photo electric emission from the cathode and initiate spurious pulses. The addition of poly-atomic gas greatly improves the characteristics and it was decided to use a mixture of up to five percent carbon dioxide in helium as the counter gas.

In polarization measurements, one of the most severe problems is that the counting rates are extremely small due to the double reaction-scattering processes involved. For this reason one must design apparatus with a maximum counting efficiency. Because of the coincidence technique to be used, a further requirement is that the pulses from the counters be as short as possible in order to improve resolving times and reduce accidental coincidences. With these criteria in mind, a basic consideration is just what size the counters should be; and this problem is discussed in the immediately following paragraphs.

Whatever the size of the counters, it is necessary that the recoiling alpha particles from scattering events be stopped within the counters and also be able to get from any part of the central counter to either of the side counters. This means that the range of the recoiling alpha particles should be such that they travel a distance slightly more than a full diagonal width of the central counter. One can express this criterion analytically by stating that for a given alpha particle energy (corresponding to a given energy for the incident neutron beam whose polarization is to be analyzed) the product of the pressure, P , in the counters and the width, w , should be constant:

$$P \cdot w = \text{constant} \quad - - - \quad 4-4$$

For a given neutron flux the scattering rate is proportional to the product of the pressure (or density of helium atoms) and the active volume of the central counter(s), from

which recoiling alpha particles are able to pass to the side counters through the vanes. One must try to make as large as practical the counting rate

$$C = \text{constant} \times (\text{pressure}) \times (\text{volume}) = \text{constant } P \cdot w \cdot h \cdot \ell \quad - - \quad 4-5$$

where P, w are the same as for equation 4-4,

h = height of active volume,

and ℓ = length of active volume.

However, providing the distance of the counters from the target can be varied, then the product, $w \times h$, really only defines the solid angle at the target. The product, $w \times h$, should be taken as a constant (maximum) quantity in determining the optimum size of counter. For maximum counting rate, then, one should maximize $P \times \ell$. But now, from equation 4-4 $P \cdot w$ is constant, so that we require that

$$C_R = \text{constant} \times \ell / w \quad - - - \quad 4-6$$

be a maximum. That is, the counter length, ℓ , should be large, and the counter width, w , small.

It can be further noted that the length and width are not entirely independent. Since the solid angle should be that defined by the middle of the active volume, then for a given length and width there is a maximum angle which can be subtended at the target (corresponding to the counters being right next to the target). This angle is given approximately by w/ℓ radians. If a given angular subtense is desired, there is a minimum value for w/ℓ . (For example, for $\Delta\theta = 10^\circ$ or 0.18 radians, then $w/\ell \geq 0.18$, or $\ell/w \leq 5.5$).

The speed of the pulses is limited by the drift velocity

of electrons and ions, and also by the distance of travel. The velocity, v , of electrons or ions increases with increasing E/p , where E is the electric field strength (which varies with radial distance from the wire). The usual form for v is given by:

$$v = \text{constant } (E/p)^x \quad - - - \quad 4-7$$

where x is some constant power, usually taken to be $\frac{1}{2}$ for electrons.

For cylindrical geometry, $E = \frac{V_o}{r \ln b/a}$ - - - 4-8

where V_o is the applied counter voltage,

b is the outer radius,

and r is the radial distance to the point of the electric field, E .

From equations 4-7 and 4-8:

$$v \equiv \frac{dr}{dt} = \text{constant} \left(\frac{1}{r} \right)^x \left(\frac{V_o}{P \ln b/a} \right)^x \quad \text{or,} \quad r^x dr = \left(\frac{V_o}{P \ln b/a} \right)^x dt.$$

Integrating, for an electron going from the mean outer radius to the counter wire:

$$b^{3/2} \approx b^{3/2} - a^{3/2} = \text{constant} \left(\frac{V_o}{P \ln b/a} \right)^{1/2} t.$$

For fast pulses, one should maximize

$$\frac{1}{t} = \text{constant} \frac{1}{b} \left(\frac{V_o}{P b \ln b/a} \right)^{1/2} \quad - - - \quad 4-9$$

The voltage increment to increase the gas gain by a factor of two is in the neighborhood of 50 to 100 volts, which is small compared with the voltage required for gas gain to start significantly. Using this fact with equation 4-1, then again, as a rule of thumb, one may say that for a

given gas gain the following equation is approximately true:

$$V / \left(P a \ln \frac{b}{a} \right) = \text{constant} \quad - - - \quad 4-10$$

Using this result, then equation 4-9 may be written

$$\frac{1}{t} = \text{constant} \frac{1}{b} \left(\frac{a}{b} \right)^{\frac{1}{2}} \quad - - - \quad 4-11$$

Thus, to increase the speed of the pulses, 'b' (or width, w) should again be small, and the wire radius 'a' should be large. Note, however, that to double the speed of the pulse by changing 'a' alone would require that 'a' be quadrupled, and so also the voltage V (according to equation 4-10) would have to be quadrupled.

Thus to satisfy the criteria of fast pulses and larger counting rates, for a given solid angle at the target, the central, active volume of the polarimeter should be as long and as thin as is practical. The central wire should be as large as possible consistent with voltage considerations. A central width of 1.25 inches was used since the accelerator beam spot for large beam currents on a target cannot be defined much better than about a quarter of an inch. It was not felt that horizontal counter wires should be more than about ten inches long; and using this value, the effective active length of the counter was limited to about 2.5 inches because of end effects and the diagonal path of the recoil alpha particles. Counter wires of .005 inch diameter were used.

Although the foregoing discussion assumed cylindrical geometry, for maximum transfer of particles with minimum

energy loss outside counters it is necessary to have flat at least the parts of the counters adjoining one another. As this in itself demands a departure from the normal cylindrical geometry for part of the walls, it was decided to make all the walls flat and the chambers rectangular in cross section. With such a shape, the counters can butt evenly against one another. Since, for proportional counting the more important design criterion is a smooth uniform wire, the unusual wall shape should not adversely affect the operation of the counter, except possibly in the low electric field regions of the corners, where recombination of ions is more likely - with consequent loss of pulse amplitude.

While one might have designed the counters to operate with their axes perpendicular to the neutron beam direction, it was thought that axes in line with the neutron direction would give a more regular geometry for scattering events occurring in different parts of the polarimeter.

In order to evaluate the effect of the flat counter walls on the collection times and gas amplifications for different parts of the counter, a simple preliminary experiment was performed to determine how the voltage and electric field can be expected to vary within the counter. An enlarged cross section of the counter was drawn on resistance paper using silver conducting ink and a voltage was applied between the central spot (representing the wire) and the rectangular outline (representing the walls of the counter). Contours of constant voltage were mapped out

using a high impedance voltmeter and the result is shown in figure 4-3. It is noted that nearer the wire the constant voltage lines are almost circular and the electric field becomes radially symmetric. The gas gain should therefore be independent of the radial direction from which the initial ionization comes.

If the counters had cylindrical walls the voltage and electric field dependence upon radial distance would be given by equations 4-12 and 4-13 respectively:

$$V \times \log(a/b) = V_0 \times \log(r/b) \quad - - - \quad 4-12$$

$$E \times r \times \log(a/b) = V_0 \quad - - - \quad 4-13$$

where a is the radius of the central electrode (wire),

b is the radius of the outer electrode (walls),

V_0 is the voltage between electrodes,

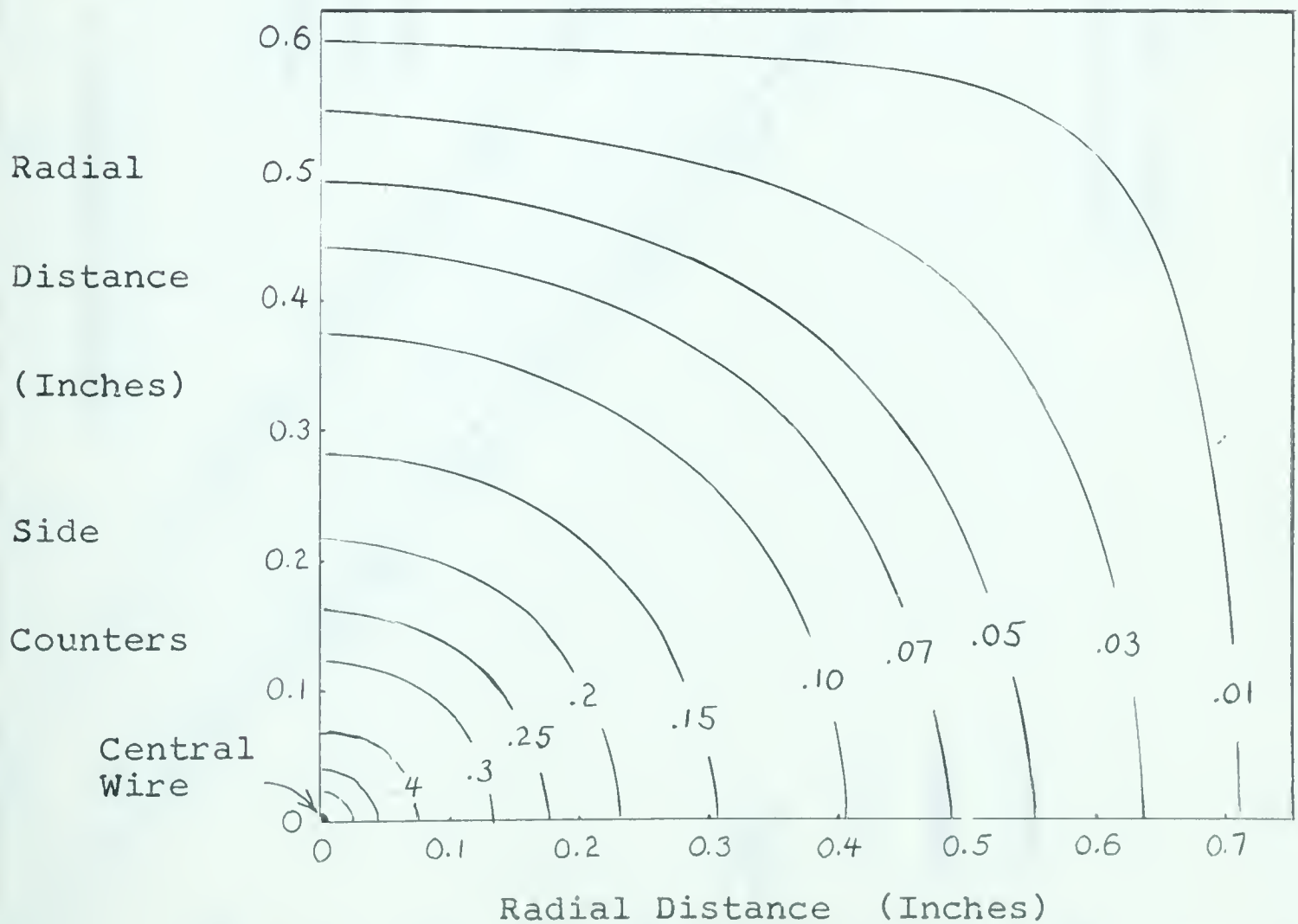
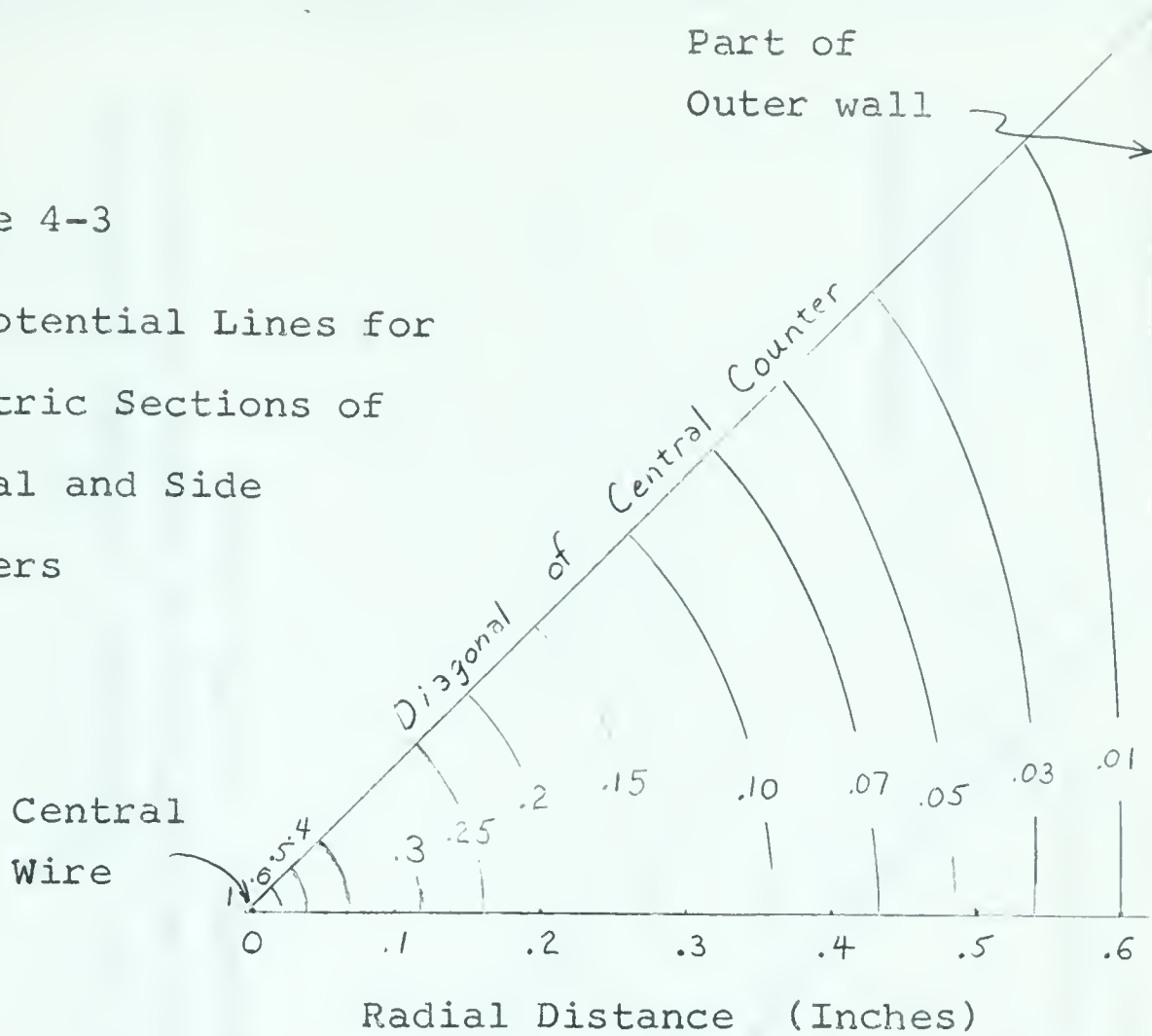
V is the voltage at radial distance r ,

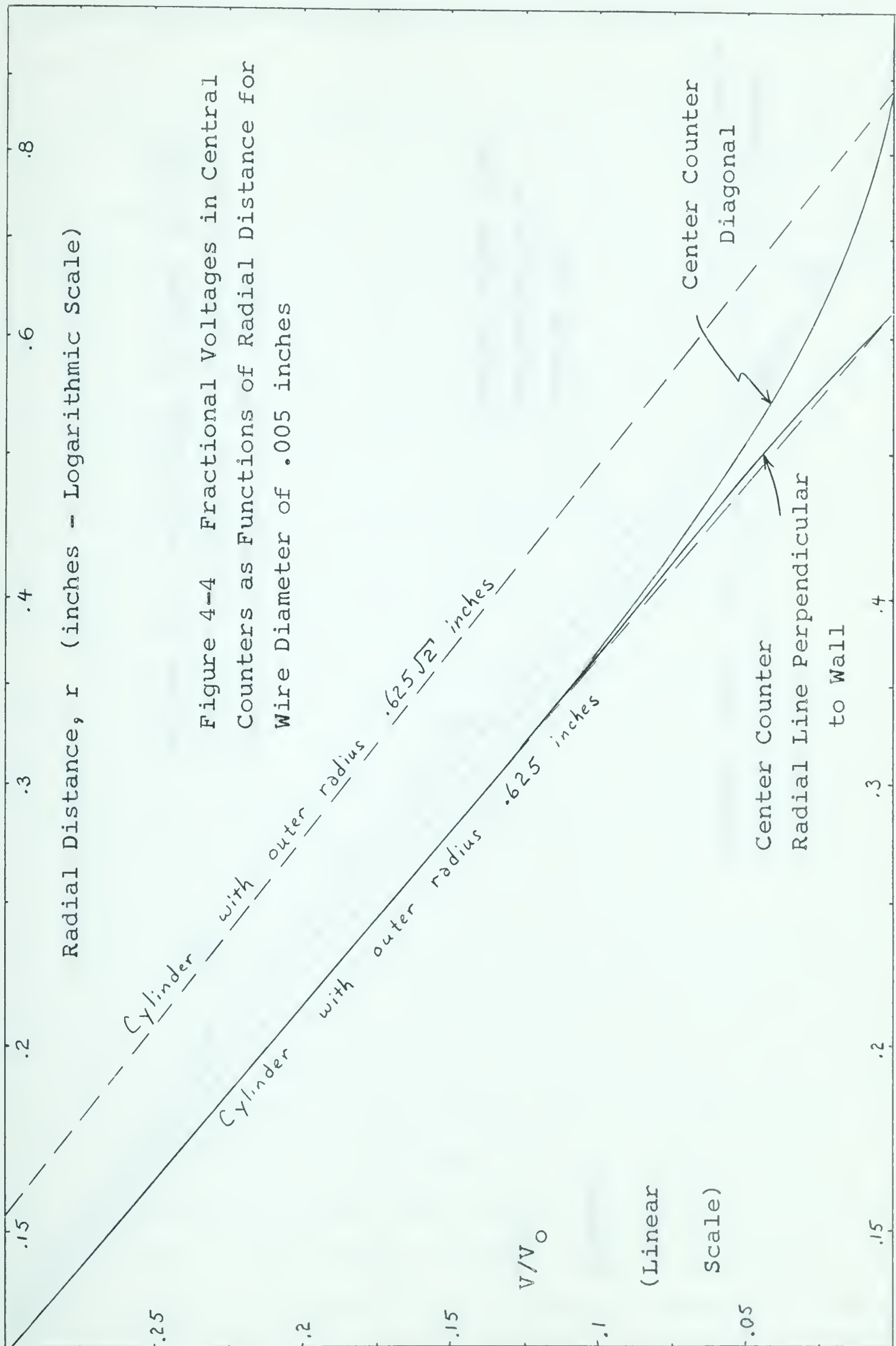
and E is the electric field at radial distance r .

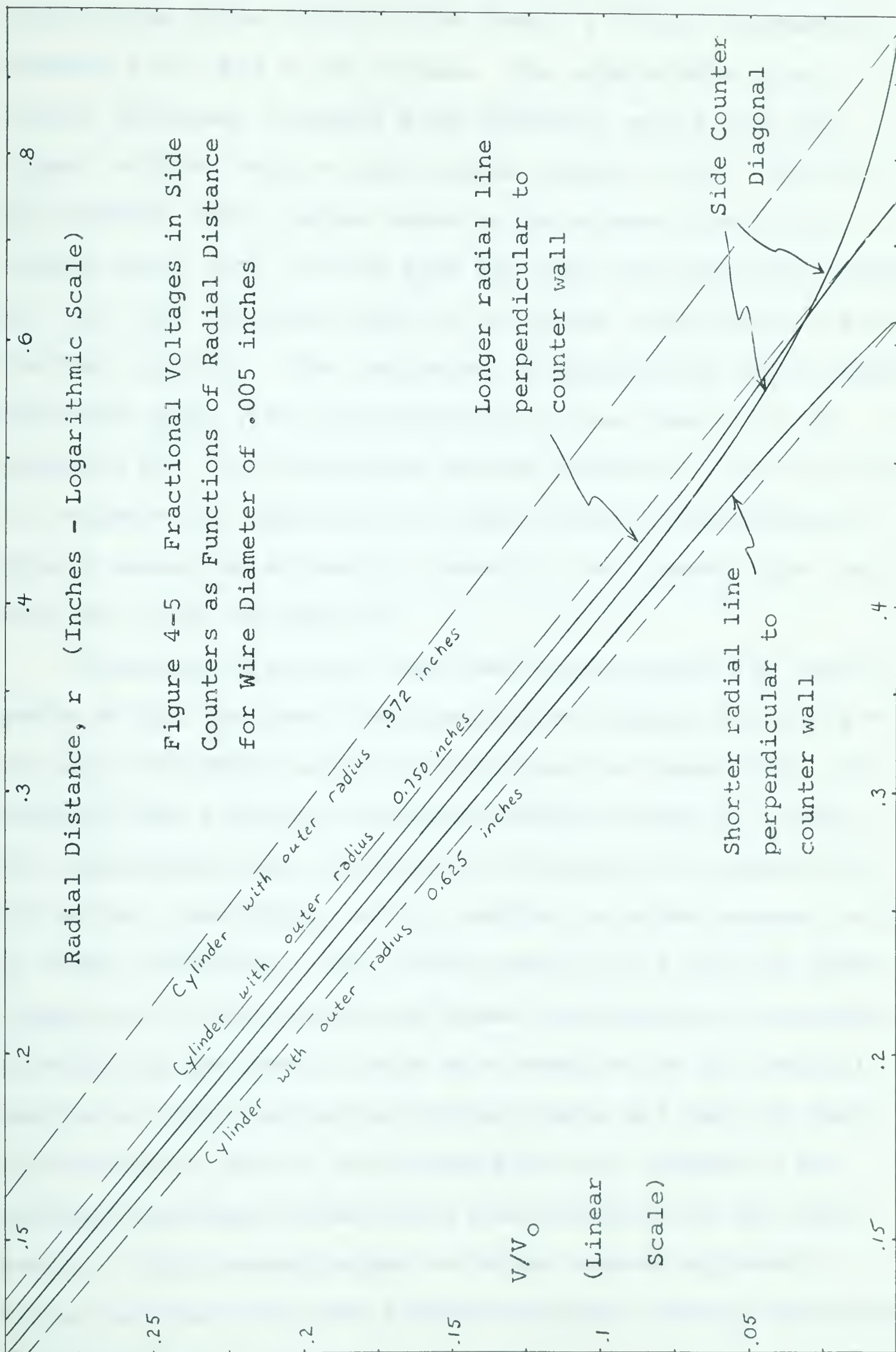
Using equation 4-12, lines are shown in figures 4-4 and 4-5 of constant voltage V as a function of radial distance r for the wire radius of 2.5 mil and for a number of values of outer radii. In these figures also are shown experimentally determined voltage values for points along counter diagonals and along radial lines perpendicular to the counter walls. For the square cross section of the middle counters the voltage values near the wire approach those for cylindrical geometry with outer radius 0.625 inches. For the rectangular cross section of the side counters the voltage values near the wire also approach those for cylindrical geometry but the

Figure 4-3

Equipotential Lines for
Symmetric Sections of
Central and Side
Counters







appropriate outer radius tends toward a value intermediate between 0.625 and 0.750 inches. The appropriate outer radius increases slightly with azimuthal angle from the closer counter wall to the farther counter wall. That the appropriate outer radius tends to be greater than 0.625 inches means that for the same gas gain the operating voltage for the side counters tends to be larger than that for the central counters. The variation in appropriate outer radius indicates that some non-uniformity in gas gain is to be expected for the rectangular walled counters. It is difficult to estimate the importance of this since the experimental points cannot be accurately taken to the counter wire, and only the trend is apparent.

Electron collection times may be estimated for various parts of the counters from the data of figures 4-4 and 4-5 and from the drift velocity data shown in figure 4-6. For example, for a typical incident neutron energy of 10 Mev, the appropriate gas pressure is 125 cm Hg of 5 percent CO₂ in helium, (see figure 4-14), and the required counter voltage is about 1500 volts. For these conditions a plot is shown in figure 4-7 of the calculated times required for an electron to drift to the central wire as a function of its initial position. The electron collection times are seen to vary significantly, and in the corners the low electric field gradients probably permit some recombination of the ionization. Such recombination could be reduced by using a larger central wire with a higher applied voltage, and perhaps a different gas mixture.

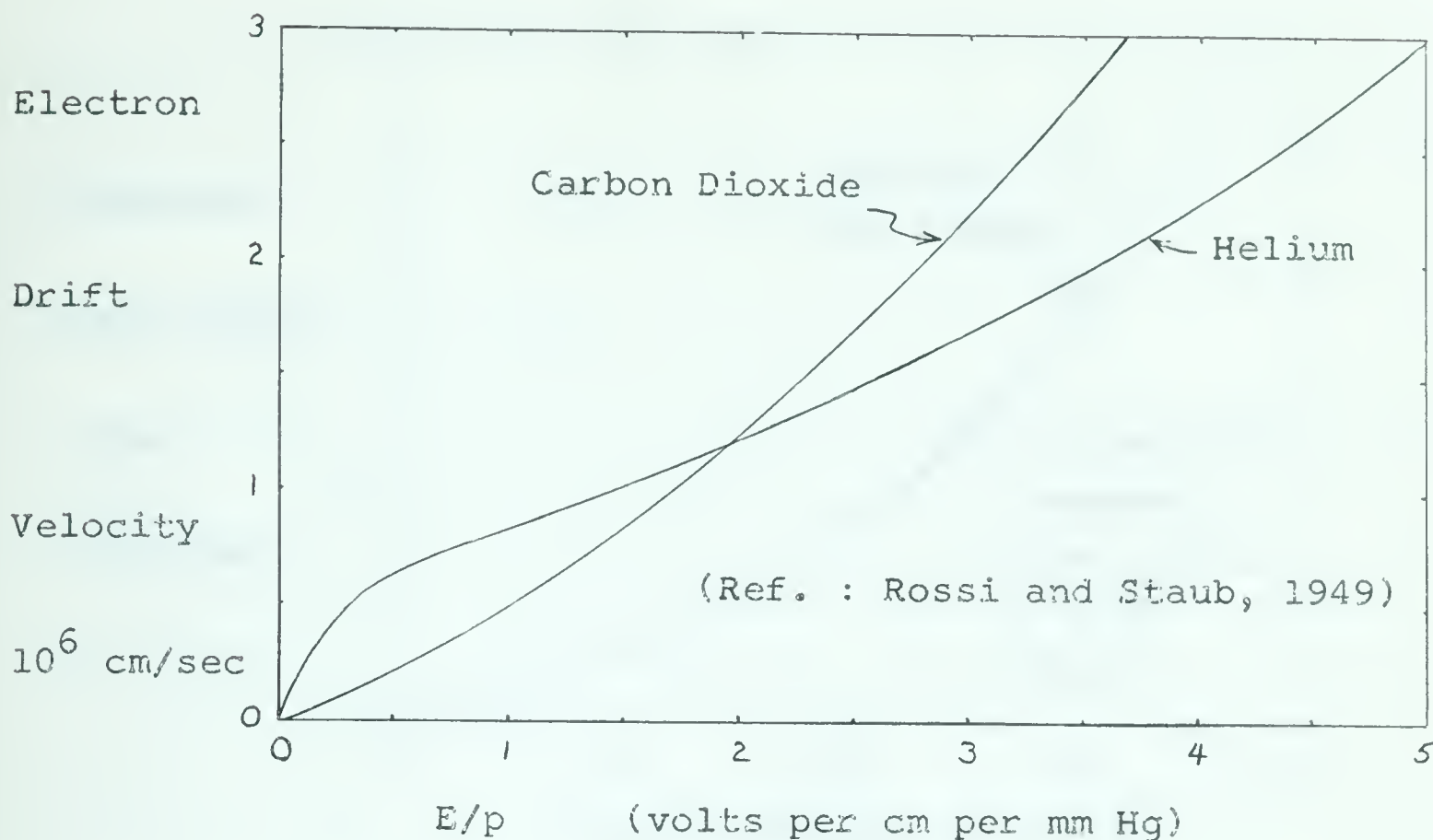


Figure 4-6 Electron Drift Velocities

Because of the solid angle defined by the grids, the alpha recoils causing coincident pulses have paths horizontal within ten degrees. The pulse shapes for horizontal paths of ionization at different heights above a central plane are shown in figure 4-8. These pulse shapes apply when the gas gain is high enough that the movement of electrons does not in itself contribute appreciably to the pulse height. It is noted that although the pulses are delayed by varying amounts the rise times are surprisingly similar. This is due to the cancellation of the effect of slower drift velocities for larger radial distances by the closer grouping in distance from the central wire for the ionization further away from the central plane. Rise times of slightly more than two microseconds are to be expected. The time delay

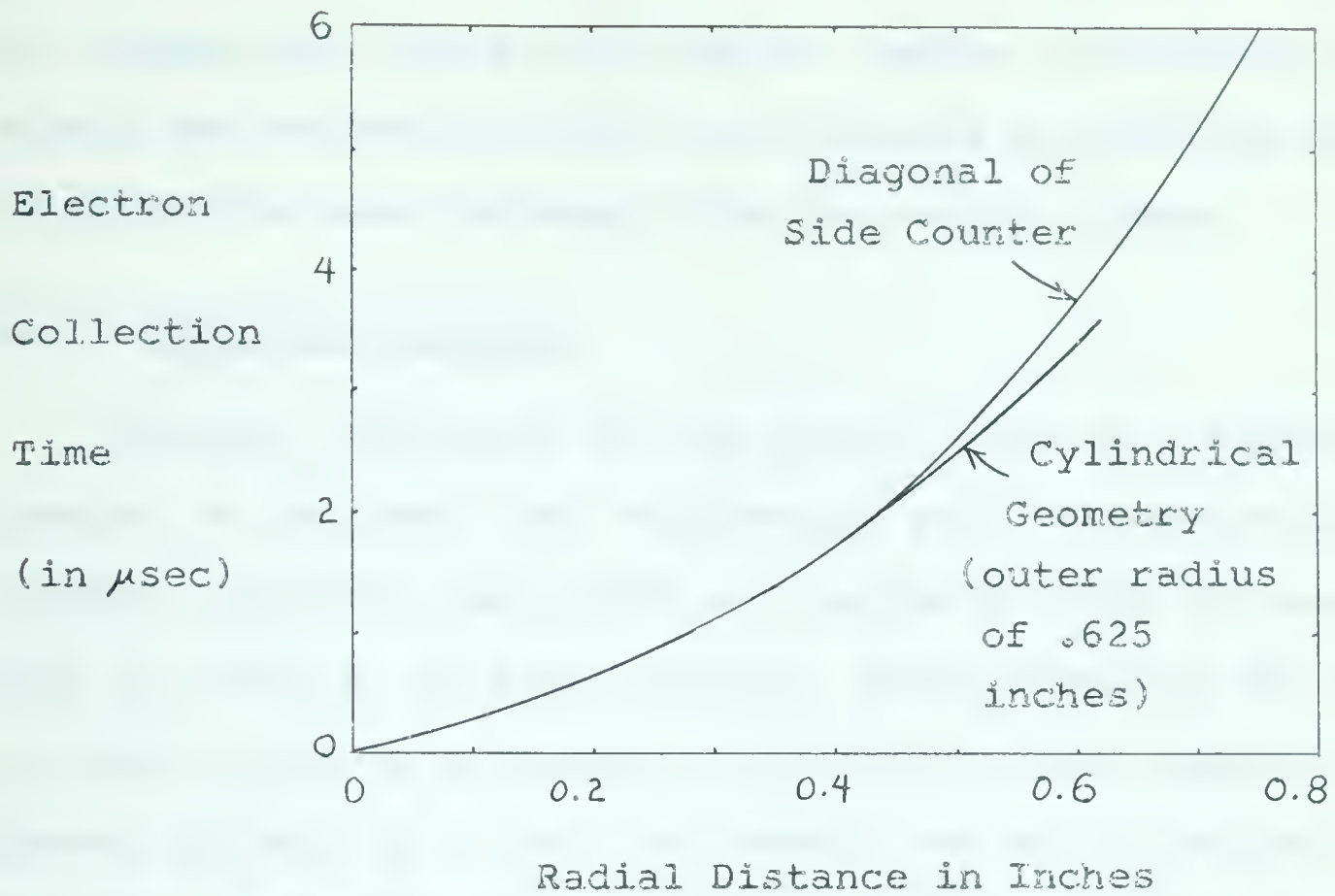


Figure 4-7 Electron Collection Times for Proportional Counters

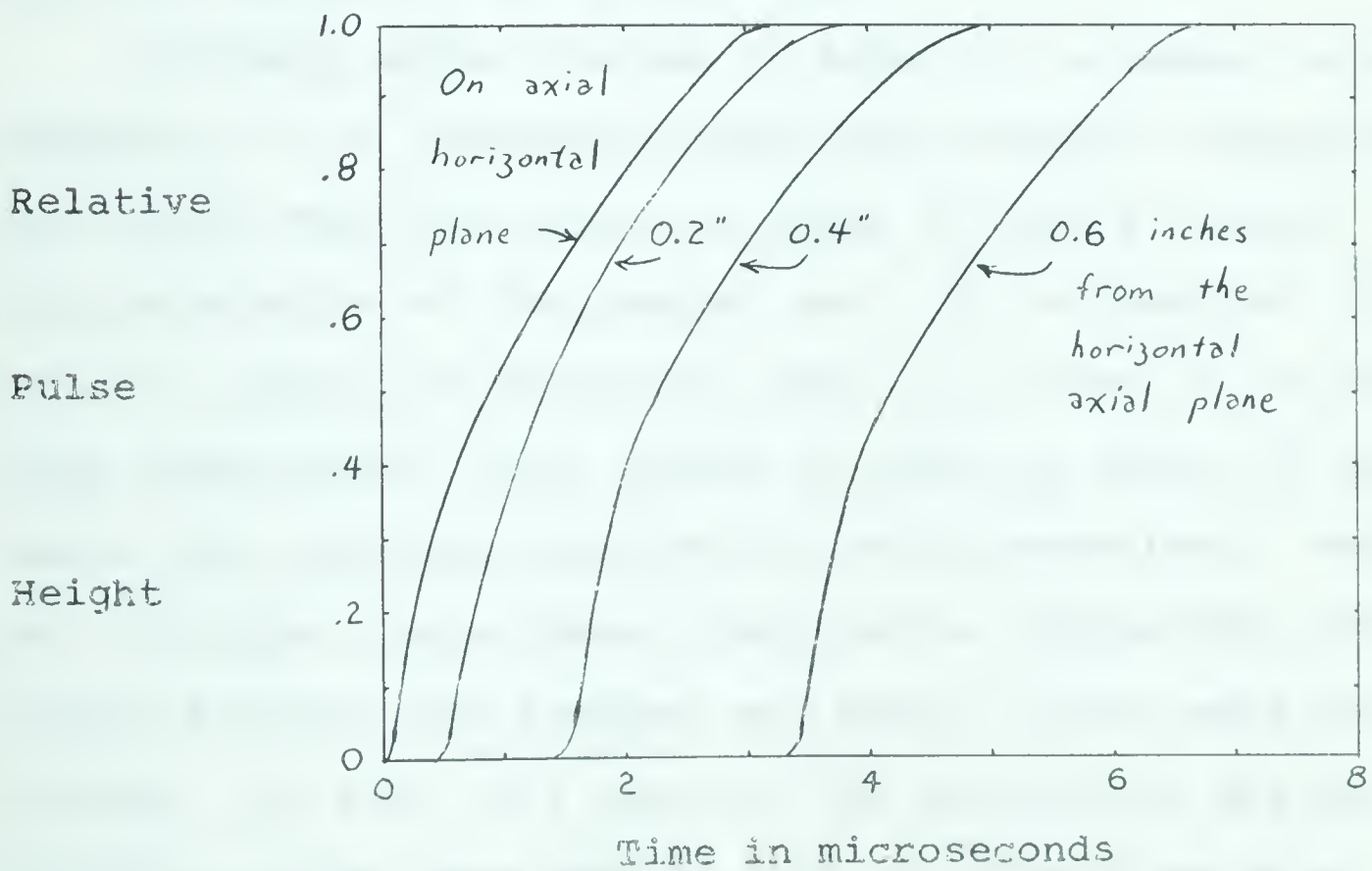


Figure 4-8 Pulse Shapes for Various Distances from Horizontal Axial Plane

for pulses relatively far from the central horizontal plane should not be serious since coincidences are between pulses at about the same distance from the central plane.

4-2 Mechanical Design

Because uniformity of the central wire of a proportional counter is important for uniform gas gain throughout the counter, special precautions are normally taken to ensure that the wire is in fact uniform. After mounting the best available wire in a counter, a high electrical current is passed through it to melt and smooth out any irregularities and also to remove dust particles. Provision for 'glowing' the wire, as this procedure is called, was incorporated into the design of the polarimeter.

Although carbon dioxide is added, in a sense, as an impurity, it is desirable that other possible impurities be removed from the helium in order to ensure regular characteristics of the counter gas. It is important to be able to outgas the apparatus; that is, to heat it to rather high temperatures under vacuum in order to drive off unwanted gases from cavities and from the walls themselves. Because of the higher temperatures required for outgassing, ordinary rubber O-rings were avoided, and metal O-rings were used instead. In fact, all parts of the polarimeter and gas handling system were made of metal or ceramic material.

The drawings for the polarimeter are shown in figures A-1 to A-11, as Appendix A of this thesis.

Basically, the proportional counters are rectangular in cross section and are housed in a cylindrical, gas tight, stainless steel tank. Nine counters in all are used - three layers of three-counter units. The central counters are each 1.25 inches square in cross section, while each side counter is 1.25 inches deep by 1.50 inches wide; all counters are about eight inches long. The reason for having the greater width on the side counters is to allow a longer path for more energetic alpha particles, if there are any, and hence to be able to discriminate against higher energy neutrons. With three three-counter units, the central active volume is three times deeper than it is wide, permitting an azimuthal divergence of about three times the polar divergence of the neutron beam from the target. This is thought to be reasonable since polarization dependence on the azimuthal angle varies as the cosine, and comparatively large divergences are possible before the cosine varies appreciably from one. At the same time, if one wants to examine the polar dependence of polarization, then the divergence of this angle should be small, consistent with reasonable counting rates.

The walls of the counters were formed from five and ten mil stainless steel sheet and were fixed in place by spot welding to a stainless steel framework. Thinner, two mil stainless steel sheet held the front end insulators in place; the sheet was flexible and elastic enough that it could keep the counter wire straight and under tension. The counter wires were normally put in while the cylindrical

shell was off; a bead held the wire in the front end insulator and the wire was soldered while under tension into a kovar seal in the back end plate.

The polarimeter tank is a twelve inch long cylinder, six and a half inches in diameter. Two end discs are bolted to flanges on the basic cylindrical shell; metal O-rings make the vacuum seal. The front end disc is easily removed so that the inner units may be conveniently inspected in situ, and so that shorting leads may be attached for glowing the counter wires, and then removed for normal counter operation. The counter assembly is held to the back-end plate, and the combined unit can be removed from the cylindrical shell of the tank.

The collimating vanes for permitting alpha particles with a particular recoil direction to pass from the central counters to the outer counters are held in slots in the frame for the counters. For maximum analyzing sensitivity over a wide range of neutron energies, the polar angle was chosen to be $22\frac{1}{2}^{\circ}$ ($\pm 5^{\circ}$), corresponding to 45° recoil and 135° neutron scattering in the center-of-mass system. As seen from figure 2-3 the analyzing factor for this angle of $n - \alpha$ scattering is close to unity over the wide range of neutron energies from about 3 to 20 Mev. The azimuthal angular variation permitted is about $\pm 10^{\circ}$.

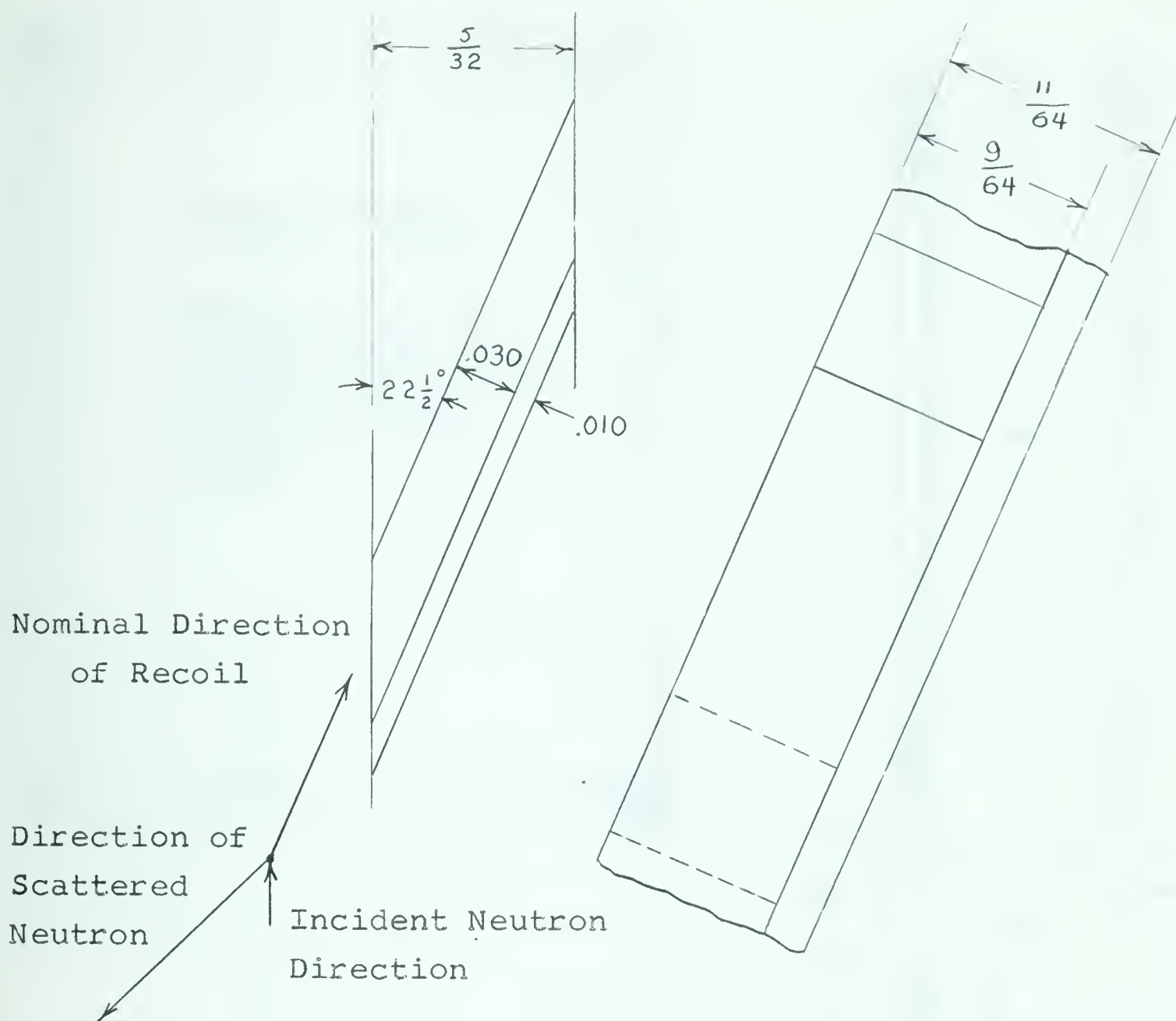
Since ionization created by alpha particle energy loss within the vanes will recombine due to negligible electric field in this region, then energy lost within the vanes will

not contribute to overall pulse height. In order to reduce this loss the vanes should be made as thin as practical.

To form the collimating vanes, it was decided⁺ to machine oblique channels in long rectangular bars and to stack the bars so cut in frames to form an array of oblique rectangular holes between counters. Figure 4-9 shows the outline of a channel hole, while figure 4-10 shows a bar with the channels cut in it. The frame for holding the vanes in place is shown in figure 4-11. These frames fit into the two slots of the counter framework illustrated in figure A-5.

Figure 4-12 shows the collimating vane positions relative to the counters, and as well the active volume and angles so defined. From this diagram it is seen that although the counters themselves are eight inches long, the exposed vane length is restricted to two and a half inches because of the small recoil angle and because of the need to define active volumes away from the counter ends where the electric field is not regular.

+ The collimating channels were produced at the Suffield Experimental Station, Ralston, Alberta, under the direction of J. T. Sample, in 1957.



Dimensions shown are in inches

Figure 4-9 Collimating Hole (not to scale)

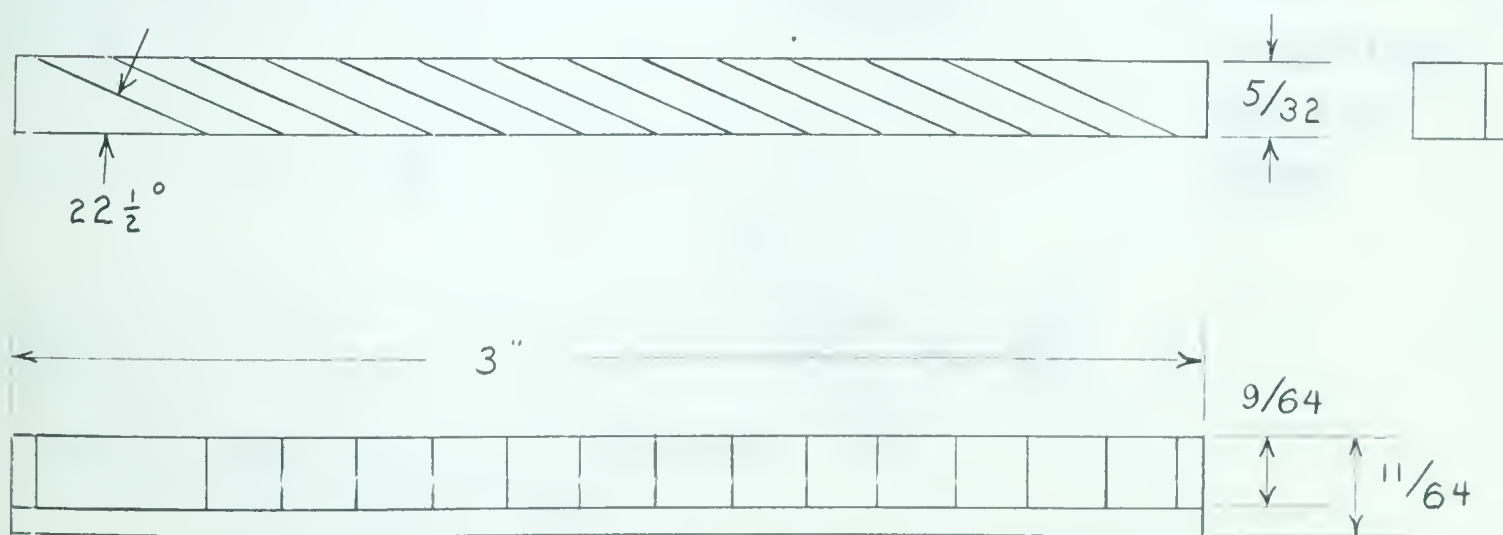


Figure 4-10 Collimating Strip (not to scale)

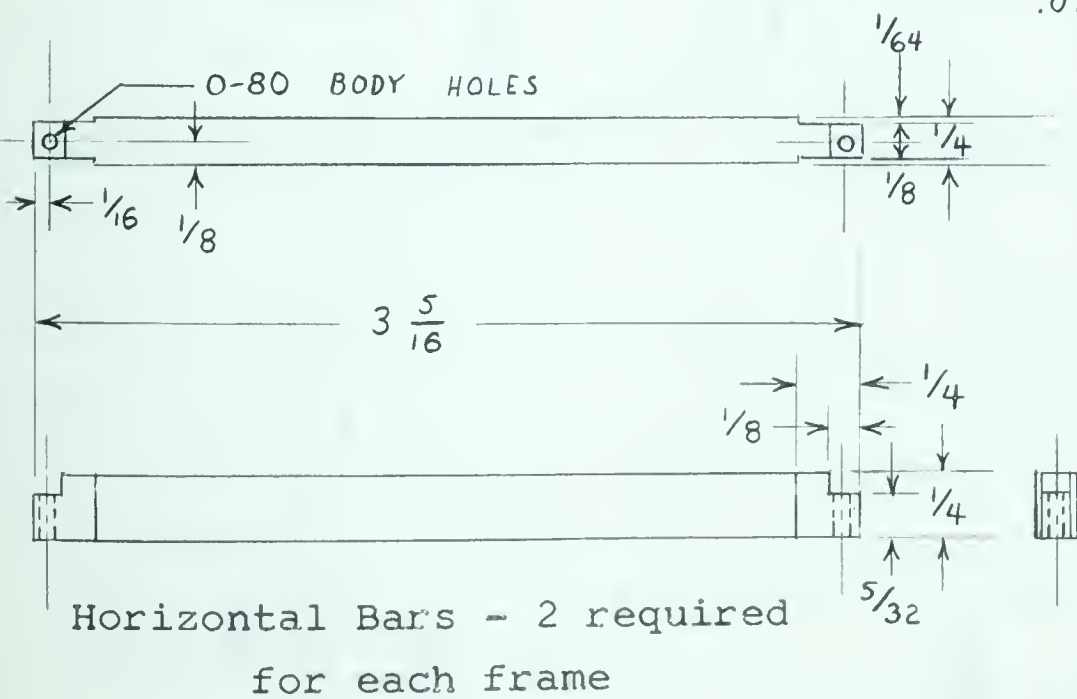
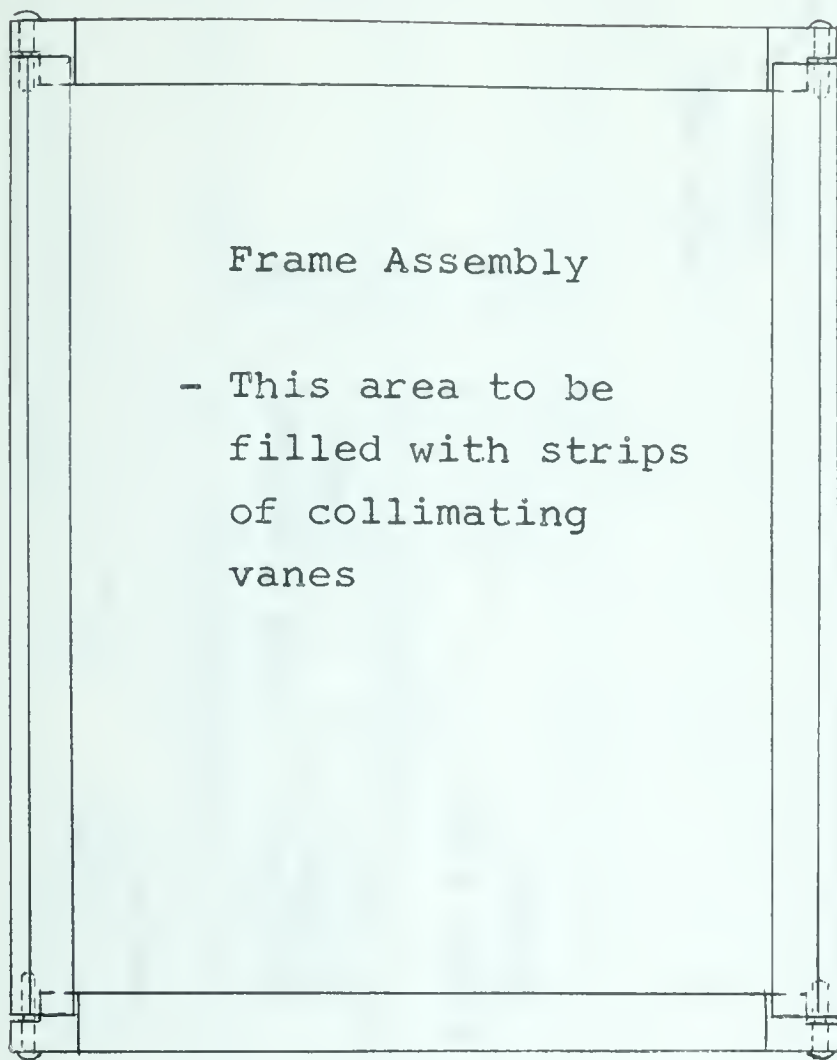


Figure 4-11 Frame for Holding Collimating Vanes

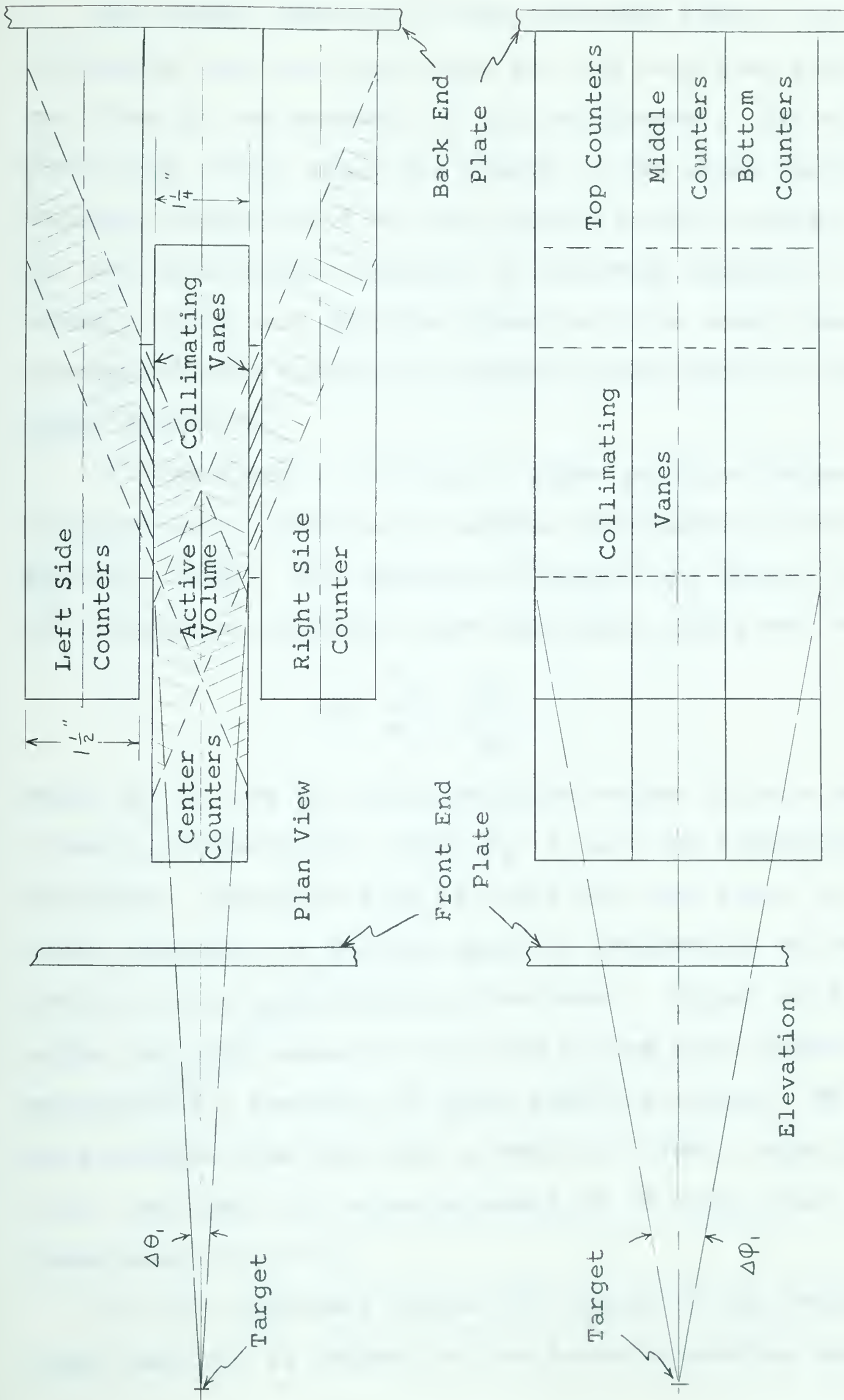


Figure 4-12 Counter Volume and Angles Defined by Vanes and Target

The recoil angle for alpha particles from $n - \alpha$ scattering and the ideal range for the recoiling particle are fixed by the geometry of the polarimeter. Since for a particular recoil angle the energy of the alpha particle is directly proportional to the incoming neutron energy, then for the polarization analysis of incoming neutrons of given energy, there is a definite alpha particle energy and correspondingly a definite pressure requirement to meet the range specified.

A comprehensive listing of alpha particle ranges and stopping cross sections in various substances is given by Whaling (1958). For mixtures of helium and carbon dioxide, the range, R , was computed from this data, using the expression

$$\frac{1}{R} = \frac{f_1}{R_1} + \frac{f_2}{R_2} \quad - - - \quad 4-14$$

where R_1 , R_2 are the alpha particle ranges in pure components 1 and 2, respectively, while f_1 , f_2 are the respective volume fractions. Equation 4-14 is valid when the ratio of stopping cross sections for the two gases is independent of energy. (This is only approximately true here). Figure 4-13 shows alpha particle ranges for various helium plus carbon dioxide mixtures as a function of alpha particle energy. The curves were derived from the data of Whaling (1958), using equation 4-14, and apply for a gas pressure of 76 cm Hg, and a temperature of 15° C.

In the laboratory system the energy of the recoiling alpha particle is related to the incoming neutron energy by

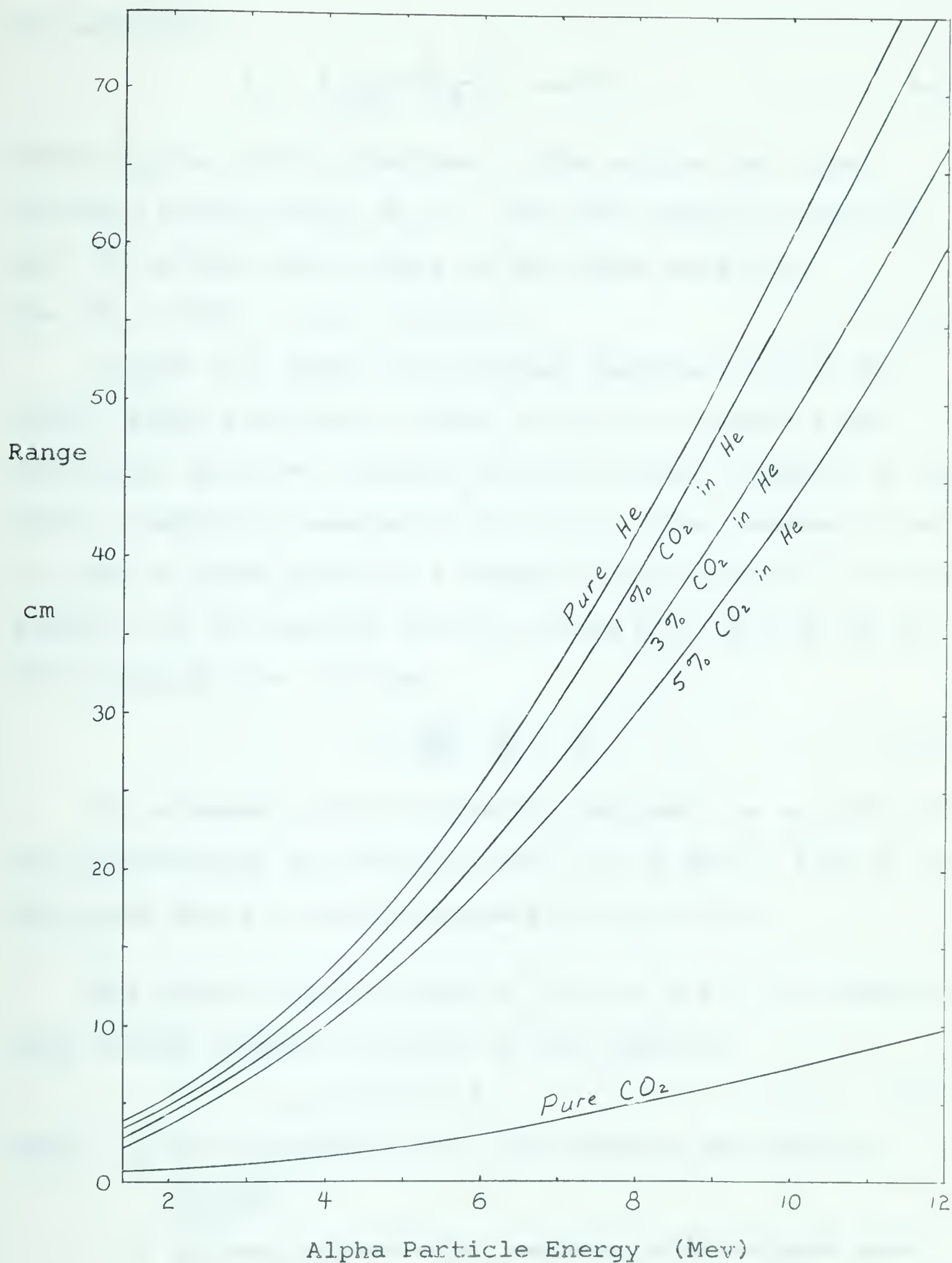


Figure 4-13 Alpha Particle Ranges in Mixtures of Helium plus Carbon Dioxide at 15°C, 76 cm Hg

the equation:

$$E_{\alpha} = E_n \left(\frac{m_{\alpha}}{m_n + m_{\alpha}} \right)^2 \cos^2 \theta_{\alpha} \quad - - - \quad 4-15$$

where E_n , E_{α} are the energies of the neutron and alpha particle respectively; m_n , m_{α} are the respective masses; and θ_{α} is the recoil angle of the alpha particle.

For $\theta_{\alpha} = 22\frac{1}{2}^{\circ}$, $E_{\alpha} = 0.546 E_n$. - - - 4-15a

Figure 4-14 shows the pressure required to give the recoil alpha particles a range of 10.0 cm, which is the horizontal diagonal distance across a center counter, at the normal operating temperature of 25° C. The pressure P required to give an alpha particle a range of 10.0 cm at 25° C as in figure 4-14 is obtained from its range R at 76.0 cm Hg and 15° C through the relation

$$P = \frac{298}{288} \cdot \frac{R}{10} \cdot 76. \quad - - - \quad 4-16$$

It is noted that the pressure required for analysis of the polarization of neutrons from 3 to 20 Mev is from 25 to 400 cm Hg for a 5 percent mixture of CO₂ in He.

The total counting rate, C_t , due to all n - α scatterings in the counters is given by the equation

$$C_t = \sigma_t n N \ell \quad - - - \quad 4-17$$

where σ_t is the total n - α cross section per nucleus, in cm²,

n is the rate at which neutrons are incident upon the counters,

N is the number of helium atoms per cc,

and ℓ is the length of the counters, in cm.

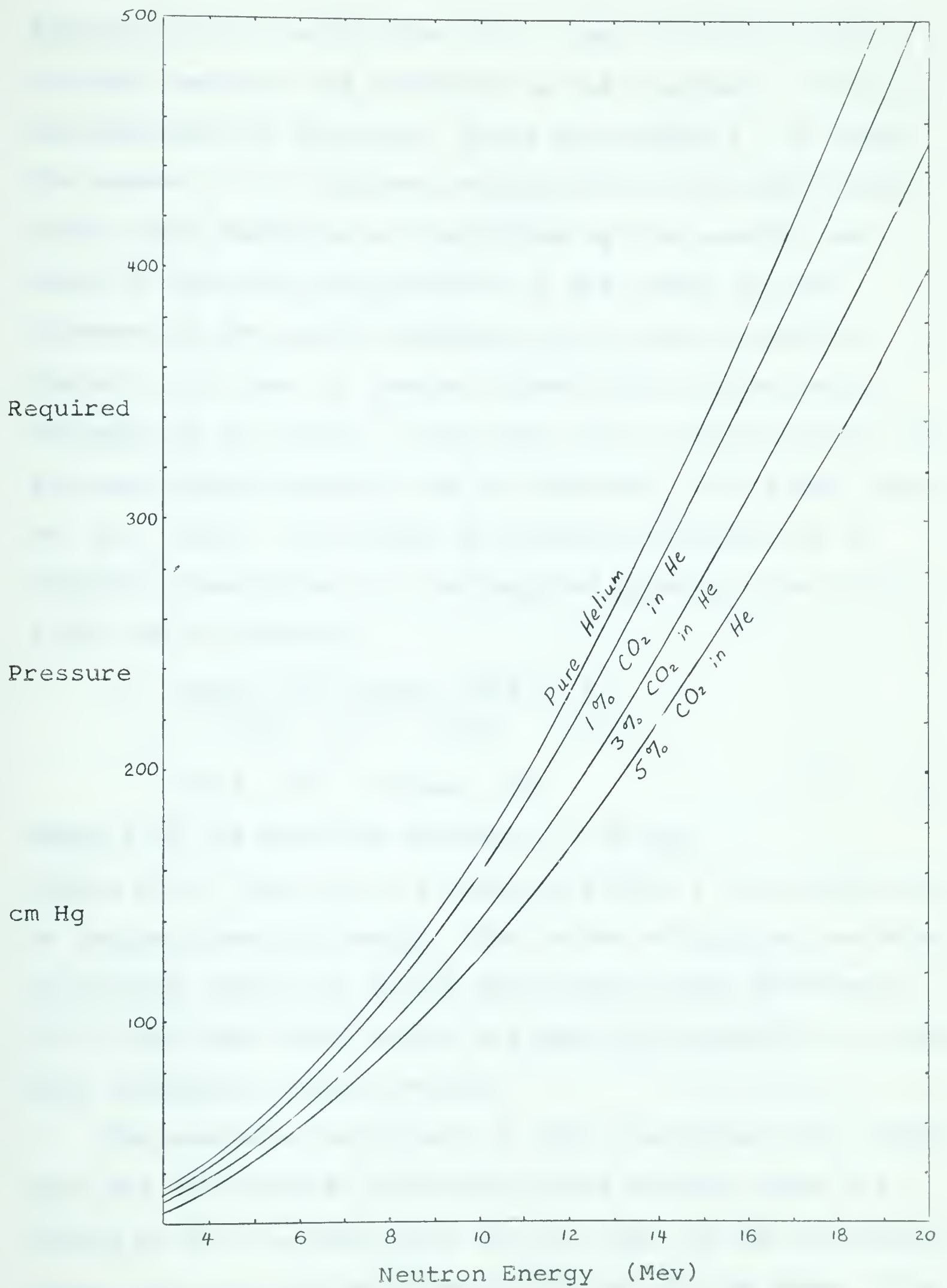


Figure 4-14 Pressures for Recoil Alpha Range of 10 cm at 25°C

Equation 4-17 is valid when only a small fraction of the incident neutrons are scattered in the counters -- and this unfortunately is the case. While the length, l , is fixed, the number, n , of incident neutrons is proportional to the solid angle subtended at the target by the counters and hence is inversely proportional to the square of the distance of the active volume of the counters from the target; n is also, of course, proportional to the source strength at the target. The total cross section varies with incident neutron energy, and is reasonably well known (Austin et. al., 1962). The number N of helium atoms per cc is directly proportional to the required pressure (see figure 4-14) and is given by

$$N = \frac{6.02 \cdot 10^{23} \text{ atoms / GAW}}{2.24 \cdot 10^4 \text{ cc / GAW}} \cdot \frac{P}{76.0}$$

$$= 3.54 \cdot 10^{16} P \text{ atoms / cc} \quad - - - \quad 4-18$$

where P is the absolute pressure, in cm Hg.

Graphs of σ_t and C_t/n are shown in figure 4-15 as functions of incident neutron energy. The values of C_t/n may be taken as a rough indication of the efficiency of the polarimeter. It is seen that these values are small but generally increase with increasing neutron energy.

The analyzing efficiency of the polarimeter will depend upon the differential scattering cross section, upon the volume of the counters which can be 'seen' by the collimating vanes, and upon the solid angle accepted by the vanes. The efficiency is reduced by a transmission factor of about 0.7,

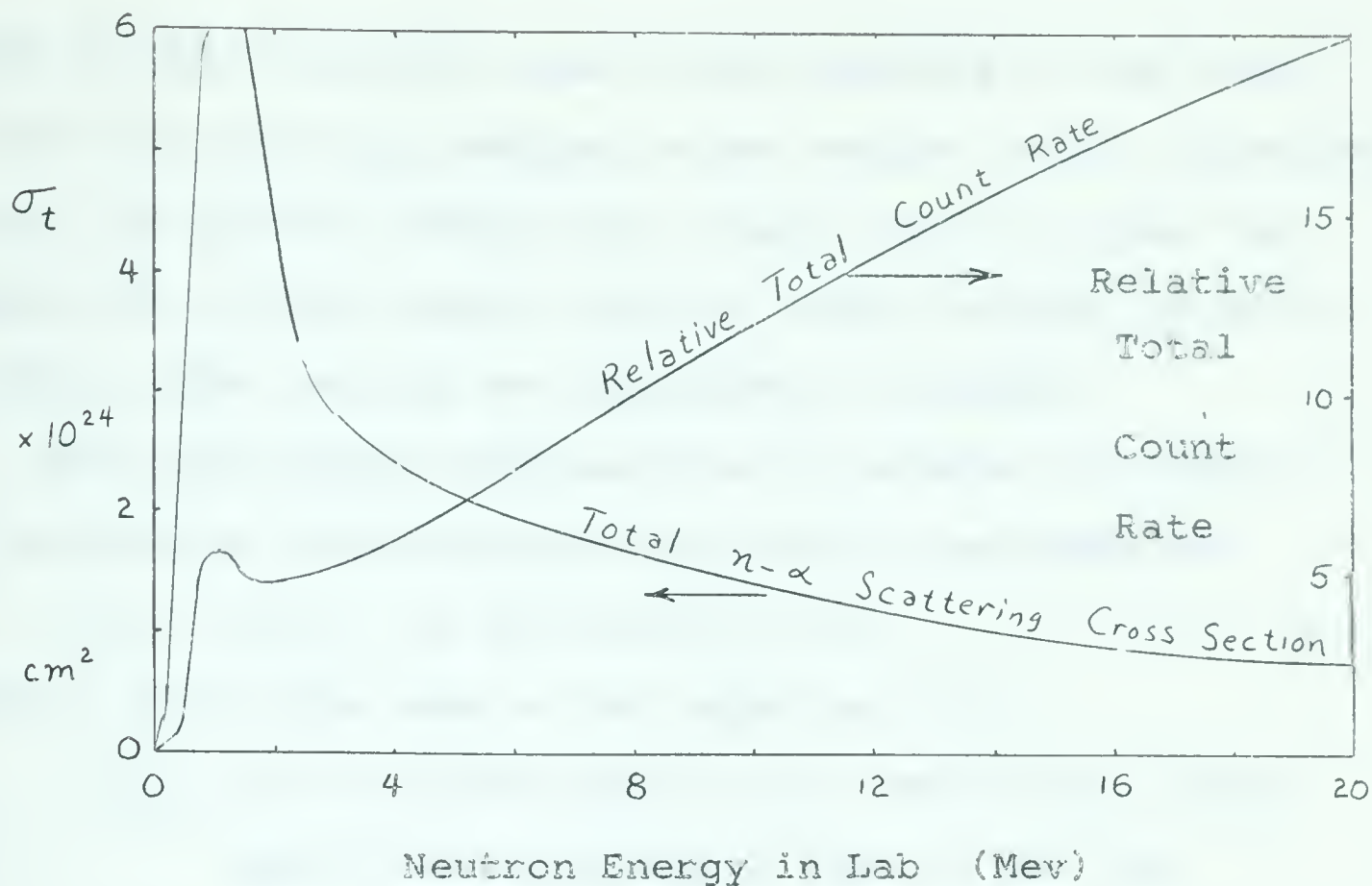


Figure 4-15 Total n- α Scattering Cross Section and Normalized Count Rate as Function of Neutron Energy

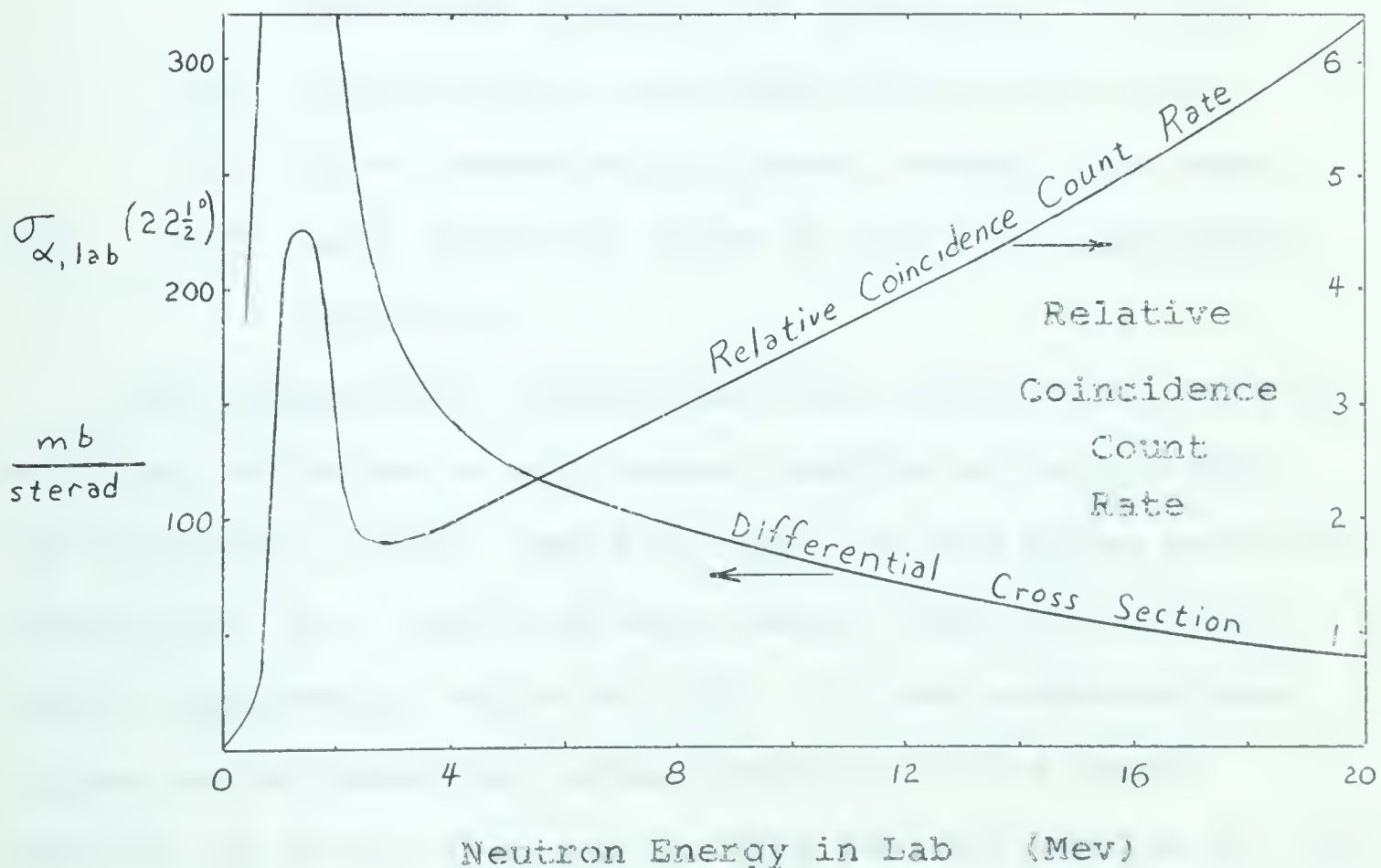


Figure 4-16 Laboratory Differential Scattering Cross Section for Alpha Recoil at $22\frac{1}{2}^\circ$ and Normalized Coincidence Rate as Function of Incident Neutron Energy

which is the fractional area of the channels in the vanes, as seen by a particle moving in the nominal recoil direction. It will be further reduced by a factor of 0.9, since ten percent of a pulse should occur in either counter in order to have a bias cut off for coincidence counting.

The coincidence counting rate C_c between the central and one set of side counters is given by the equation

$$C_c = \sigma_{\alpha, lab} n N l_r \Delta\Omega_r (0.7)(0.9) \quad - - - \quad 4-19$$

where n , N are the same as for equation 4-17,

$\sigma_{\alpha, lab}$ is the differential cross section for alpha particles recoiling at $22\frac{1}{2}^\circ$ in the lab,

l_r is the active length of the counters for coincidences, and as defined by the length of the vanes equals 2.75 inches (or 7.0 cm),

$\Delta\Omega_r$ is the solid angle defined by the vanes,

0.7 is a transmission factor through the vanes,

and 0.9 is a factor to allow a bias for coincidence counting.

The differential scattering cross section of neutrons by alpha particles is well known (Austin et. al., 1962). The laboratory recoil angle of $22\frac{1}{2}^\circ$ for the alpha particles corresponds to a center-of-mass recoil angle of 45° and neutron scattering angle of 135° . In the center-of-mass system the differential cross section for the recoil particle at 45° is the same as that for the neutron at 135° . To change to the lab system however, for $n-\alpha$ scattering the recoil cross section is obtained from that for the

center-of-mass by the equation (Schiff, 1955)

$$\sigma_{\alpha, lab} = \frac{\sin(\Theta_{\alpha, c.m.})}{\sin(\Theta_{\alpha, lab})} \cdot \sigma_{\alpha, c.m.} \quad - - - \quad 4-20$$

where $\Theta_{\alpha, c.m.}$ is the center-of-mass recoil angle. For

$$\Theta_{\alpha, lab} = 22\frac{1}{2}^\circ, \quad \Theta_{\alpha, c.m.} = 45^\circ \quad \text{so that}$$

$$\sigma_{\alpha, lab} = 1.85 \cdot \sigma_{\alpha, c.m.}(45^\circ) = 1.85 \cdot \sigma_{h, c.m.}(135^\circ) \quad - - - \quad 4-21$$

The solid angle for passage of the recoiling alpha particles through the vanes is given by

$$\Delta\Omega_v = \int_{-10}^{+10} d\phi \int_{17.5}^{27.5} \sin\theta d\theta = 0.0233 \text{ steradians} \quad - - - \quad 4-22$$

where ϕ is the azimuthal angle, and θ is the polar angle of recoil. The laboratory differential cross section for alpha recoil, and the expected coincidence rates between the central set of three counters and a side set are shown in figure 4-16 as a function of energy per neutron incident on the central active volume.

The distance of the polarimeter from the target is typically five inches or more so that the active volume of the central three counters subtends a solid angle at the target of about 0.47 steradians, or less for greater polarimeter-to-target distances. For a source strength at the target of 10^6 per steradian per second, the total counting rate at 10 Mev incident neutron energy is about 58 per second. The corresponding coincidence counting rate is 1.55×10^{-2} per second, or 55 per hour.

A random, or accidental, coincidence rate results from the finite time resolution and is given by

$$C_R = 2 N' N'' \tau \quad - - - \quad 4-23$$

where N' , N'' are the counting rates in the two counters between which coincidences are being monitored, and τ is the coincidence resolving time, (which obviously should be as small as possible).

For a resolving time of one microsecond and a total counting rate of 58 per second (as before), then one may expect an accidental coincidence rate of

$$C_r \doteq 2 (58)^2 (10^{-6}) = 0.67 \cdot 10^{-2} \text{ per sec.} \quad - - - \quad 4-24$$

This rate is comparable to the true coincidence rate and must be reduced. Some possible ways, in order of decreasing preference, are:

- (1) reduction of the coincidence resolving time,
 - (2) reduction of the counting rate in the side counters by shielding,
 - (3) reduction of total counting rate by moving polarimeter further from the target to reduce the subtended angle,
- and (4) reduction of total counting rate by reducing the neutron source strength at the target.

Several other sources of unwanted coincidences also exist. While it is not possible for the alpha particles to recoil back through the vanes and while the recoil of heavier nuclei such as the carbon or oxygen would not have sufficient energy to cause any trouble, numerous other reactions such as (n,p) and (n,α) appear to have appreciable cross sections at higher neutron energies (Hughes, 1958). It is expected that such reactions contribute to low energy coincidences

which must be discriminated from higher-energy true coincidences.

Since nuclear reactions may proceed to various states of a given final nucleus it is necessary to be able to distinguish between neutron groups of different energy. The energy resolution of the apparatus is limited for various reasons, but a major source of poor resolution lies in the finite angular acceptance of the vanes. The recoil energy is given by equation 4-15. For a given incident neutron energy

$$\frac{dE_{\alpha}}{E_{\alpha}} = -2 \tan \theta_{\alpha} d\theta_{\alpha} \quad - - - \quad 4-25$$

For $\theta_{\alpha} = 22\frac{1}{2}^{\circ}$ and $d\theta_{\alpha} = 10^{\circ} \equiv 0.175$ radians, then

$$\frac{dE_{\alpha}}{E_{\alpha}} = 2(.414)(.175) = 0.145. \quad \text{The energy resolution due to}$$

the vanes, defined as the relative width at half maximum, is then about seven percent.

Other sources of poor energy resolution for the polarimeter system lie within the counters and vanes themselves. Because of low electric fields within the vane passages one must expect recombination to occur and that ionization in this region is lost. The average path length within the grids is 1.0 cm compared to a counter path length of 10 cm. Assuming the ionization rate to be constant along the length of the path of the alpha particle then nine percent of the ionization is lost within the grids. For different path orientations the nine percent figure varies between about seven and eleven percent, with a resulting resolution loss

in the detected portion of the pulse of about two percent.

For the rectangular shaped counters, the voltage configuration near the wire was seen to progress uniformly from one appropriate for a cylindrical wall of radius about 0.65 inches to one for a radius of about 0.70 inches. For constant gain one must keep the electric field at the wire constant. From equation 4-13:

$$dE = \frac{\partial E}{\partial b} db + \frac{\partial E}{\partial V_o} dV_o$$

$$\frac{dE}{E} = - \frac{1}{\ln \frac{b}{a}} \left(\frac{db}{b} \right) + \frac{dV_o}{V_o} \quad - - - \quad 4-26$$

It was found while operating the counters at 1500 volts that a voltage change of one volt resulted in a change of one percent in pulse amplitude. Using this result and equation 4-26, it is seen that a change in b of .05 in .68 would result in a gain change of 20 percent. The expected resolution is then about 10 percent for the width at half maximum for the portion of the pulse in the side counters. Since, on the average, half the pulse is from the side counter then the overall resolution due to this cause is about five percent.

In another preliminary experiment, an alpha source was directed through the grids toward the center counters in order to determine whether any variations in pulse height could be detected across the counter. A plot of the results is shown in figure 4-17. It is seen that the pulse height drops off noticeably near the sides of the counter and this is attributed to recombination in low field regions. The

effect has an estimated contribution to a worsening of the resolution of about five percent.

While these preliminary checks were being made, a general variation of pulse height with position along the length of the counter was observed, and attributed to a temperature variation along the length of the polarimeter (the end closest to the pre-amplifiers was heated by the electronics). A blower was directed against the back end of the polarimeter and the pre-amplifiers to keep the apparatus at a uniform temperature and to eliminate this effect.

The resolution attributable to the counter gas and wire was determined by directing a collimated alpha source along the length of the counter. While this resolution was often as low as three percent it was more usually five percent.

The overall resolution R due to all the above effects within the counters can then be calculated from equation 4-27:

$$R^2 = R_1^2 + R_2^2 + R_3^2 + R_4^2 + R_5^2 \quad - - - \quad 4-27$$

For $R_1 = 7$, $R_2 = 3$, $R_3 = 5$, $R_4 = 5$, $R_5 = 5$ percent, then $R = 12$ percent.

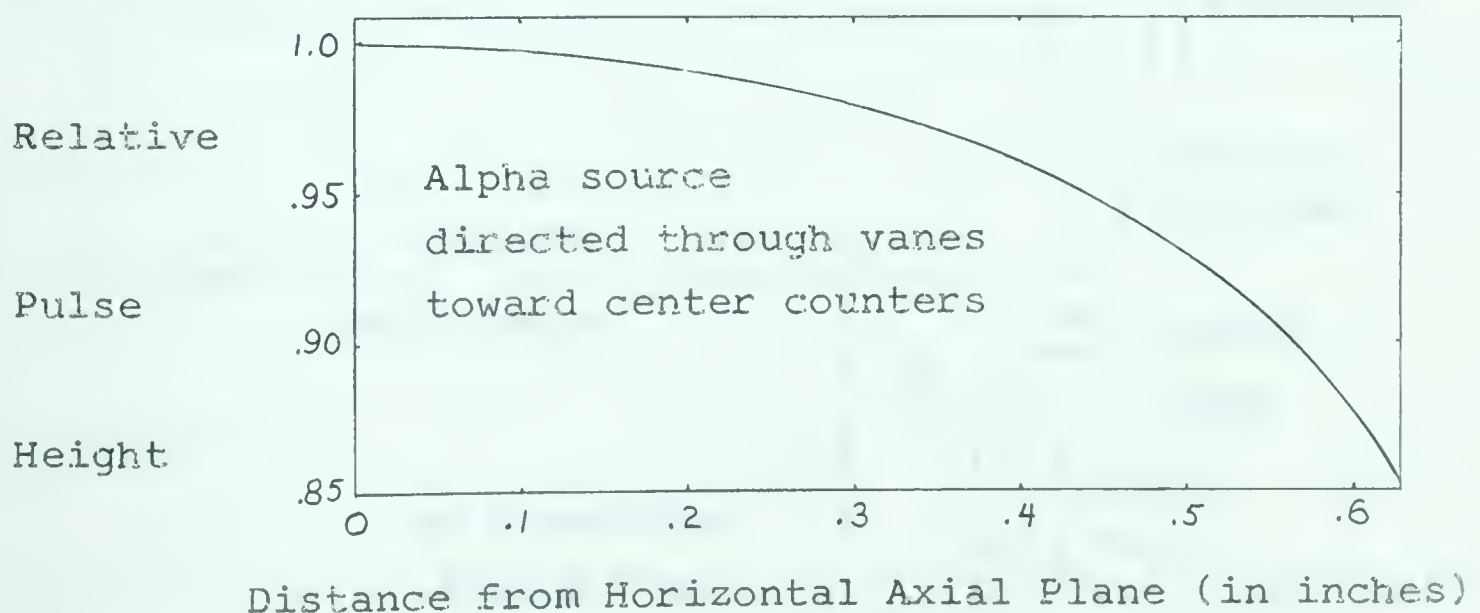


Figure 4-17 Pulse Height Variation Across Counters

To fill the polarimeter with purified gas of the desired composition, a gas handling system was built as shown schematically in figure 4-18. Four gauges are shown for monitoring the pressure in the system over different ranges. The hot calcium purifier (Segre, 1953) and the liquid air cold trap are for purifying commercial helium.

Before being filled, the system and polarimeter were first evacuated with the mechanical pump, and outgassed for about two hours at an estimated temperature of 250° C, by directing a hot air blower at the metal parts while they were enclosed in an asbestos paper tent. The pump was then valved off, and commercial helium allowed to flow into the system and polarimeter through the cold trap and calcium purifier. After being filled to the desired pressure, the system was isolated from the cold trap.

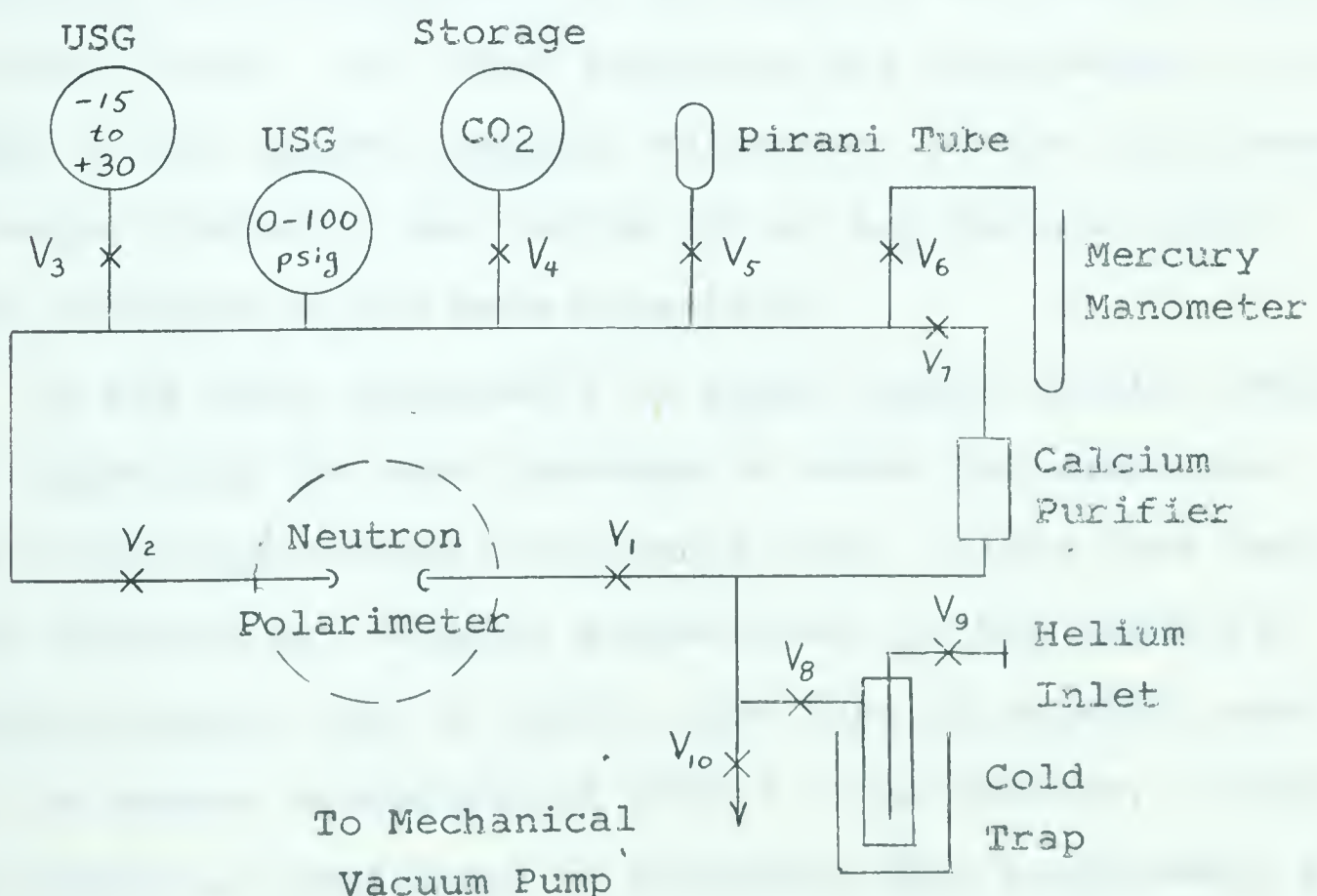


Figure 4-18 Gas-handling System

The basic part of the gas system is a rectangular loop, with the hot calcium purifier at the bottom of one of the vertical arms; the intention of this design is to promote circulation of the gas through the purifier by convection.

After several hours of purifying, the polarimeter was valved off. The rest of the system was then evacuated and filled with high grade pure CO_2 to a pressure which would give the desired mixture of CO_2 in helium, on the basis of ideal gas laws, when mixed with the helium in the polarimeter. For this latter operation, of course, the relative volumes of the system and polarimeter had to be known. A period of several hours had to elapse before the CO_2 had diffused uniformly from the system tubing into the polarimeter.

After being filled with an appropriate mixture of CO_2 in helium, the polarimeter is attached to the mount depicted in figure 4-19. The mount maintains the polarimeter at the height of the target, permits adjustment of the polarimeter to target distance, and can be set at any desired polar angle relative to the beam direction.

It was found desirable to place shadow shields between the target and the side counters in order to reduce the relatively high random coincidence rate. Since fast neutron cross sections are roughly proportional to the geometric cross-sectional area of nuclei, the type of material used for the shadow shield should have a large density. Ordinary mild steel was used since it satisfies this requirement and as well is self supporting and relatively inexpensive. The

measured transmissions were 0.1 for a 12 inch shadow shield and 0.3 for a 6 inch shadow shield.

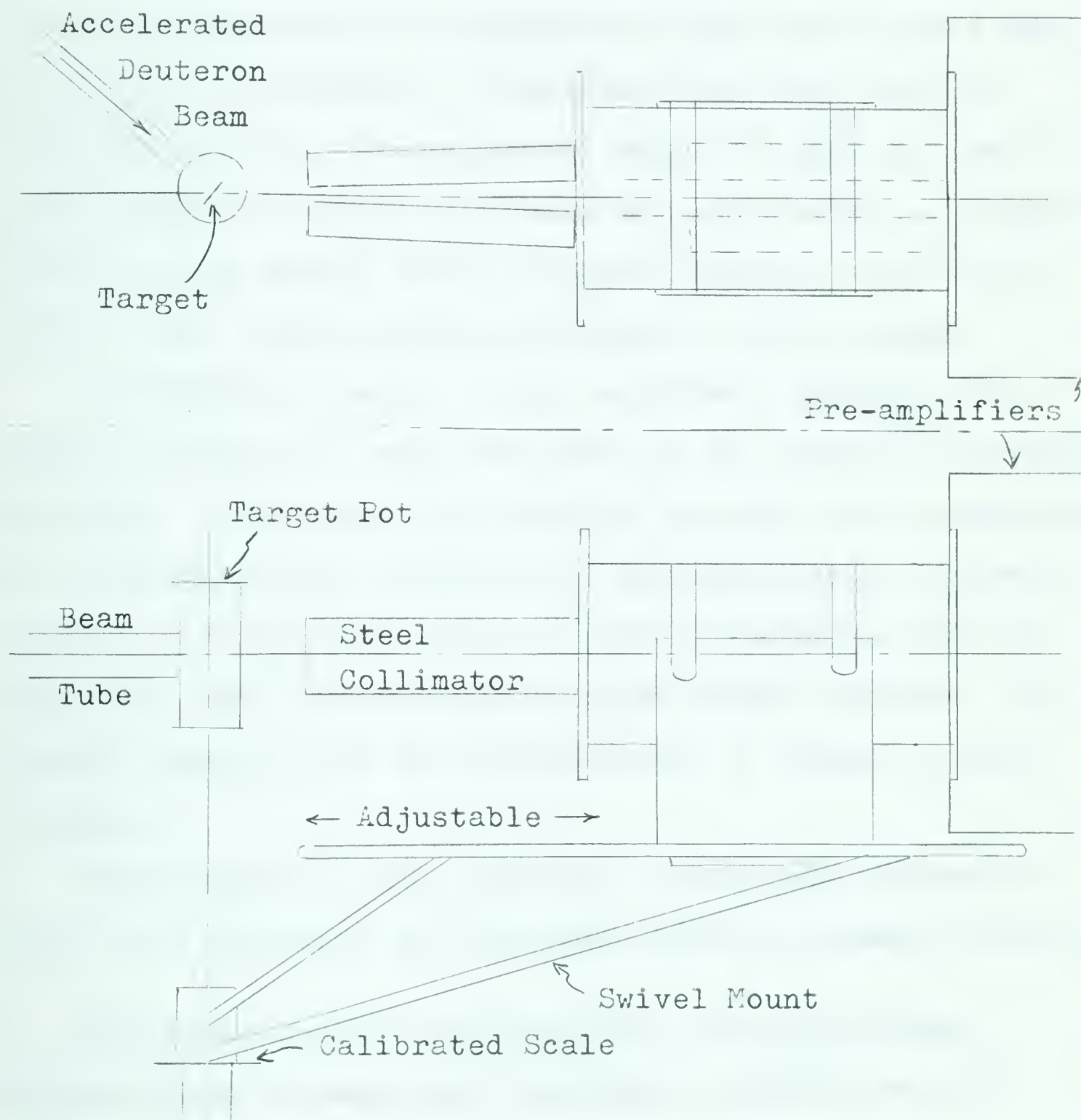


Figure 4-19 Polarimeter Mount and Collimating Shield

CHAPTER 5

ELECTRONICS

For determining the left-right scattering asymmetry, electronic apparatus is required to detect and record left and right coincidences. In addition, for each pair of coincident pulses, the apparatus should be able to sum the pulse heights in order to obtain an output which is proportional to the energy of the original neutron, and then to sort out the summed pulses according to their energy.

A schematic diagram of the electronic apparatus is shown in figure 5-1 with the paths of the signals indicated by arrows. There are two identical systems, each consisting of two proportional counters and pre-amplifiers, an adding circuit, a coincidence unit, an anti-coincidence unit, an amplifier, and a multi-channel pulse height analyzer. The central counter with its pre-amplifier is common to both systems.

The component units and their operational characteristics and functions are described below in greater detail.

The basic design considerations for proportional counters have already been discussed in chapter 4, and drawings for the counters are shown in figure 4-12 and Appendix A.

The voltage pulse size from the counters is given by the equation $V = Ane/C$ - - - 5-1
where A is the gas gain,

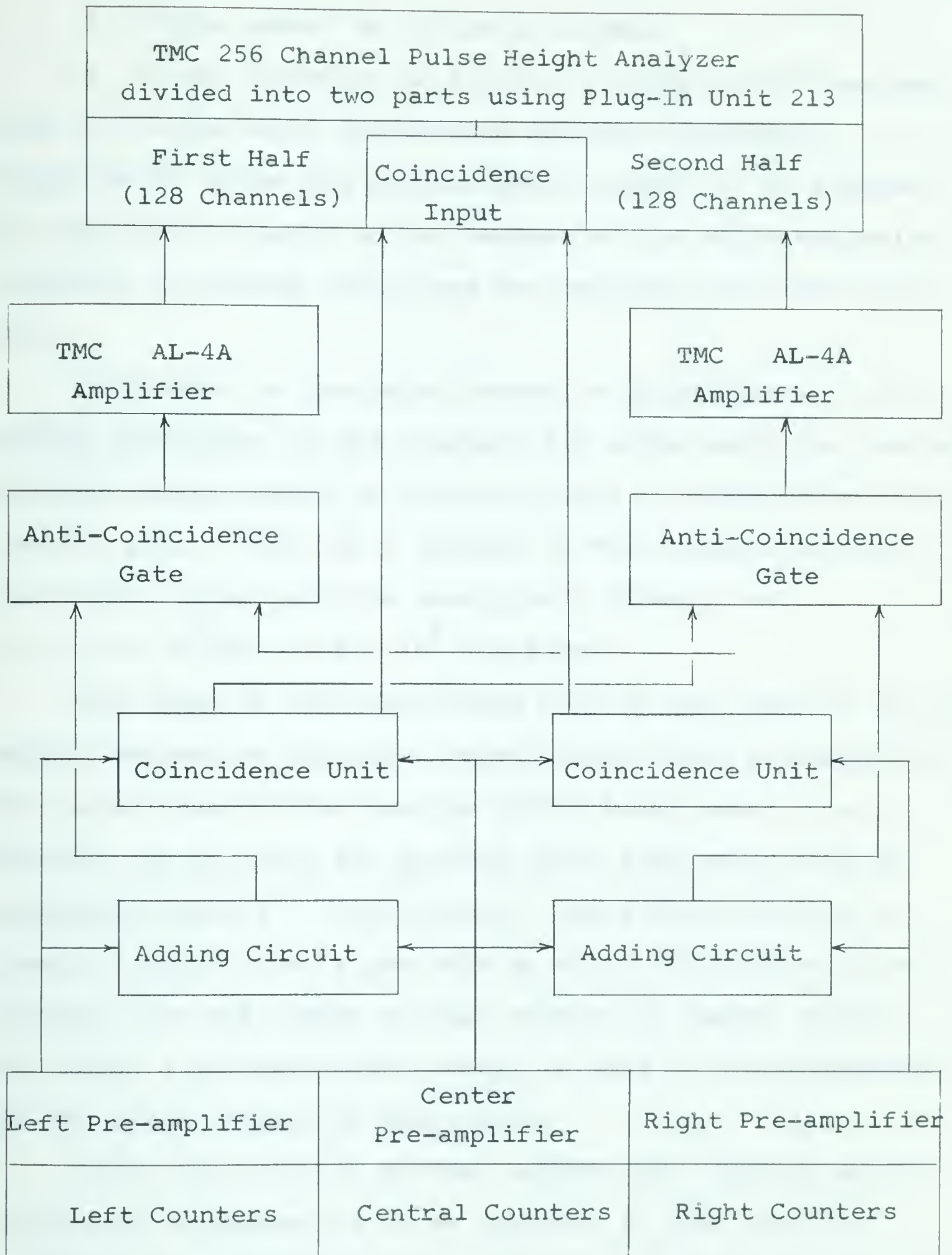


Figure 5-1 General Schematic Diagram of the Electronics for the Neutron Polarimeter

n is the number of ion pairs formed,

e is the charge on an electron $= 1.602 \cdot 10^{-19}$ coulomb,

and C is the total capacitance between electrodes.

Equation 5-1 gives the maximum pulse height; it is reduced by more than a factor of two because of the differentiation required to shorten the pulses for counting and coincidence use.

The number of ion pairs formed is proportional to the energy dissipated in the counter; for alpha particles passing through helium, about 30 electron volts is required to form one ion pair. Thus for a typical 10 Mev incident neutron, the recoil alpha particle energy is 5.46 Mev, and $n = 5.46 \cdot 10^6 / 30 = 1.82 \cdot 10^5$ ion pairs.

The value of the capacitance C is of the order of $15 \mu\mu f$, mainly because of the input capacitance of the pre-amplifier, the capacitance of the counter itself being about $2 \mu\mu f$. Without any gas gain the maximum pulse size would then be typically about $V = 2$ millivolts. While this would be a useable output size, a gas gain of about 100 reduces noise problems and the higher voltage results in faster pulses. Too large a gas gain would result in loss of proportionality as the geiger region is approached.

Since the pulse is divided between two counters and as little as 10 percent is to be detected in one, then the smallest output pulse height to be used is about 10 millivolts if the gas gain is 100 and differentiation reduces the pulse height by a factor of two.

A single, stabilized high voltage supply was used to operate all nine counters. Since the counters had to function independently with the same gas gain, pulse filters and voltage adjustments were made for each counter as shown in figure 5-2.

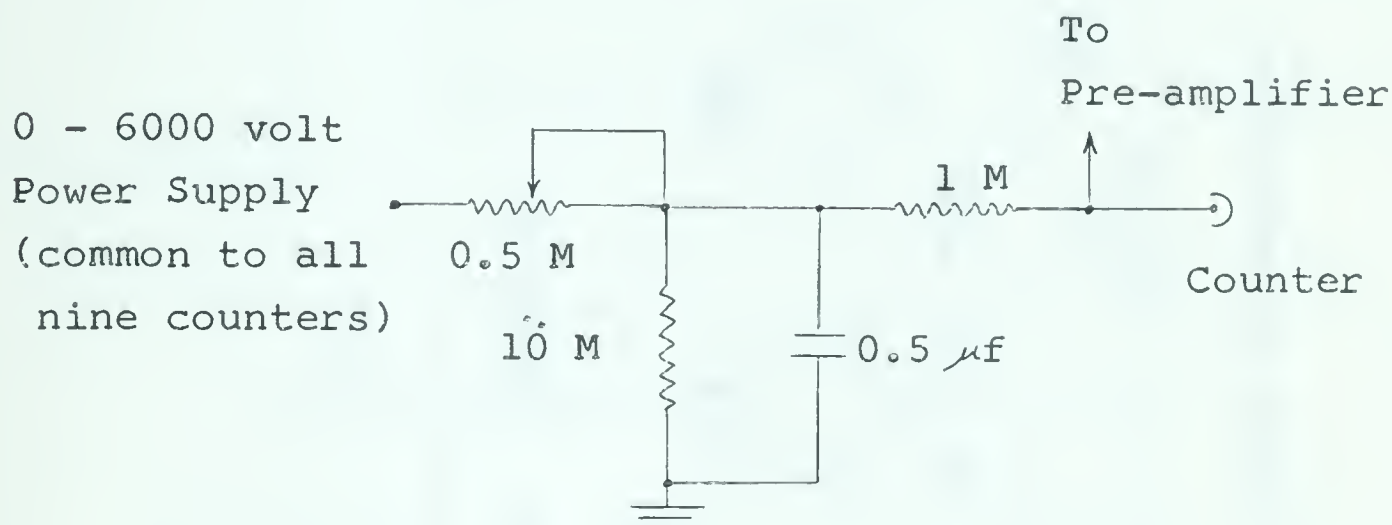


Figure 5-2 High Voltage Adjustment and Filter for each Counter

The pre-amplifiers were standard ring-of-three tube amplifiers, one for each vertical set of three counters; the gain of each unit was 90. The upper and lower cut-off frequencies were measured to be 3.5 mc and 1 kc respectively; the rise time is $0.1 \mu s$. Between each counter and the ring-of-three amplifier, an isolating tube was used; and the circuit is shown as figure 5-3. Three such pre-amplifier units were operated in a box mounted behind the polarimeter tank. Since the remaining electronic units were used in the control room, away from the target area, a cathode follower was required after each ring-of-three to drive the pulses

through the cable.

The adding circuits used are shown in figure 5-4. The cathode follower outputs add linearly to within three percent; the pulse amplitude on passing through the adding circuit is reduced by a factor of three.

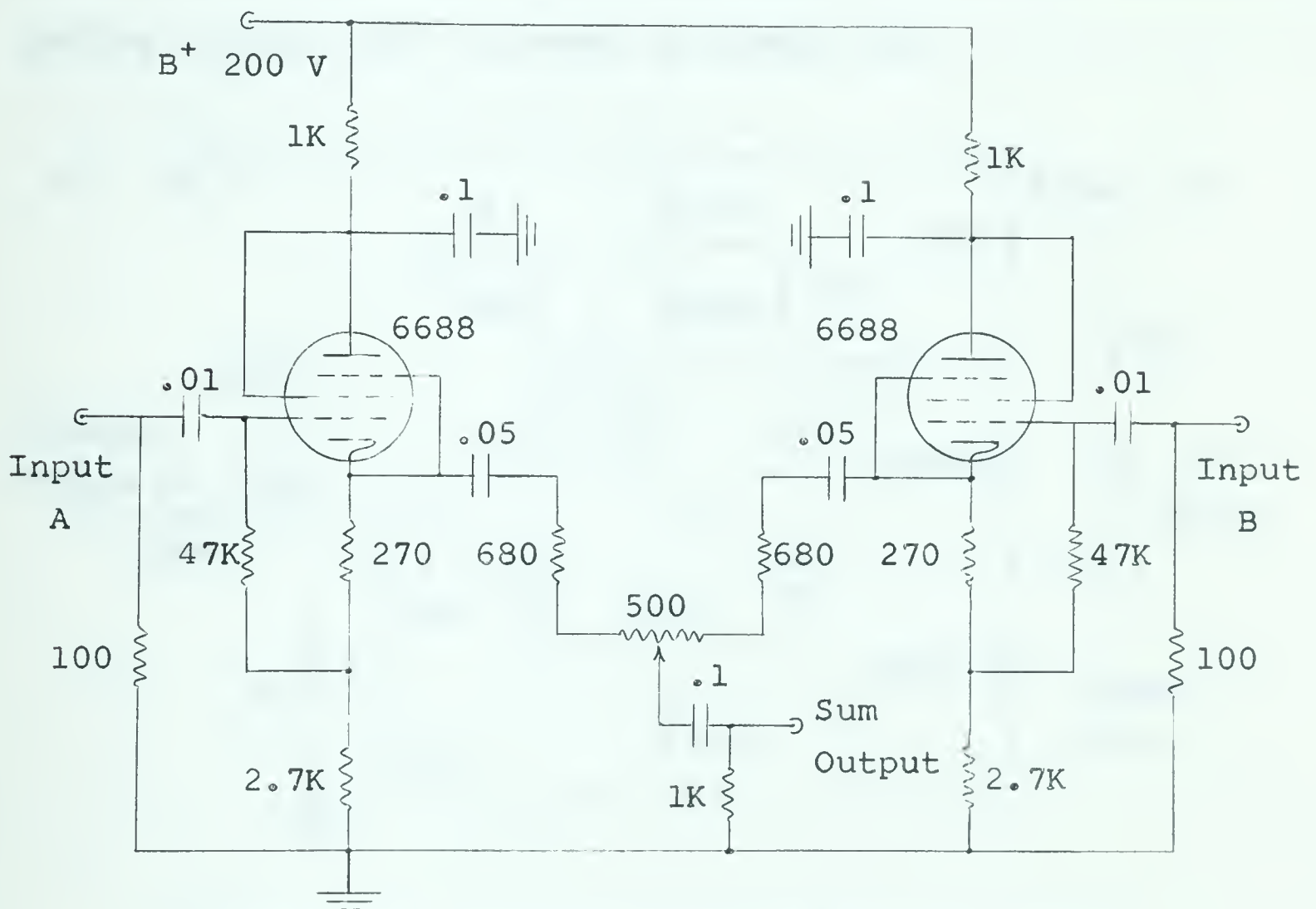


Figure 5-4 Adding Circuits

The coincidence units are basically the type designed by Krawciw (1960). For coincident input pulses, each greater than a set lower limit (the minimum is 0.25 volts), a 10 volt output pulse is obtained. Both the coincidence resolving time and the discriminator levels are variable.

Since the center counter outputs are common to both sides of the circuitry, whenever a coincidence occurs in one half of the electronics then the center counter pulse passing through the other half must be prevented from reaching the pulse height analyzer. This is essential because for a coincidence in either half there must always be a pulse in both halves due to the central counter. The anti-coincidence gating circuit used is shown in figure 5-5.

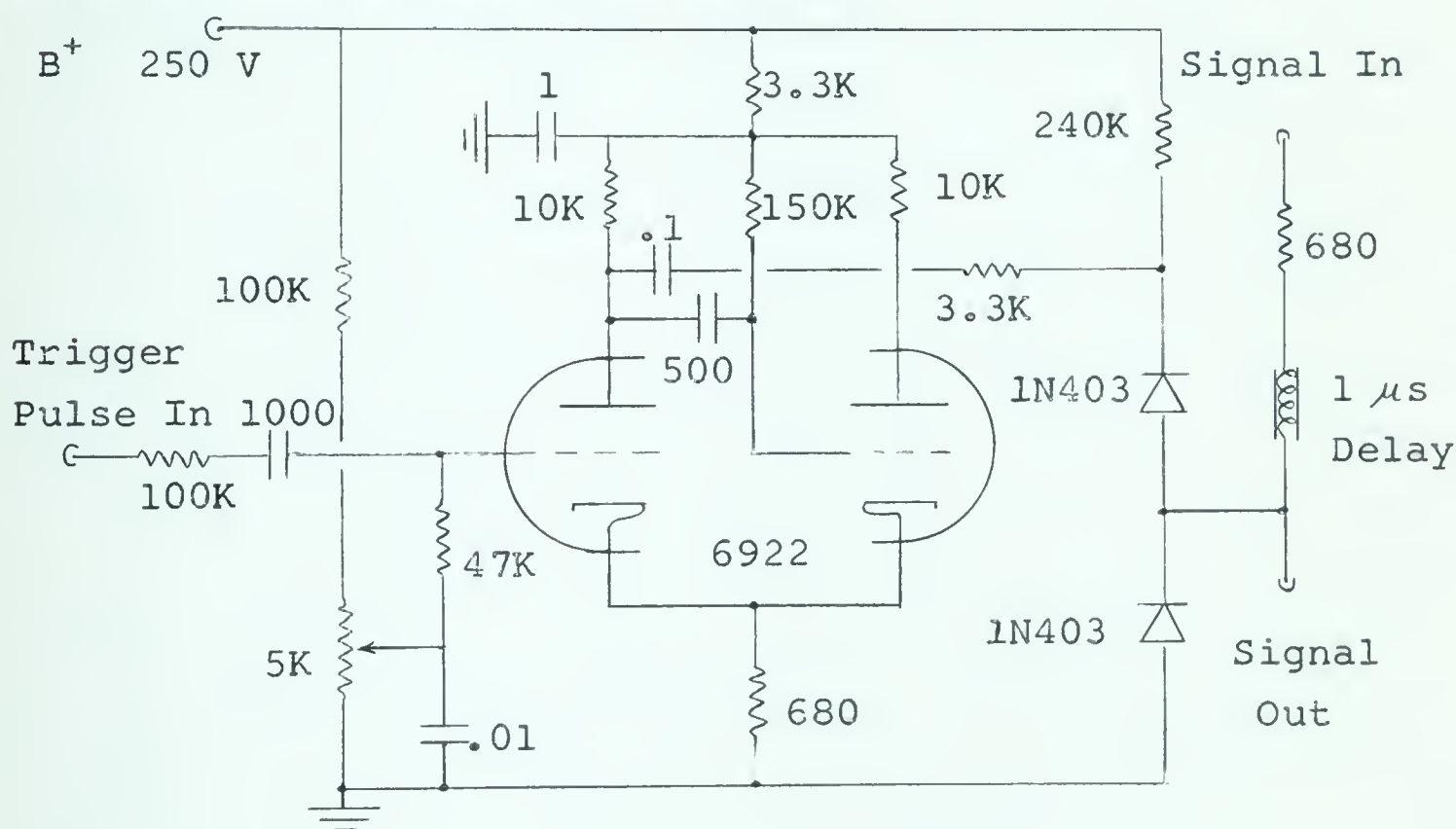


Figure 5-5 Anti-coincidence Gating Circuit

The amplifiers preceding the pulse height analyzer were necessary to produce the required high-level pulses for the multi-channel pulse height analyzer plug-in units. Linear amplifier model AL -4A, manufactured by the Technical Measurement Corporation, was used since it gives the correct shape of output pulse; it has more than enough gain.

The Technical Measurement Corporation 256 Channel Model CN110 Pulse Height Analyzer was available and adaptable for the required purpose through the use of the plug-in unit number 213. The plug-in unit enables four inputs to be used feeding separate quarters of the basic analyzer. Only two of these inputs of course were used at any one time. Only one coincidence input however was available, which controlled all inputs. Because of this the anti-coincidence gating circuits were required as described earlier.

CHAPTER 6

EXPERIMENTAL PROCEDURE, UNCERTAINTIES, AND CORRECTIONS

As a preliminary check on the operation of the counters and electronics, plutonium 239 alpha sources* were mounted in a collimator one inch long and .073 inches inside diameter, and directed through holes in the sides of the front part of the central counters diagonally toward the opposite side counters. The counter gas pressure was set at 207 cm Hg to allow the 5.5 Mev alpha particles to traverse both the central and the opposite side counter. Pictures were taken of the summed pulse going to the multi-channel analyzer using a Tektronix type 555 oscilloscope and type C12 camera. While the resolution obtained with the collimated sources in such an arrangement was about seven percent, the pictures showed that the rise times of the summed pulses were about $1.2 \mu s$, and the time spread between coincident pulses was as much as $1.0 \mu s$. This meant that the coincidence resolving time set on the coincidence units should be $1.0 \mu s$.

Before beginning an actual experimental run several checks were made to ensure that the apparatus was functioning properly.

* The sources were punched with a 3/32 inch die from a plated source, MA 162, supplied by Monsanto Research Corporation, Mound Laboratory, Miamisburg, Ohio, U.S.A.

About a day before an experimental run was to begin on the 2 Mev van de Graaff accelerator*, the polarimeter tank was filled to the pressure appropriate for the particular experiment with a helium plus five percent CO₂ mixture as outlined in chapter 4. At least two hours before the start of a run all the electronics were turned on so that the units would have time to stabilize, and the pre-amplifiers were checked for proper operation.

Each day, immediately before starting a series of runs, test pulses, simulating the outputs from the pre-amplifiers, were fed into the adder and coincidence units to check the overall operation of the electronics in the control room area. The coincidence units had a tendency to drift and sometimes oscillate; they had to be checked and adjusted about twice a day.

With the accelerator beam on the target, and the polarimeter mounted, the pulse spectrum from each proportional counter was recorded on the TMC CN110 Pulse Height Analyzer. The voltages to the counters were adjusted, if necessary, until the ends of the spectra fell in the same channel. This procedure was followed to ensure a uniform gain for all counters. The end of a spectrum corresponds to those scattering events where a neutron strikes a helium nucleus directly and the alpha particle recoils at zero degrees,

* van de Graaff electrostatic accelerator, model AN2 manufactured by High Voltage Engineering Corporation, Burlington, Massachusetts, U.S.A.

with the maximum energy transfer to it of 0.64 times the neutron energy.

Because of the very low coincidence rates, long runs were necessary; however, to avoid possible loss due to equipment failure of data already collected, individual, uninterrupted runs were usually restricted to not more than one hour duration. For a given reaction angle, consecutive runs were made on either side of the beam direction in order to eliminate any false asymmetry that might exist either in the counter geometry itself or in the electronics. For a given setting of the polarimeter on either side of the beam, the run was further divided in two to reverse the electronics in the control room associated with given halves of the polarimeter at the target; this was to compensate for possible drift in the electronics. During some of the earlier experiments, on the $D(d,n)He^3$ reaction, the polarimeter was rotated within its mount as well, as a further precaution to eliminate false asymmetries. However, this practice was not continued as it was felt that the movement of the polarimeter between the two sides of the beam was adequate.

A BF_3 neutron detector was used to monitor the reaction rate at the target during runs. As well, several scalers were used to monitor the count rates at various points in the electronics. Usually, the total number of trigger pulses within the coincidence units were monitored for each input from the polarimeter and, further, the coincidence

pulses from each coincidence unit were counted.

Because of the extremely small counting rates for the polarization measurements it was necessary to use rather thick targets. The average energy, \bar{E} , of deuterons in the target was then considerably less than the bombarding energy, E_0 , and is determined from the relation

$$\bar{E} = \frac{\int_0^t E \cdot \sigma \cdot dx}{\int_0^t \sigma \cdot dx} \quad - - - \quad 6-1$$

where E is the deuteron energy at distance x into the target material,

σ is the reaction cross section,

and t is the thickness of the target.

The energy, E , at distance, x , is given by

$$E = E_0 + \int_0^x \frac{dE'}{dx'} \cdot dx' \quad - - - \quad 6-2$$

where $\frac{dE'}{dx'}$ is the rate of energy loss (Whaling, 1958) at energy E' and distance x' into the target.

Although the cross section, σ , should be the differential cross section corresponding to the particular angle at which a measurement is made, total cross sections were used in evaluating the integrals because differential cross sections are not all available and because, for the bombarding energies used, the variations of the different cross sections with energy seem to be similar.

For the $D(d,n)He^3$ reaction the target was prepared by freezing D_2O vapor onto a gold backing cooled by liquid air. With the gold backing mounted in the evacuated target region,

a fixed volume of D_2O vapor was allowed to diffuse out of a small hole in a pipe leading from a storage flask. With the hole directed at the gold backing, the vapor would immediately freeze when it diffused out of the pipe and struck the gold. Only a very crude estimate can be made of the target thickness because of uncertainties in the area of the target, in the efficiency of freezing, and in uniformity of the target; further, energy from the accelerator beam would tend to evaporate the target. As a crude estimate, however, a thickness of about 0.5 mg/cm^2 would result if the 97 cc volume of D_2O were spread uniformly over a 4 cm^2 area; these are thought to be reasonable values. Since 0.5 mg/cm^2 of D_2O would reduce the incident deuteron energy by about 300 kev at 1.5 Mev bombarding energy and since a number of volumes of vapor were used, then the targets were very thick. It is estimated that the average deuteron reaction energy in the target material is 1.1 Mev for 1.5 Mev bombarding energy, and 1.5 Mev for 1.9 Mev bombarding energy.

The $T(d,n)He^4$ reaction has a large maximum in its cross section at 0.1 Mev, and is isotropic below about 0.5 Mev (Brolley and Fowler, 1960). The 2 Mev van de Graaff accelerator, on the other hand, was not designed to operate below 0.75 Mev. As a compromise between a low energy beam for maximum reaction rate, in this particular case, and the stability of the accelerator at lower energies, a bombarding energy of 0.5 Mev was used. The thickness of the 17 curie target was uncertain since it was imbedded in a stainless

steel backing. However, for a bombarding energy of 0.5 Mev, the average deuteron energy for reactions in the target was thought to be about 0.3 Mev.

For all the $B^{11}(d,n)C^{12}$ measurements a rather thick, 1.2 mg/cm^2 , natural boron target was used. Total cross sections for both the ground state neutrons and the first excited state neutrons are given for energies below 1 Mev by Ames and Owen (1958). Their results were extrapolated to higher energies with the help of some crude cross section values obtained from a BF_3 neutron monitor during experimental runs. For bombarding energies of 1.5, 1.6, 1.8 and 2.0 Mev the average deuteron energies were estimated to be 1.35, 1.45, 1.65, and 1.85 Mev respectively.

The result obtained from a given run consists basically of two numbers, the numbers of coincidence counts due to 'right' and to 'left' scattering. If the side to which a neutron is scattered is in the same sense as the reaction angle then it is called a 'left' scattering; otherwise it is called a 'right' scattering. The asymmetry factor may then be written (see also equation 1-4)

$$\epsilon = \frac{l - r}{l + r} = \frac{l/r - 1}{l/r + 1} \quad - - - \quad 6-3$$

where l is the number of 'left' counts,

and r is the number of 'right' counts.

When the run for a given reaction angle is repeated to eliminate false asymmetries then the false asymmetries will be eliminated if the roles of the two sides of the polarimeter

are interchanged and if the ℓ/r ratio is taken as the square root of the product of the individual ℓ/r ratios (Haeberli, 1963). In general, for an even number of n corresponding readings one should take

$$\frac{\ell}{r} = \sqrt[n]{\prod_{i=1}^n (\ell/r)_i} \quad - - - \quad 6-4$$

For uncertainties $\Delta \ell_i$, Δr_i in the measurements, the uncertainty in ℓ/r is

$$\begin{aligned} \Delta\left(\frac{\ell}{r}\right) &= \sqrt{\sum_{i=1}^n \left[\left(\Delta \ell_i \cdot \frac{\partial(\ell/r)}{\partial \ell_i} \right)^2 + \left(\Delta r_i \cdot \frac{\partial(\ell/r)}{\partial r_i} \right)^2 \right]} \\ &= \frac{1}{n} \left(\frac{\ell}{r}\right) \sqrt{\sum_{i=1}^n \left[\left(\frac{\Delta \ell_i}{\ell_i} \right)^2 + \left(\frac{\Delta r_i}{r_i} \right)^2 \right]} \quad - - - \quad 6-5 \end{aligned}$$

The uncertainty in ϵ is then given by

$$\Delta \epsilon = \Delta\left(\frac{\ell}{r}\right) \frac{\partial \epsilon}{\partial (\ell/r)} = \frac{2}{\left[\left(\frac{\ell}{r}\right) + 1\right]^2} \Delta\left(\frac{\ell}{r}\right) \quad - - - \quad 6-6$$

A set of typical experimental results is shown in figure 6-1 for neutrons from the $B^{11}(d,n)C^{12}$ reaction. The peaks for the ground state and the 4.43 Mev state neutrons lie about channels 49 and 30 respectively. The accidental coincidence counts are mainly in the lower channels but they extend slightly into the region of true coincidences. The shape of the background curve shown was obtained from runs for which accidental coincidences only were possible, as between a top side counter and the bottom center counter. For each spectrum, the number of ground state coincidences was obtained by adding all counts in channels 36 to 54

inclusive and subtracting a background correction; the 4.43 Mev state coincidences were taken to lie in channels 23 to 35 inclusive, again with a correction indicated by the background curve. The uncertainty in a given corrected count was taken as the square root of the sum of the total counts in a peak and the corresponding background correction. The numbers so obtained are shown in the figure.

From the measured asymmetry, ϵ , and a knowledge of the analyzing power of the helium gas one can compute the polarization of the neutron group incident upon the polarimeter using equation 1-5: $\epsilon = P_1 \cdot P_2 \cos \phi$. The apparatus is set up so that $\cos \phi$ is nominally either plus or minus one. However, the active volume of the polarimeter subtends an appreciable solid angle at the target, and also the variation in the angle of recoil of the alpha particle is considerable - with the result that $\cos \phi$ is, on the average, somewhat less than one. Also, the analyzing power, P_2 , varies about its nominal value. A value for $P_2 \cos \phi$ must therefore be averaged over the active volume of the polarimeter and over the angles of recoil accepted by the vanes. A computer program was written to do this; the development of the necessary equations, a flow diagram, and a program written in Fortran II for the IBM 1620 computer are given as Appendix B.

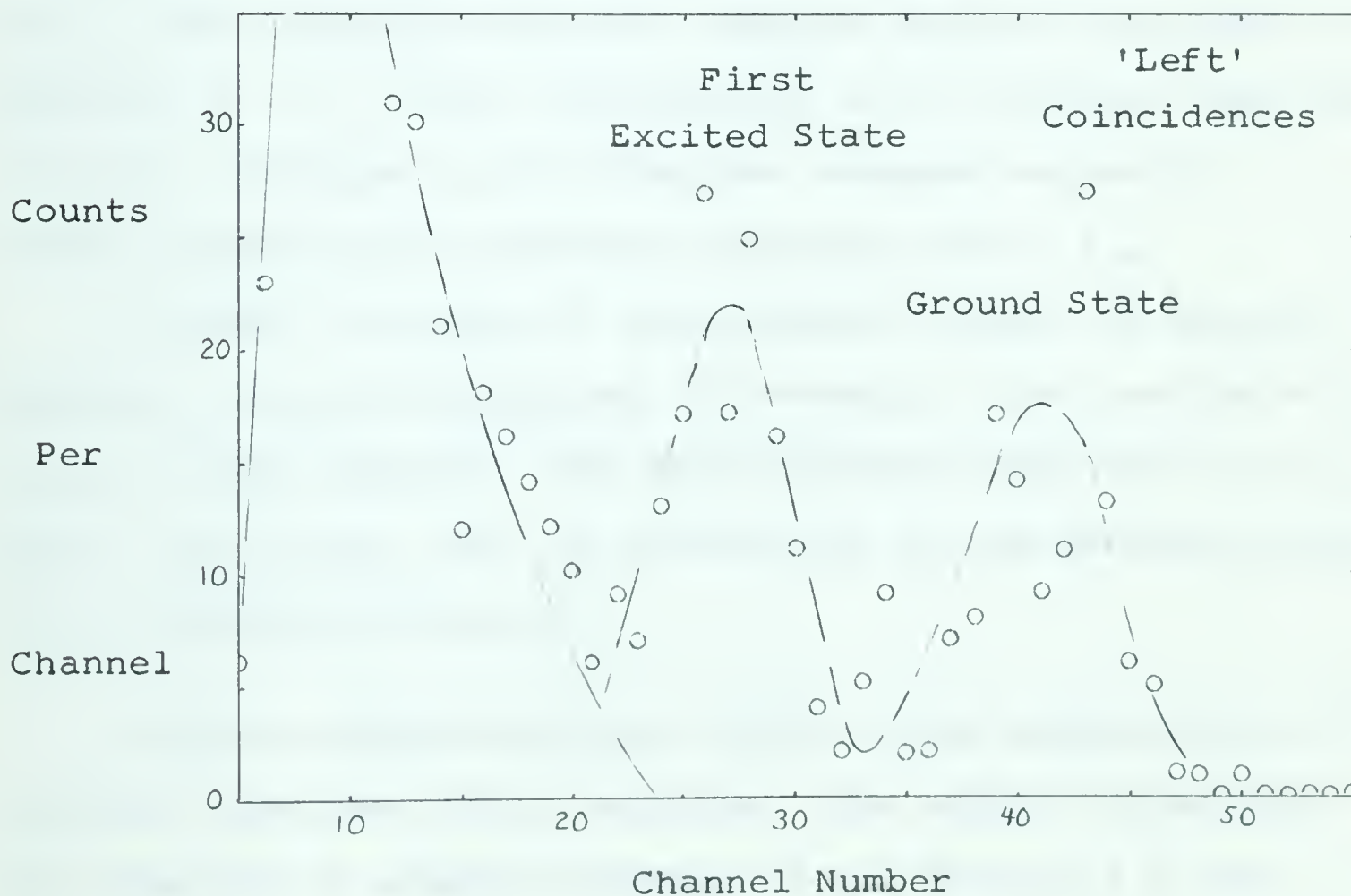
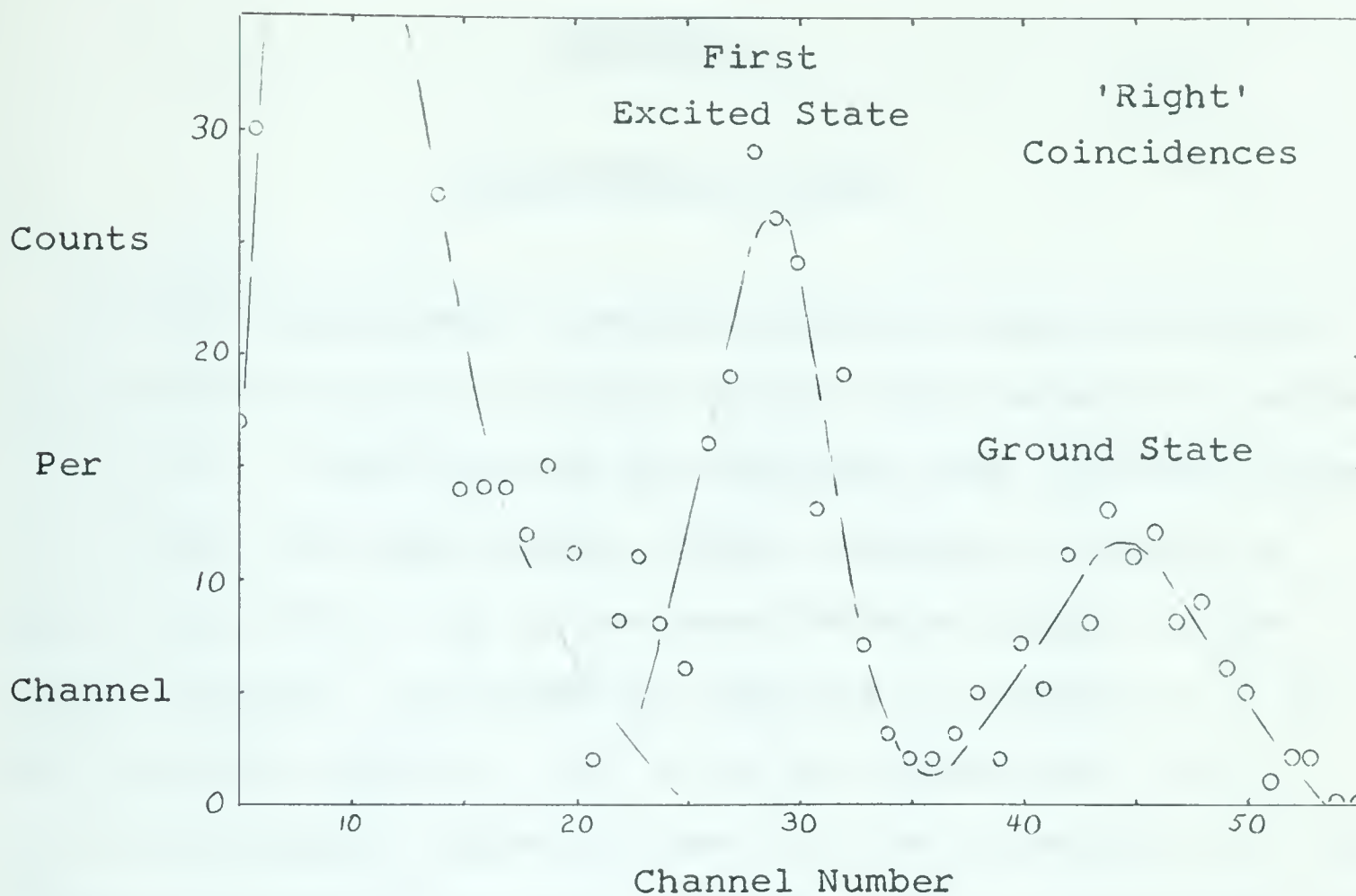


Figure 6-1 Some Experimental Data for the $B^{11}(d,n)C^{12}$ Reaction (Sum of Runs 11, 12, and 13; September 23, 1963; Polarimeter 120° West)

CHAPTER 7

EXPERIMENTAL RESULTS

All the experimental results obtained using the neutron polarimeter described in this thesis are tabulated in tables 7-1 to 7-4. While most of the headings used in these tables are almost self-explanatory, their meanings are given in more detail here. \bar{E}_d is the mean deuteron energy in the target material, estimated as outlined in chapter 6. ϵ is the measured asymmetry, and $\Delta\epsilon$ is the uncertainty in ϵ . P_2 is the nominal analyzing power of the polarimeter for the energy of neutrons from the reaction. \bar{P}_2 is an average value of $P_2 \cdot \cos\theta$ obtained using the computer program described in Appendix B. P_n is the polarization of the neutrons from the reaction, obtained by dividing the measured asymmetry, ϵ , by the geometrically-averaged analyzing power, \bar{P}_2 .

A number of graphs of polarization values and also of products of polarization and differential cross section are shown in this chapter. The uncertainties indicated, in all cases, are solely from the uncertainty in the measured value of the asymmetry factor, ϵ .

Numerous measurements were made of the polarization of neutrons from the $D(d,n)$ reaction; the angular dependence was measured at average energies of 1.1 Mev and 1.5 Mev, corresponding respectively to 1.5 and 1.9 Mev bombarding energies on rather thick targets. Since the polarization of

Table 7-1 Neutron Polarizations for $D(d,n)He^3$

\overline{E}_d	Lab Angle	En Lab	ϵ	$\Delta\epsilon$	P_2	\overline{P}_2	P_n
1.1	10	4.665	-.010	.031	.993	.833	-.011
1.1	20	4.561	-.048	.031	.993	.889	-.035
1.1	30	4.395	-.098	.026	.993	.906	-.108
1.1	40	4.178	-.160	.021	.990	.897	-.178
1.1	47	4.003	-.223	.039	.986	.896	-.249
1.1	50	3.925	-.127	.042	.984	.896	-.142
1.1	60	3.649	-.158	.058	.974	.892	-.177
1.1	70	3.365	-.112	.059	.960	.885	-.127
1.1	75	3.224	-.278	.095	.941	.879	-.318
1.5	20	4.962	-.154	.039	.994	.887	-.174
1.5	30	4.764	-.085	.024	.994	.906	-.088
1.5	40	4.506	-.108	.045	.993	.904	-.120
1.5	50	4.206	-.197	.077	.990	.903	-.218

Table 7-2 Neutron Polarizations for $T(d,n)He^4$

\overline{E}_d	Lab Angle	En Lab	ϵ	$\Delta\epsilon$	P_2	\overline{P}_2	P_n
0.3	30	15.26	+.015	.035	.995	.870	+.017
0.3	45	15.03	-.018	.020	.995	.869	-.021

neutrons from this reaction has been studied by many workers, these measurements mainly provided a necessary check on the operation of the polarimeter.

The measured neutron polarization values for the $D(d,n)He^3$ reaction are summarized in table 7-1, and are plotted in figures 7-1 and 7-2, along with the corresponding results of previous workers. It is seen that most of the values are in good agreement. The solid curve shown for each graph has the shape (Blin-Stoyle, 1952):

$$P_n(E, \theta) = C \frac{A(E_d) \sin \theta \cos \theta}{1 + A(E_d) \cos^2 \theta} \quad - - - \quad 7-1$$

The fitted values are $A(E_d) = 2$ and $C = 0.35$ for both energies.

Using differential cross sections, σ , from Brolley and Fowler (1960), the products $P_n \cdot \sigma$ were computed for the $D(d,n)He^3$ reaction, and are shown in figures 7-3 and 7-4. On the basis of equation 2-10, a weighted least squares fit to associated Legendre functions was made. (See, for example, Mathews and Walker, 1964). A good fit is obtained in both cases using only $\ell = 2$.

Two values are shown in table 7-2 for the $T(d,n)He^4$ reaction. In agreement with other workers (see, for example, Haeberli, 1963), the polarizations are small. This reaction was used primarily to check the operation of the neutron polarimeter for neutrons with energy similar to those from the $B^{11}(d,n)C^{12}$ reaction.

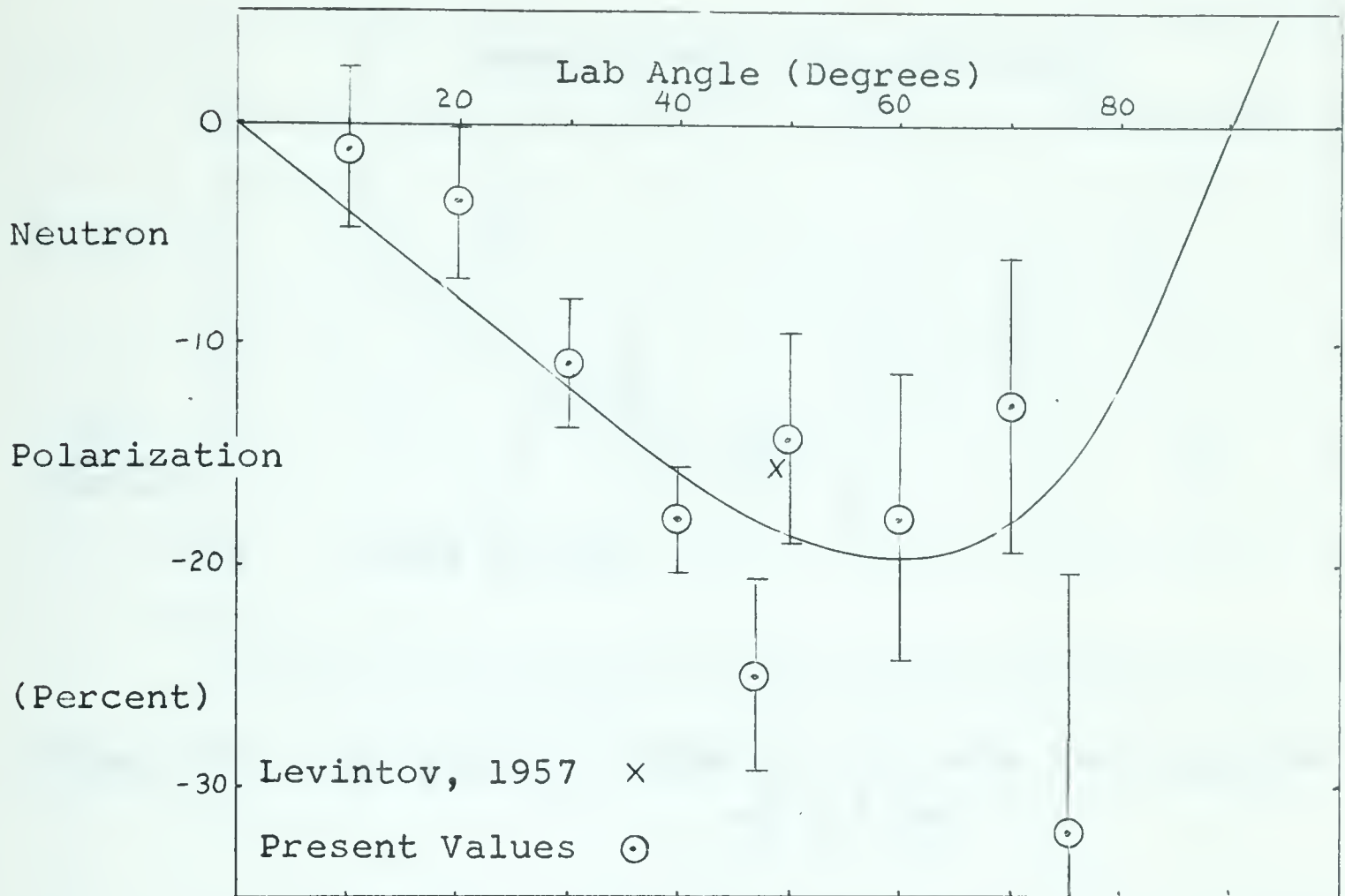


Figure 7-1 Measured Neutron Polarizations for $D(d,n)He^3$ for Mean Energy of 1.1 Mev

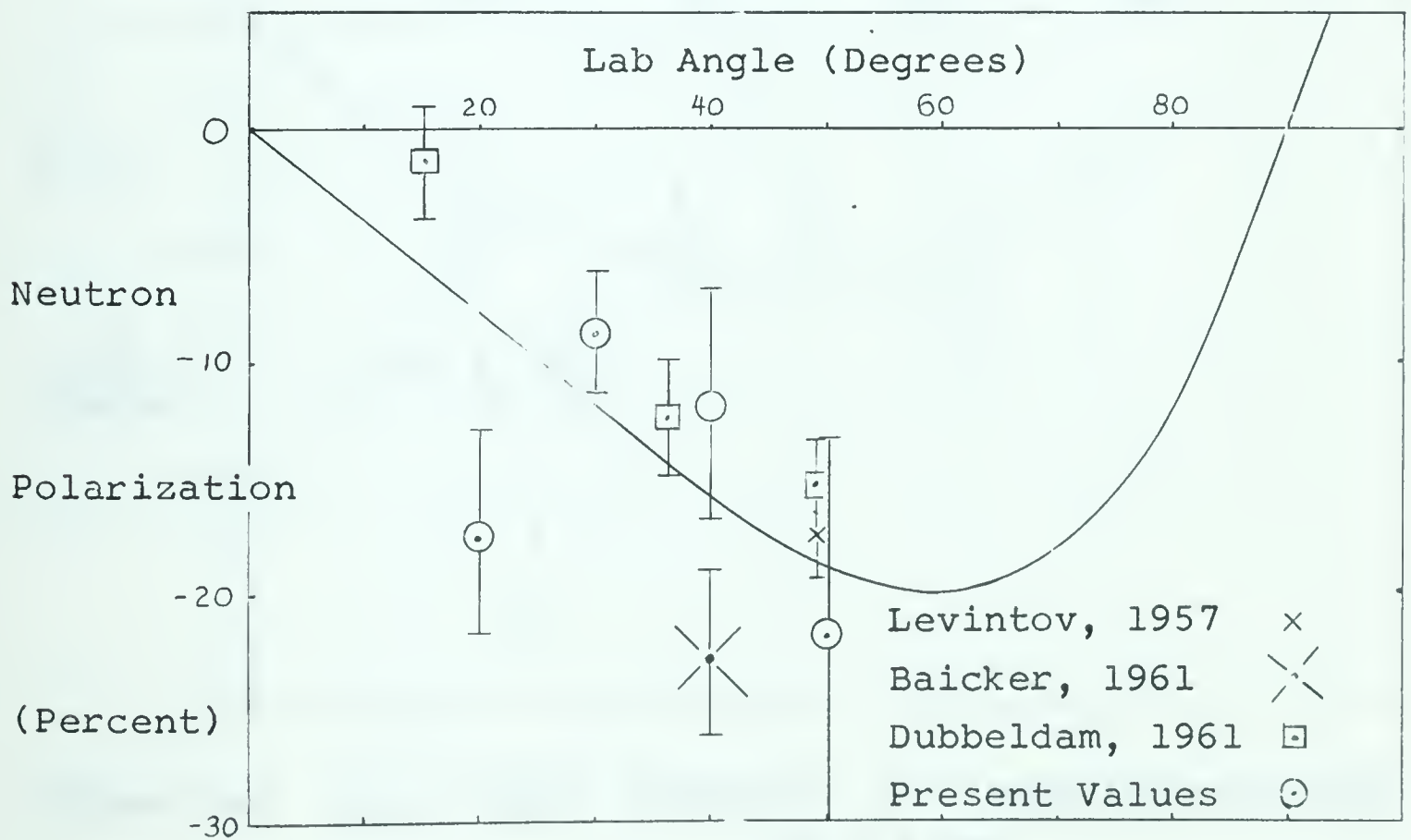


Figure 7-2 Measured Neutron Polarizations for $D(d,n)He^3$ for Mean Energy of 1.5 Mev

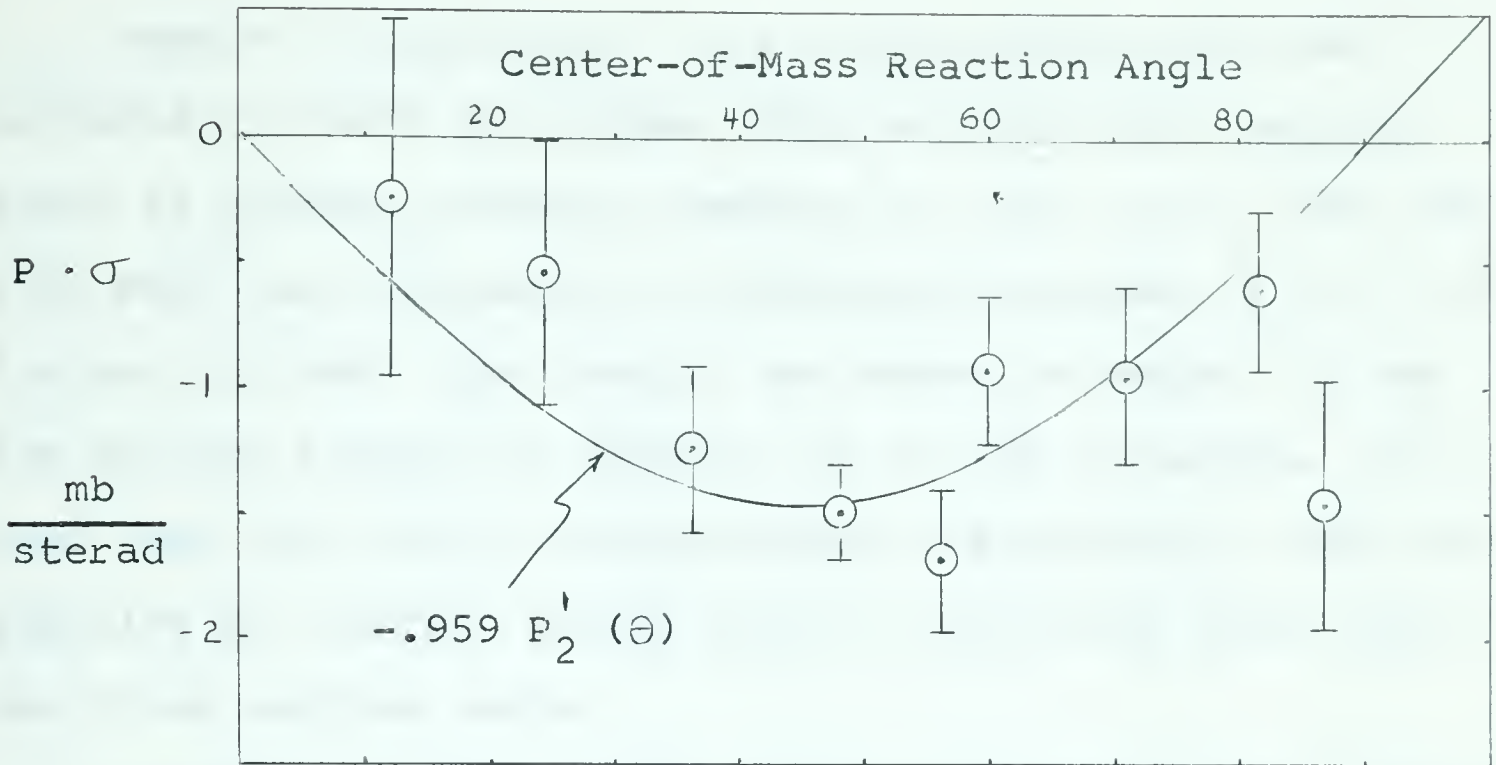


Figure 7-3 $\sum a_\ell P_\ell'(\theta)$ fitted to $P \cdot \sigma$ data for $D(d,n)He^3$ at 1.1 Mev

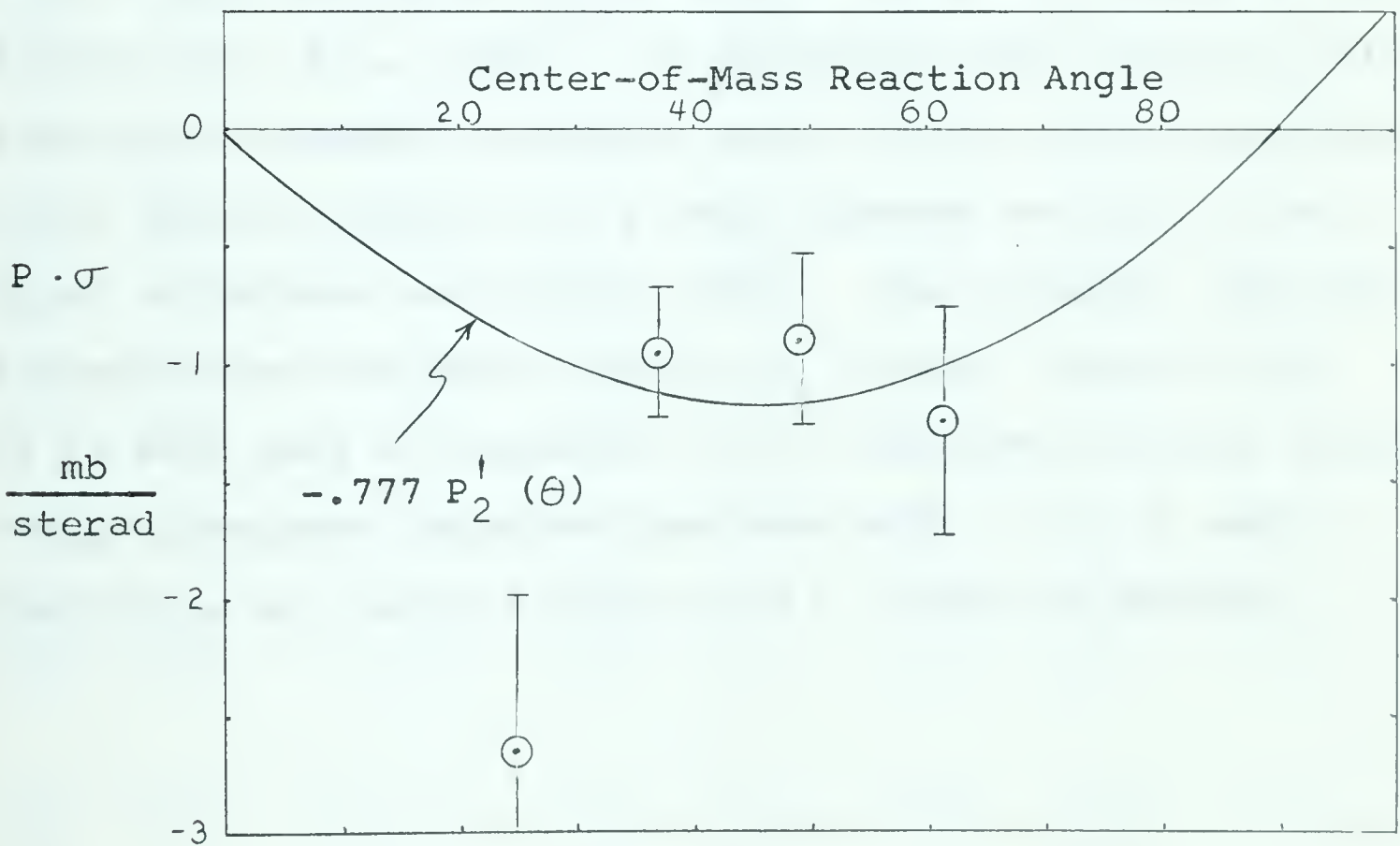


Figure 7-4 $\sum a_\ell P_\ell'(\theta)$ fitted to $P \cdot \sigma$ data for $D(d,n)He^3$ at 1.5 Mev

Angular distributions of neutron polarization were measured for both the ground state and the first excited state at average deuteron energies of 1.35, 1.45, 1.65 and 1.85 Mev - corresponding to bombarding energies of 1.5, 1.6, 1.8 and 2.0 Mev. The results are shown in tables 7-3 and 7-4 and are plotted in figures 7-5 to 7-8 inclusive. It is seen that the neutron polarizations are generally small and positive for neutron groups both to the ground state and to the first excited state.

Products of polarization and cross section were computed for the 1.45 Mev results. Cross sections for the ground state neutrons were derived from Owen and Madansky (1957), while values for the first excited state were obtained from Neilson, et. al., (1960). In accordance with equation 2-10, associated Legendre functions were fitted to the polarization - cross section products by a least squares analysis as outlined in Mathews and Walker (1964). The products, and the fitted curves are shown plotted in figures 7-9 and 7-10. It is seen that a reasonable fit is obtained for both states using associated Legendre functions with $\ell = 1, 2$, and 3. The fit is not as good with the $\ell = 2$ function omitted.

Table 7-3 Neutron Polarizations for $B^{11}(d,n)C^{12}$ g.s.

\bar{E}_d	Lab Angle	En Lab	ϵ	$\Delta\epsilon$	P_2	\bar{P}_2	P_n
1.35	20	14.79	+.094	.12	.996	.858	+.109
1.35	30	14.71	+.166	.09	.996	.872	+.189
1.35	40	14.60	+.107	.09	.996	.879	+.122
1.35	60	14.33	+.159	.12	.996	.886	+.179
1.35	90	13.83	+.138	.12	.995	.892	+.155
1.45	2.5	14.96	+.060	.063	.996	.391	+.153
1.45	5	14.96	+.148	.052	.996	.635	+.233
1.45	15	14.93	+.109	.054	.996	.832	+.131
1.45	30	14.82	+.045	.056	.996	.868	+.052
1.45	45	14.64	+.075	.053	.996	.879	+.085
1.45	60	14.42	+.050	.047	.996	.884	+.057
1.45	75	14.16	+.073	.053	.996	.888	+.082
1.45	90	13.90	-.041	.058	.995	.895	-.046
1.45	105	13.63	+.013	.044	.995	.894	+.014
1.45	120	13.39	+.082	.051	.995	.897	+.091
1.45	135	13.20	+.166	.056	.995	.901	+.184
1.45	145	13.08	+.275	.100	.995	.901	+.305
1.45	150	13.03	-.100	.089	.995	.901	-.111
1.65	20	15.12	.000	.12	.997	.857	-.001
1.65	40	14.92	+.170	.11	.996	.878	+.194
1.65	60	14.61	+.119	.11	.996	.885	+.135
1.65	90	14.05	+.134	.12	.995	.891	+.150
1.85	20	15.34	+.329	.11	.997	.895	+.368
1.85	40	15.12	+.258	.14	.997	.898	+.288
1.85	60	14.80	-.061	.18	.996	.899	-.068
1.85	90	14.21	-.103	.17	.996	.901	-.113

Table 7-4 Neutron Polarizations for $B^{11}(d,n)C^{12}_{4.43}$

\bar{E}_d	Lab Angle	En Lab	ϵ	$\Delta\epsilon$	P_2	\bar{P}_2	P_n
1.35	20	10.55	+.033	.13	.995	.873	+.038
1.35	30	10.48	+.020	.12	.995	.892	+.022
1.35	40	10.39	+.093	.13	.995	.892	+.104
1.35	60	10.16	+.028	.24	.995	.898	+.031
1.35	90	9.73	+.081	.20	.996	.903	+.090
1.45	2.5	10.71	+.028	.063	.995	.397	+.071
1.45	5	10.71	+.023	.043	.995	.644	+.036
1.45	15	10.68	+.127	.051	.995	.845	+.150
1.45	30	10.58	+.166	.078	.995	.882	+.188
1.45	45	10.44	+.163	.055	.995	.892	+.183
1.45	60	10.25	+.098	.054	.995	.898	+.109
1.45	75	10.03	+.034	.049	.996	.901	+.038
1.45	90	9.81	-.061	.082	.996	.904	-.067
1.45	105	9.58	+.081	.044	.996	.907	+.089
1.45	120	9.38	-.065	.049	.996	.910	-.071
1.45	135	9.21	+.107	.049	.996	.912	+.117
1.45	145	9.12	-.007	.140	.996	.914	-.008
1.45	150	9.08	+.097	.072	.996	.914	+.106
1.65	20	10.86	-.027	.17	.995	.870	-.031
1.65	40	10.70	-.038	.17	.995	.891	-.043
1.65	60	10.43	+.004	.15	.995	.897	+.004
1.65	90	9.96	-.023	.21	.996	.904	-.025
1.85	20	11.80	+.063	.16	.995	.907	+.069
1.85	40	10.90	+.126	.13	.995	.910	+.139
1.85	60	10.62	-.048	.18	.995	.912	-.053
1.85	90	10.12	+.028	.14	.995	.915	+.031

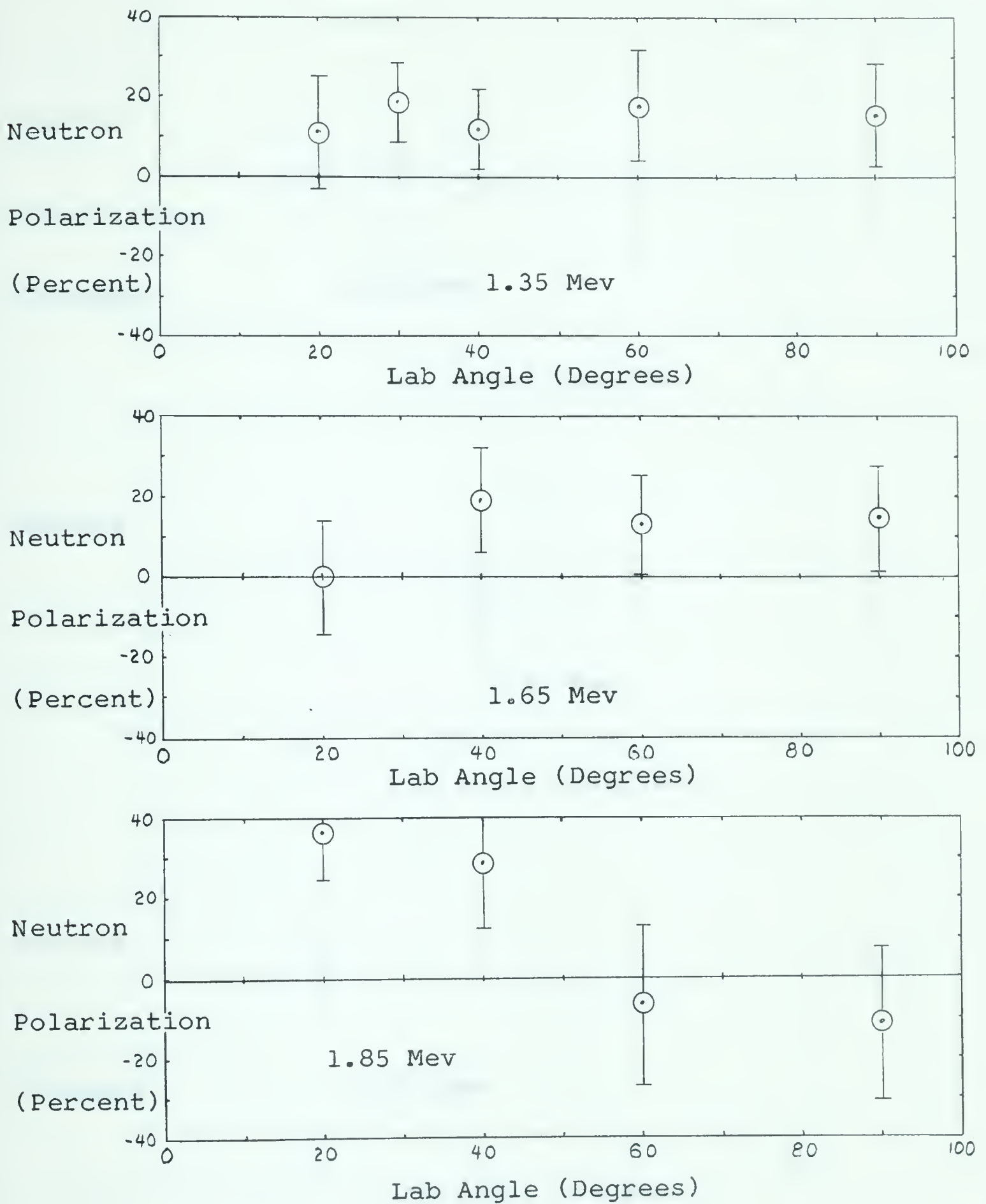


Figure 7-5 Neutron Polarizations for $B^{11}(d,n)C^{12}$ Ground State for Mean Deuteron Energies of 1.35, 1.65, and 1.85 Mev

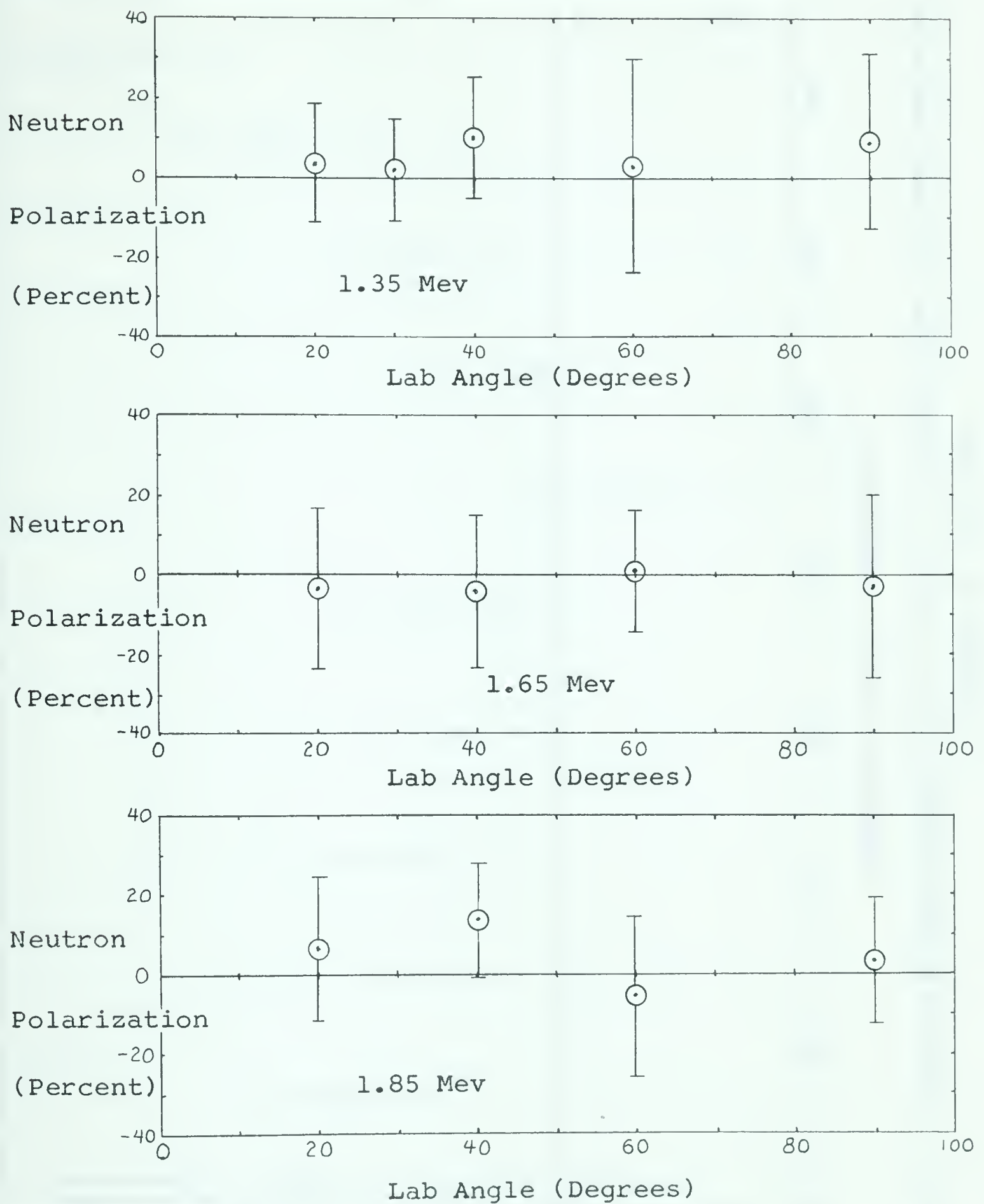
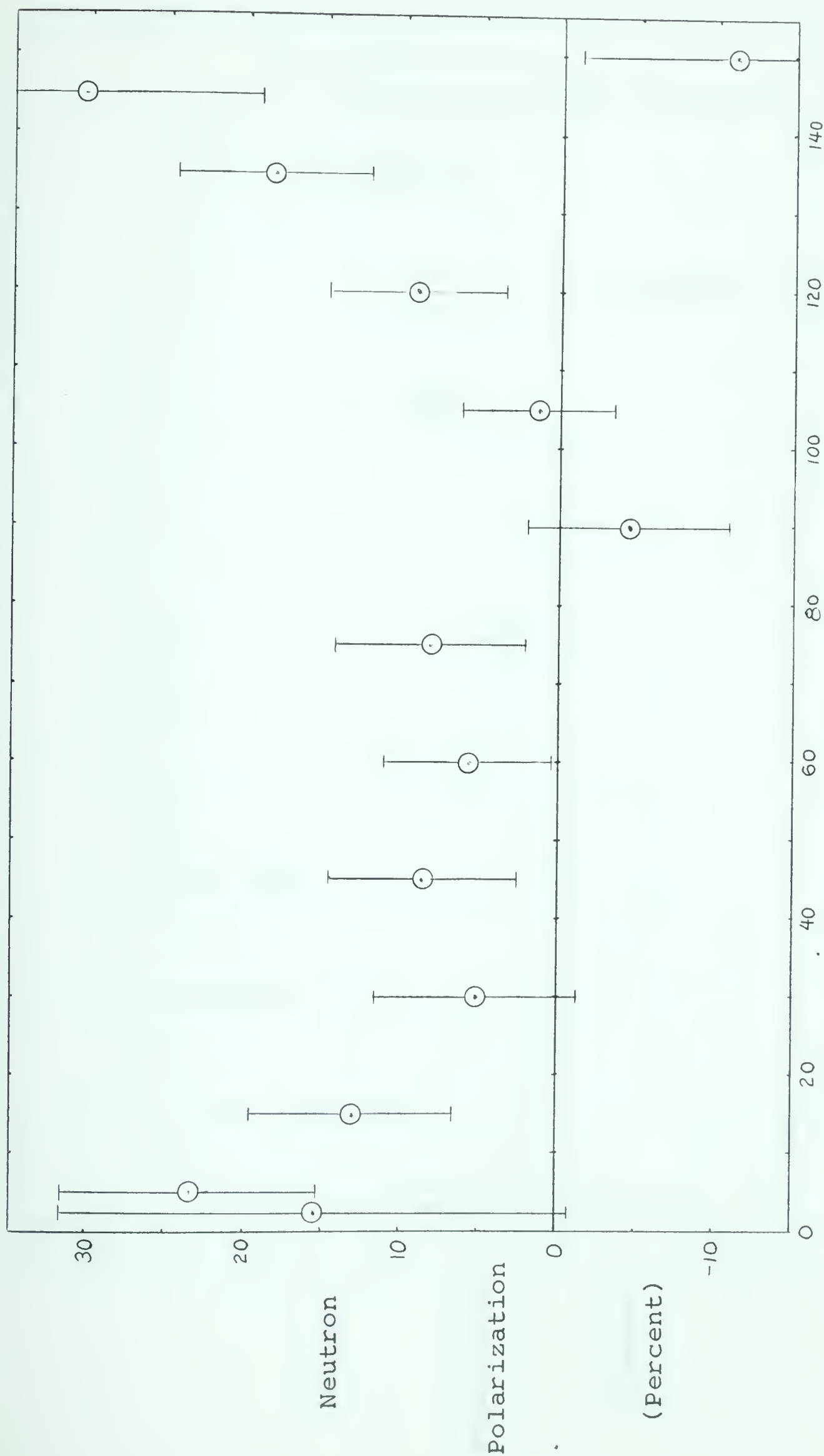


Figure 7-6 Neutron Polarizations for $B^{11}(d,n)C^{12}$ First Excited State (4.43 Mev Excitation) for Mean Deuteron Energies of 1.35, 1.65, and 1.85 Mev



Laboratory Angle (Degrees)

Figure 7-7 Neutron Polarizations for $B^{11}(d,n)C^{12}$ Ground State for Mean Deuteron Energy of 1.45 Mev

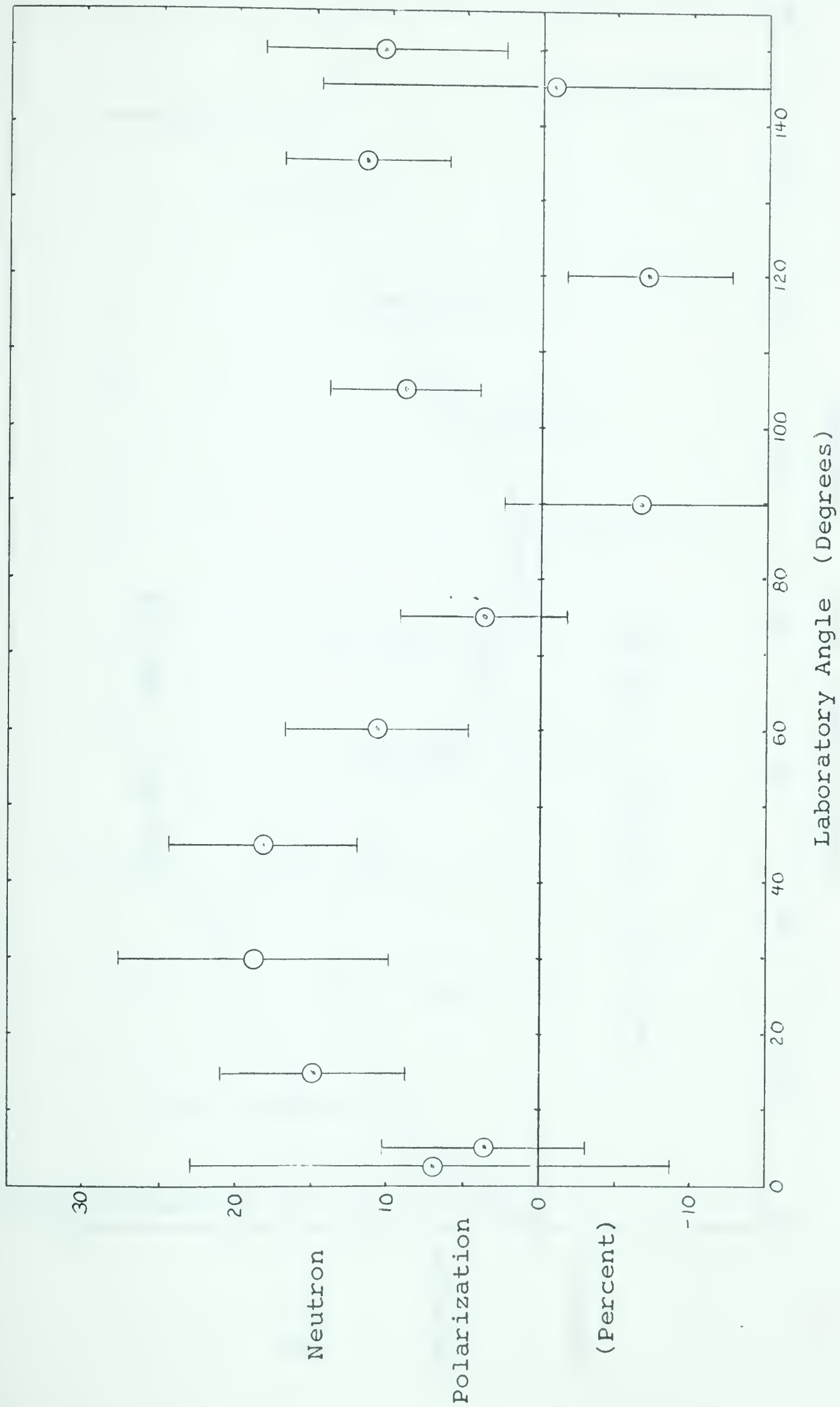


Figure 7-8 Neutron Polarizations for $B^{11}(d,n)C^{12}$ First Excited State for
Mean Deuteron Energy of 1.45 Mev

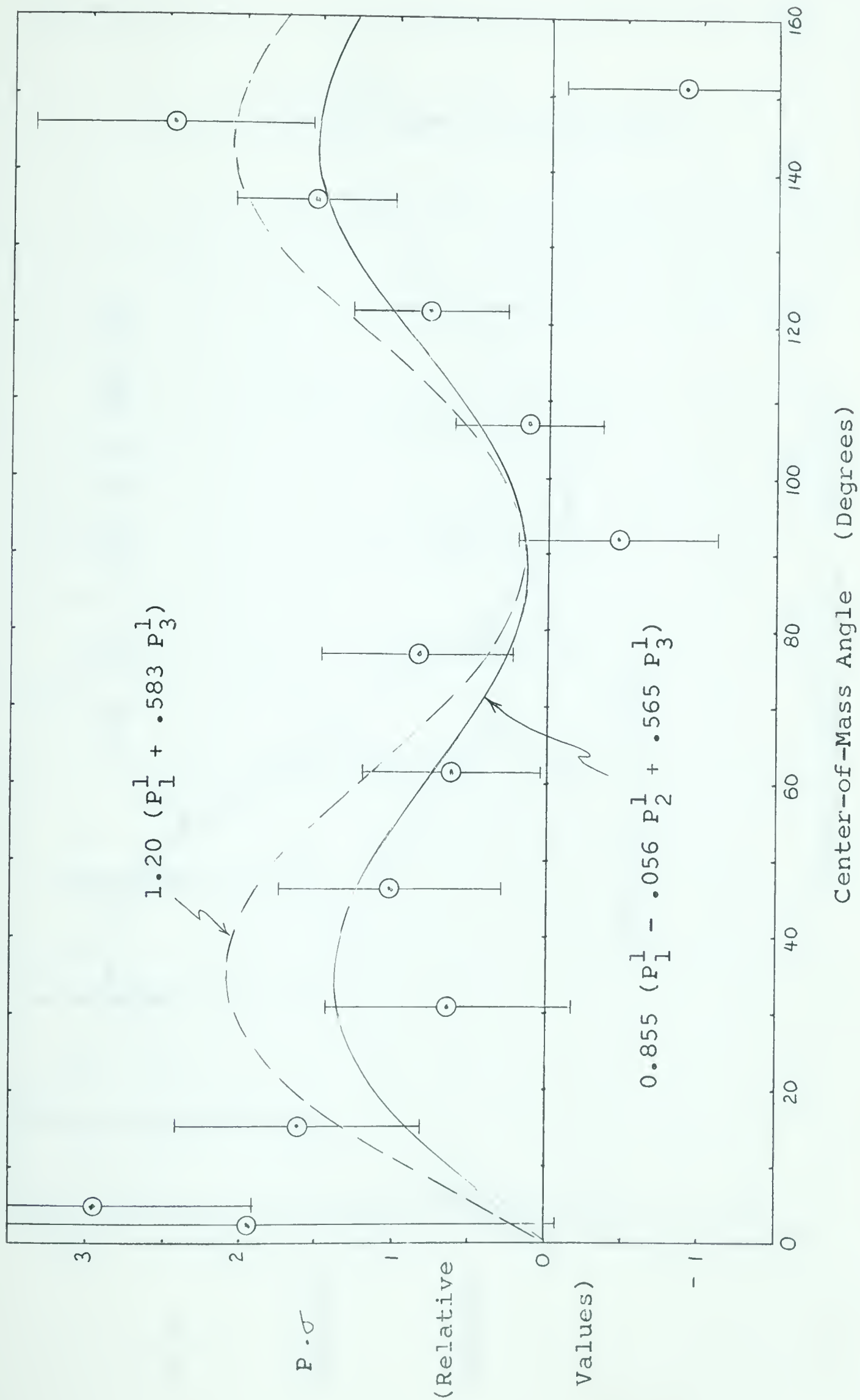


Figure 7-9 $\sum a_\ell P'_\ell(\theta)$ Fitted to $P \cdot \sigma$ Data for $B^{11}(d,n)C^{12}$ Ground State Neutrons at a Mean Deuteron Energy of 1.45 Mev

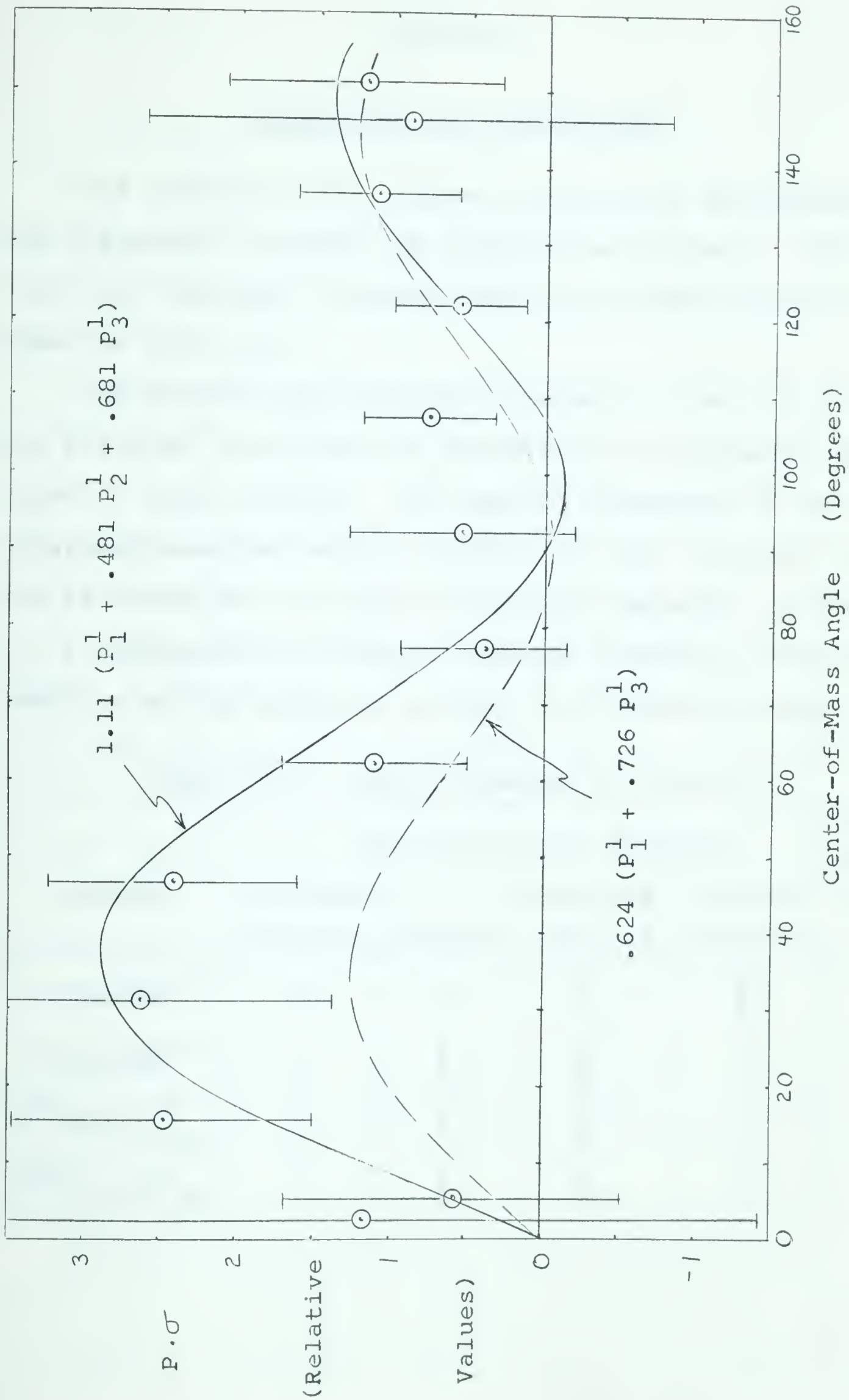


Figure 7-10 $\sum a_\ell P'_\ell(\theta)$ Fitted to $P \cdot \sigma$ Data for $B^{11}(d,n)C^{12}$ First Excited State Neutrons at a Mean Deuteron Energy of 1.45 Mev

CHAPTER 8

DISCUSSION AND CONCLUSIONS

The results of the neutron polarization measurements are displayed in tables and diagrams in chapter 7. The spins and parities of nuclei involved in the reactions are shown in table 8-1.

The neutron polarizations measured for the $D(d,n)He^3$ and $T(d,n)He^4$ reactions are essentially in agreement with those of other workers. The angular dependence of the polarization-cross-section product for the $D(d,n)He^3$ reaction can be fitted by the single associated Legendre function for $\ell = 2$, indicating an angular momentum transfer of two in the reaction and no change in parity, as is already known.

Table 8-1 Angular Momenta and Parities

Reaction	Spin Values and Parities				Angular Momentum Transfer (ℓ_p)
	Incident Particle	Target	Observed Particle	Residual Nucleus	
$D(d,n)He^3$	1^+	1^+	$\frac{1}{2}^+$	$\frac{1}{2}^+$	2
$T(d,n)He^4$	1^+	$\frac{1}{2}$	$\frac{1}{2}^+$	0^+	0
$B^{11}(d,n)C_{g.s.}^{12}$	1^+	$\frac{3}{2}^-$	$\frac{1}{2}^+$	0^+	1
$B^{11}(d,n)C_{4.43}^{12}$	1^+	$\frac{3}{2}^-$	$\frac{1}{2}^+$	2^+	1

The neutron polarizations measured for the first two states of C^{12} in the reaction $B^{11}(d,n)C^{12}$ had not previously been measured by anyone. Generally, the results at all energies of 1.35, 1.45, 1.65, and 1.85 Mev, and all angles, tend to be positive and less than one-third, in agreement with the distorted wave Born approximation. The fairly extensive measurements of the angular dependence of the polarization-cross-section products at a mean deuteron energy of 1.45 Mev are fitted quite well by linear combinations of associated Legendre functions, in accordance with equation 2-10 and the theory of polarization presented by Welton (1963). The predominant functions for both states are those with ℓ values of 1 and 3; they are odd, in agreement with the changes in parity. However, the $\ell = 2$ function seems also to be required for a good fit to the experimental results. It is interesting that the trend for the polarizations at angle θ for the first excited state follows that for the ground state at angle $\pi - \theta$.

The $B^{11}(d,n)C^{12}$ ground state polarizations at a mean deuteron energy of 1.85 Mev show a definite trend from positive values at small angles to negative values at larger angles, the sign change occurring at about 60° . Although an analytical fit was not made, such an angular dependence indicates a predominant $\ell = 3$ associated Legendre function for the product $P \cdot \sigma$.

The neutron polarimeter has proven useful for the reaction $B^{11}(d,n)C^{12}$, but it does not work as well as had been hoped. Two serious faults lie in its low detection

efficiency for incoming neutrons, and in its poor time resolution for coincidence counting.

The detection efficiency would be increased either by lengthening the polarimeter or by raising the gas pressure. The first method requires longer counters and wires and a longer array of collimating vanes. These lengths could probably be increased without any difficulty, although a problem might arise in getting long enough uniform wires and in keeping such long wires straight and central. With an increase in gas pressure the counters would have to be narrower in order that recoils could still reach the side counters. With narrower counters, energy loss within the collimating vanes would be more serious so that thinner vanes would be desirable. Thinner vanes however would be difficult to construct, and as well might be prohibited because of breakdown problems near the vane edges. Breakdown problems could be reduced by covering the array of vanes with very thin metallic sheaths, but only at the expense of further energy loss in the sheaths themselves.

Better time resolution would be obtained using a wire with a larger diameter; a larger voltage would be required for operation at a given gas gain and this would produce faster collection of ionization. Again, however, voltage breakdown problems might arise because of the higher voltage. The principal reason for wanting better time resolution lies in the increasing proportion of accidental coincidences with higher counting rates (see equation 4-23). And in the experiments reported here it was found necessary to place

shadow shields in front of the side counters in order to reduce accidental coincidence rates. An alternative way of trying to avoid this difficulty would be to replace the side counters with solid state detectors placed so that they count the recoil alpha particles passing through the collimating vane passages.

An improvement, entirely within the present design, would be to make the side counters square in cross section rather than rectangular. This would result in some improvement both in energy and in time resolution. Discrimination against higher energy neutrons could probably be made by using a slightly larger counter pressure.

Other improvements in counting efficiency and time resolution lead away from the use of helium gas proportional counters with resultant increased complexity and cost and worsened energy resolution.

True coincidence rates of about 100 per hour per side were obtained for each neutron group from the $B^{11}(d,n)C^{12}$ reaction with 3 micro amperes of 1.6 Mev deuteron beam on a 1.2 mg/cm^2 natural boron target. (Although the cross section for neutrons from the first excited state is greater than that for the ground state, the range in the polarimeter of the lower energy recoil alpha particles is shorter, with a resultant decrease in the number that can reach side counters and produce coincidences.) By comparison, the methods of Levintov et. al. (1957), and of Pasma (1959) yield counting rates an order of magnitude higher (see Haeberli, 1960), while the liquid helium scintillator system of Perkins and

Simmons (1963) is more than one hundred times as efficient. This latter method has a resolving time of about 10 nano-seconds and an energy resolution of about twenty-five percent.

The merits of the present system lie in its simplicity, low cost, and somewhat better energy resolution than can be obtained with other neutron polarimeters.

REFERENCES

- Adair, R. K., Darden, S. E., and Fields, R. E., Phys. Rev. 96 (1954) 503.
- Ames, O., and Owen, G. E., Phys. Rev. 109 (1958) 1639.
- Austern, N., Fast Neutron Physics II, ed: Marion and Fowler, Interscience Publishers (1963) 1113.
- Austin, S. M., Barschall, H. H., and Shamu, R. E., Phys. Rev. 126 (1962) 1532.
- Baicker, J. A., and Jones, K. W., Nuclear Physics 17 (1960) 424.
- Barshall, H. H., Helv. Phys. Acta 29 (1956) 145.
- Basel Convention, Helv. Phys. Acta, Supplementum VI (1961) 436.
- Baumgartner, E., and Huber, P., Helv. Phys. Acta 26 (1953) 545.
- Bhatia, A. B., Huang, K., Huby, R., and Newns, H. C., Phil. Mag. 43 (1952) 485.
- Biendenharn, L. C., Boyer, K., and Charpie, R. A., Phys. Rev. 86 (1952) 619.
- Blin-Stoyle, R. J., Proc. Phys. Soc. A65 (1952) 949.
- Blin-Stoyle, R. J., and Grace, M.A., Handbuch der Physik 42 (1957) 555.
- Brinkman, H., Helv. Phys. Acta., Supplement 6 (1960) 166.
- Brolley, J. E., Jr., and Fowler, J. L., Fast Neutron Physics I, eds: Marion and Fowler, Interscience Publishers (1960) 73.
- Burke, P. G., Nuclear Forces and the Few Nucleon Problem, 2, eds: Griffith and Power, Pergamon Press (1960).
- Butler, S. T., Phys. Rev. 80 (1950) 1095.
- Butler, S. T., Proc. Roy. Soc. (London) A208 (1951) 559.
- Dubbeldam, P. S., Jonker, C. C., and Heemskerk, F. J., Nucl. Instr. 4 (1959) 234.

- Dubbeldam, P. S., Jonker, C. C., and Boersma, Nucl. Phys. 15 (1960) 452.
- Dubbeldam, P. S., and Walter, R. L., Nucl. Phys. 28 (1961) 414.
- Gallagher, L. J., and Cheston, W. B., Phys. Rev. 88 (1952) 684.
- Glendenning, N. K., Annual Review of Nuclear Science 13 (1963) 191.
- Haeberli, W., Fast Neutron Physics II, ed: Marion and Fowler, Interscience Publishers (1963) 1379.
- Hughes, D. J., and Schwartz, R. B., Neutron Cross Sections, B.N.L. 325, Brookhaven National Laboratories, (1958).
- Jonker, C. C., Helv. Phys. Acta, Supplementum VI (1961) 160.
- Krawciw, W., M.Sc. Thesis, University of Alberta (1960).
- Levintov, I. I., Miller, A. V., Tarumov, E. Z., and Shamshev, V. N., Soviet Physics, JETP 5 (1957) 258.
- Levintov, I. I., Miller, A. V., Tarumov, E. Z., and Shamshev, V. N., Soviet Physics, JETP 5 (1957a) 310.
- Levintov, I. I., Miller, A. V., and Shamshev, V. N., Soviet Physics, JETP 7 (1958) 712.
- Macfarlane, M. H., and French, J. B., Rev. Mod. Phys. 32 (1960) 567.
- Mather, K. B., and Swan, P., Nuclear Scattering, Cambridge University Press (1958) 427.
- Mathews, J., and Walker, J. L., Methods of Mathematical Physics, Benjamin, (1964).
- McCormac, B. M., Steuer, M. F., Bond, C. D., and Hereford, F. L., Phys. Rev. 104 (1956) 718.
- Monahan, J., Fast Neutron Physics I, ed: Marion and Fowler, Interscience Publishers (1963) 49.
- Neilson, G. C., Dawson, W. K., Johnson, F. A., and Sample, J. T., Suffield Technical Report 176, Defence Research Board of Canada (1960).
- Newns, H. C., Proc. Phys. Soc. (London) A66 (1953) 477.
- Owen, G. E., and Madansky, L., Phys. Rev. 105 (1957) 1766.

- Pasma, P. J., Nucl. Phys. 6 (1958) 141.
- Ricamo, R., Helv. Phys. Acta 26 (1953) 423.
- Rossi, B. B., and Staub, H., Ionization Chambers and Counters, McGraw-Hill (1949).
- Sample, J. T., Ph.D. Thesis, University of British Columbia (1955).
- Satchler, G. R., and Spiers, J. A., Proc. Phys. Soc. (London) A65 (1952) 980.
- Schiff, L. I., Quantum Mechanics, McGraw-Hill, (1955) 99.
- Seagrave, J. D., Phys. Rev. 92 (1953) 1222.
- Segre, E., Experimental Nuclear Physics, Wiley (1953).
- Simon, A., Phys. Rev. 92 (1953) 1050.
- Simmons, J. E., and Perkins, R. B., Rev. Sci. Instr. 32 (1961) 1173.
- Tobocman, W., Theory of Direct Nuclear Reactions, Oxford University Press (1961).
- Welton, T. A., Fast Neutron Physics II, ed: Marion and Fowler, Interscience Publishers, (1963) 1317.
- Whaling, W., Handbuch der Physik 34 (1958) 193.
- Wilkinson, D. H., Ionization Chambers and Counters, Cambridge University Press (1950).
- Willard, H. B., Bair, J. K., and Kington, J. D., Phys. Rev. 95 (1954) 1359.
- Williams, R. W., Methods of Experimental Physics, 5A ed: L. Marton, Academic Press, (1961) 118.
- Wolfenstein, L., Annual Rev. Nucl. Sci. 6 (1956) 43.

APPENDIX A

NEUTRON POLARIMETER DRAWINGS

Figures A-1 to A-11 show details of the construction of the polarimeter counters and pressure tank.

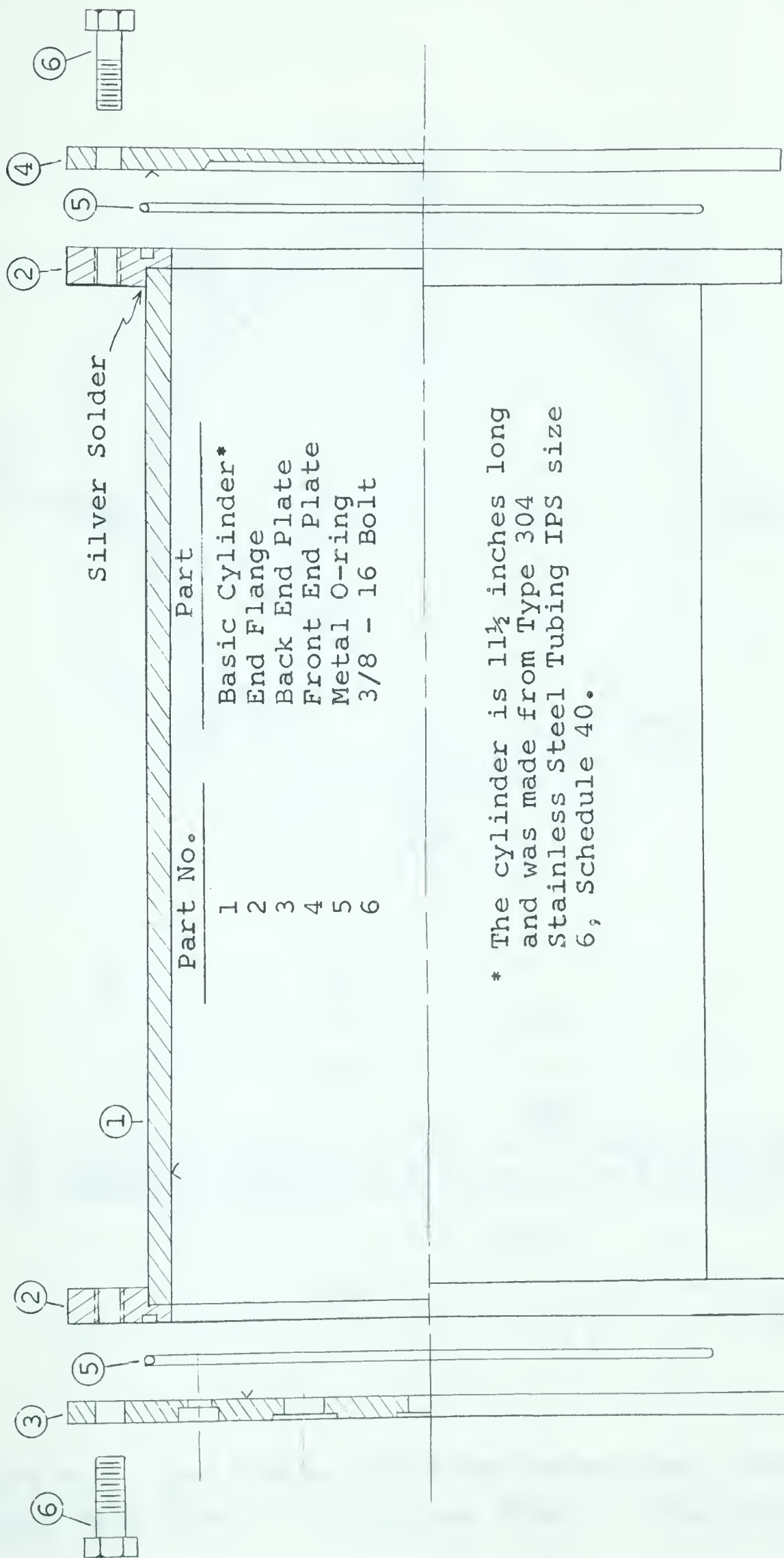


Figure A-1 Polarimeter Tank Assembly (Approx. Half Size)

Figure A-2 End Flange for Polarimeter Tank (Part No. 2)
(Shown Half Size - - Stainless Steel - - Two Required)

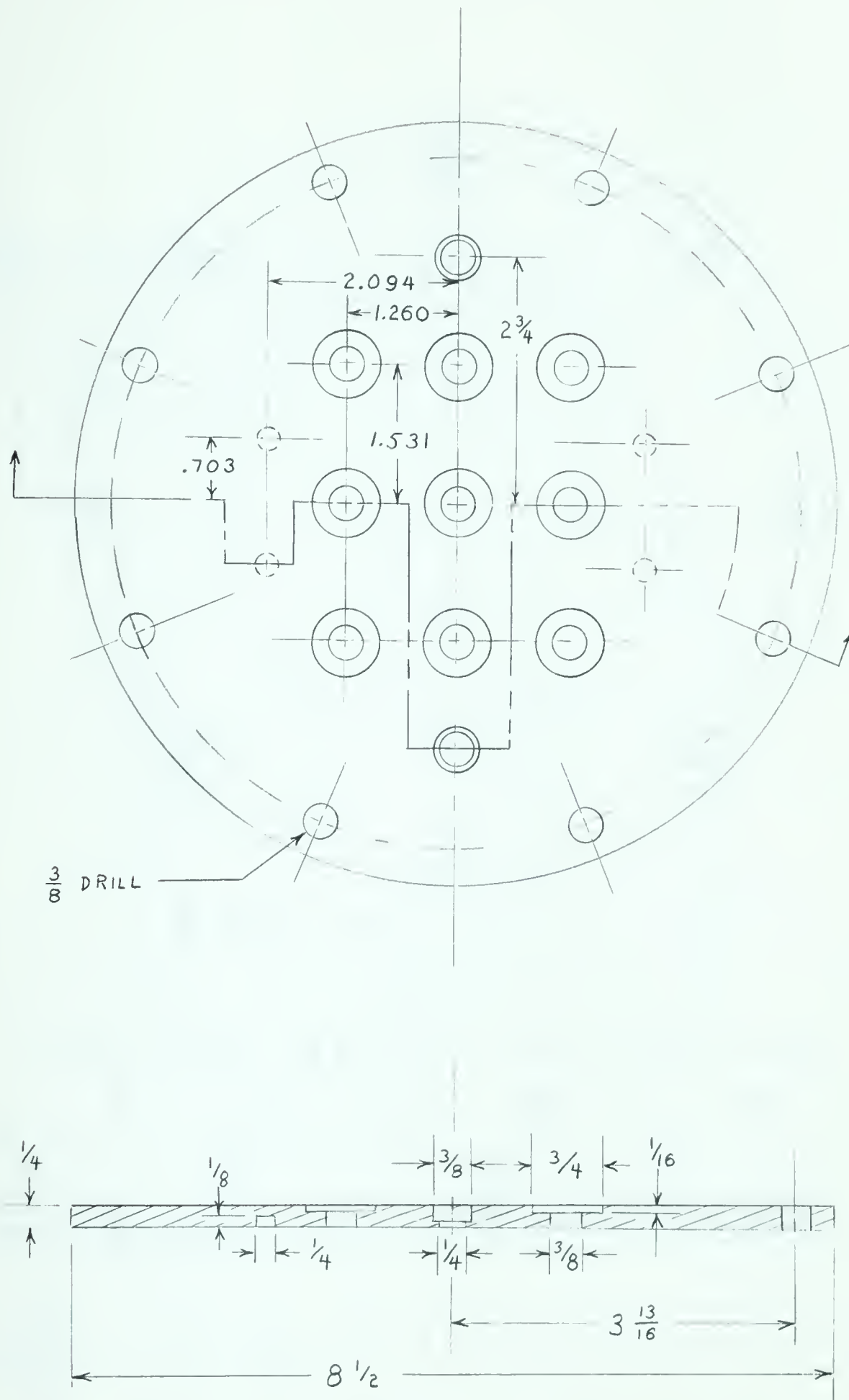


Figure A-3 Back End Plate for Polarimeter Tank (Part No. 3)
(Shown Half Size - - Stainless Steel - - One Required)

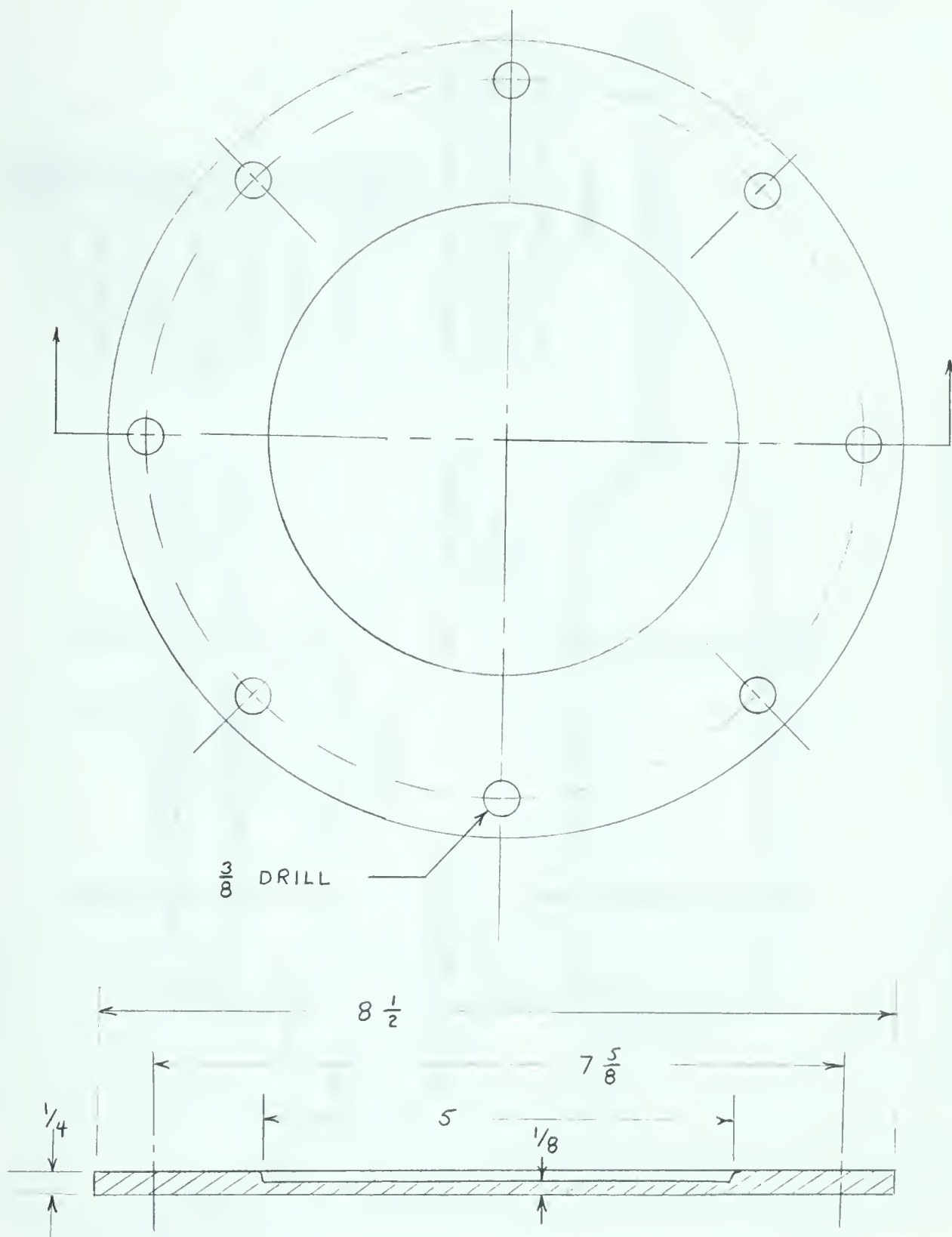


Figure A-4 Front End Plate for Polarimeter Tank (Part No.4)
(Shown Half Size - - Stainless Steel - - One Required)

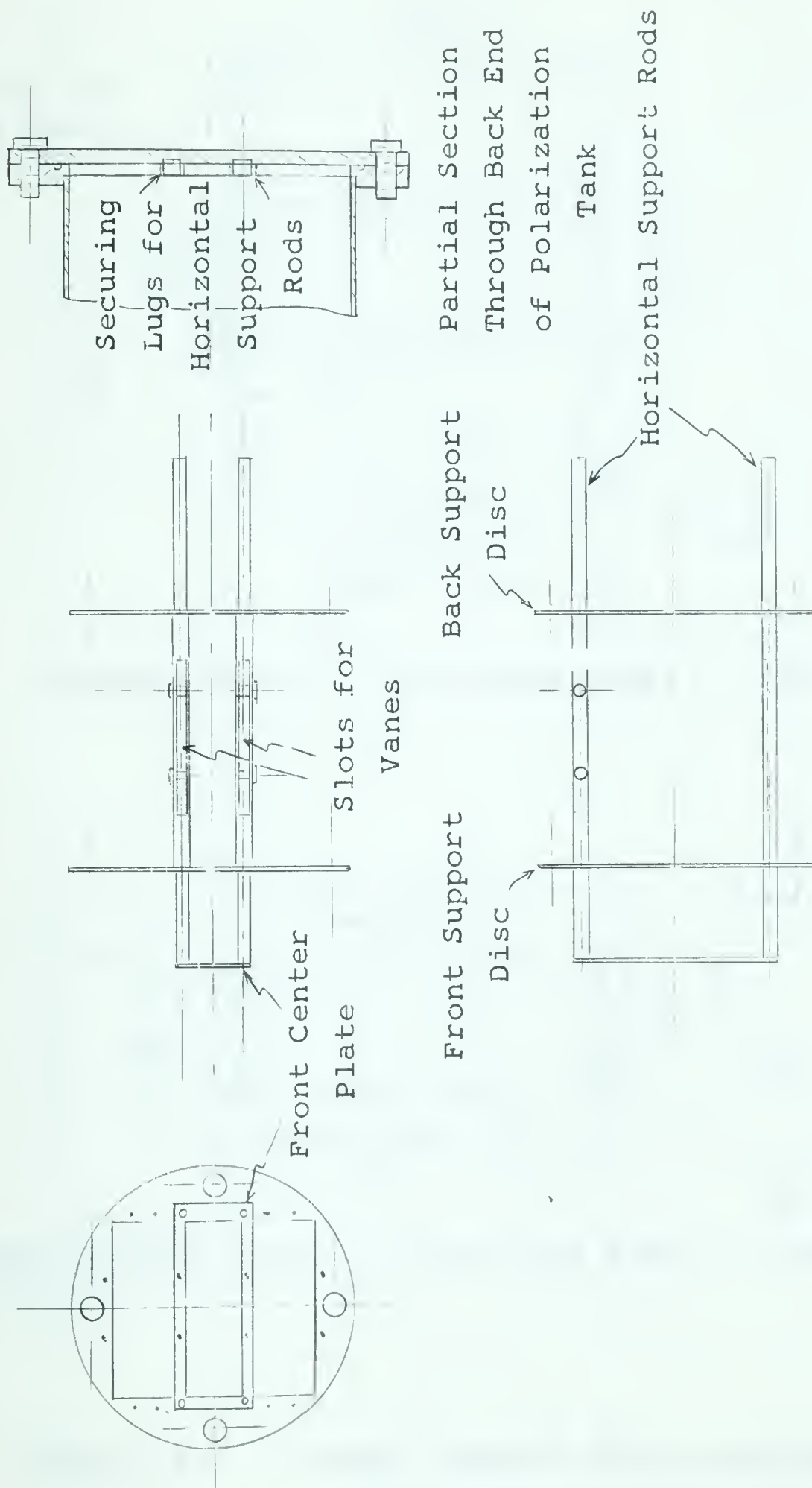
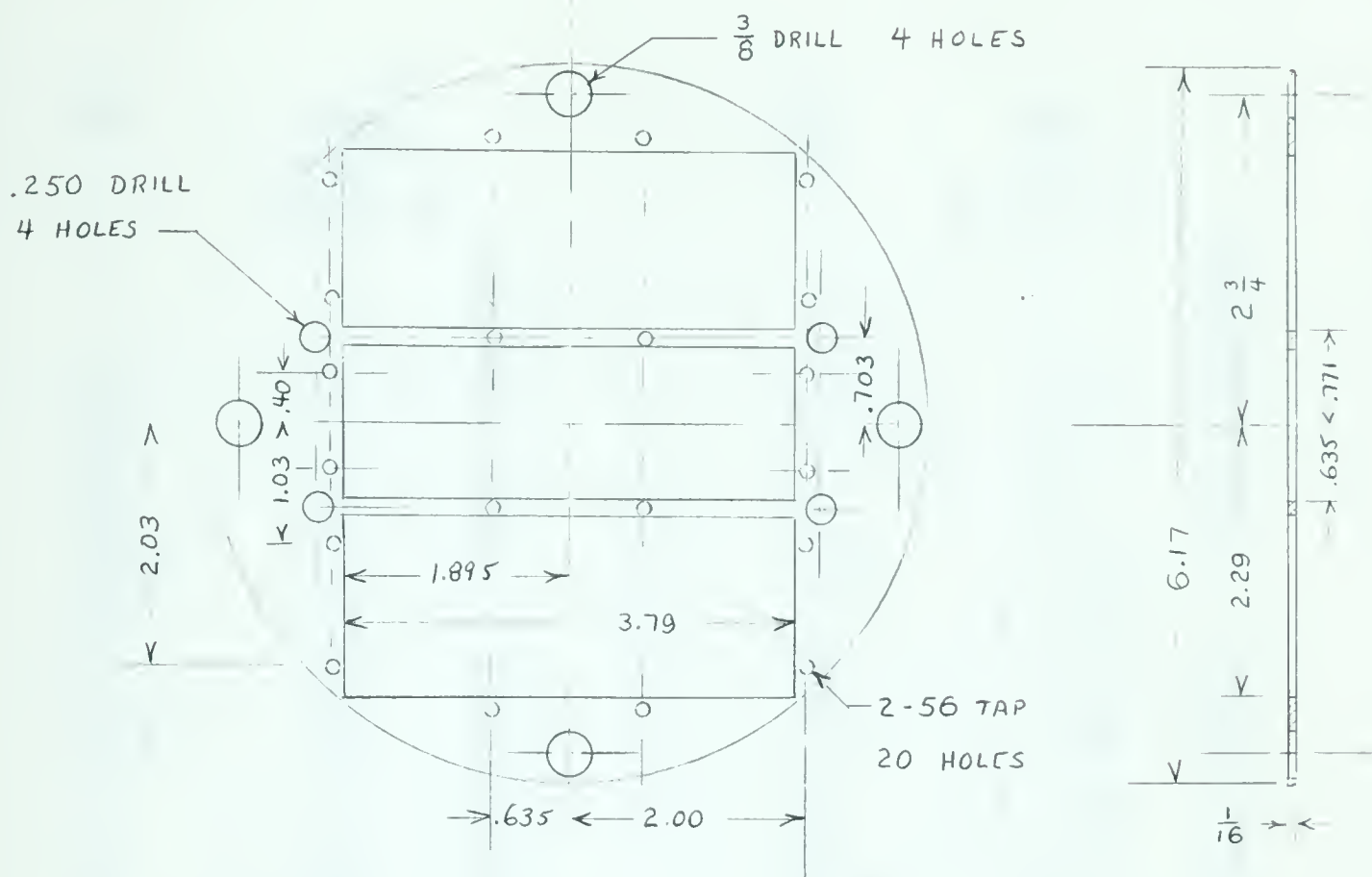
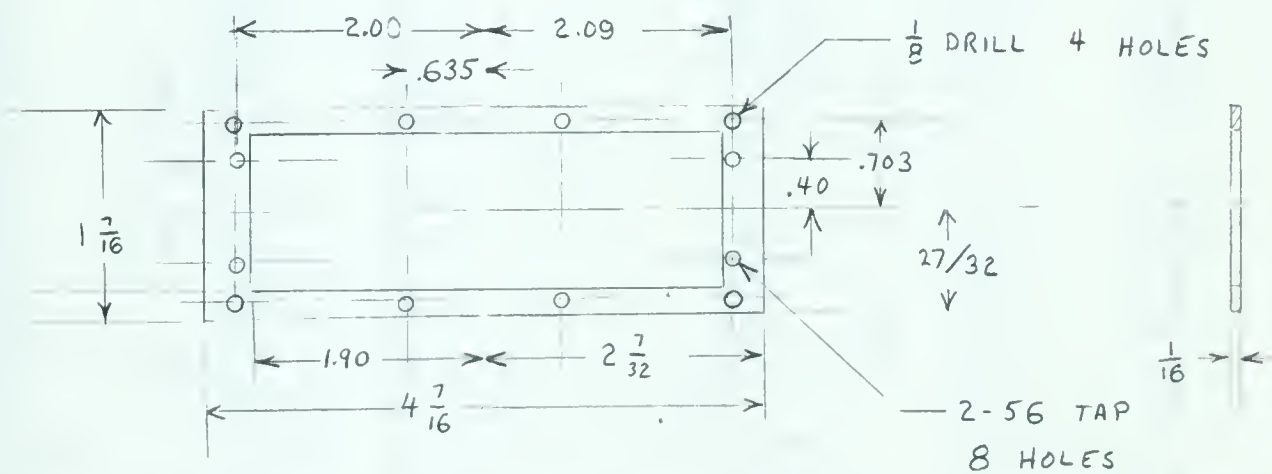


Figure A-5 Counter Frame Assembly

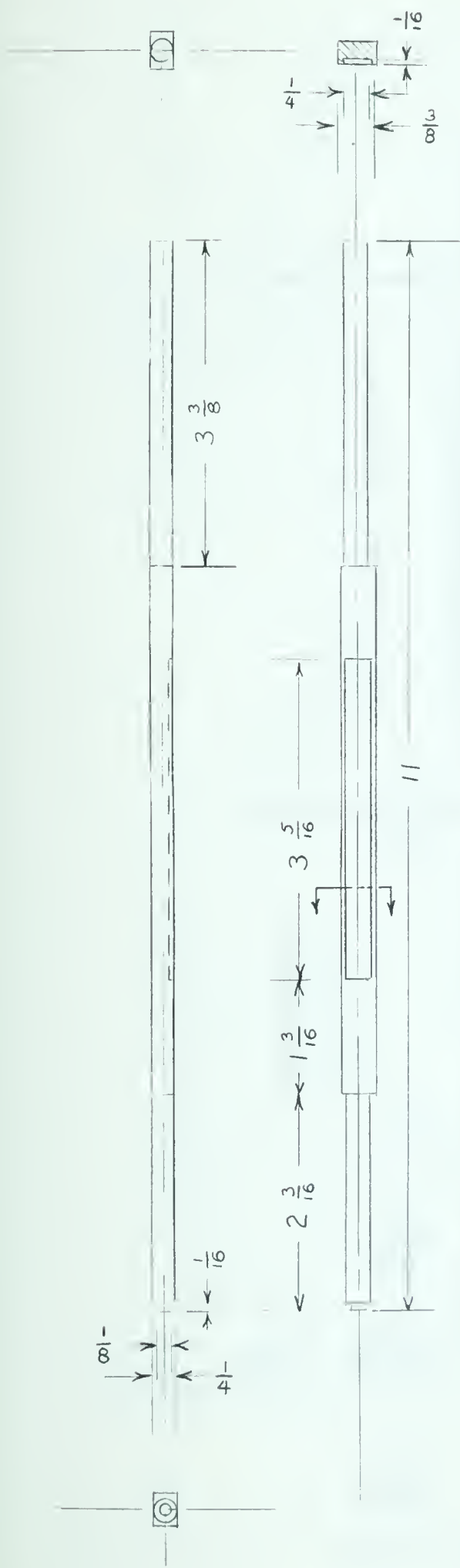


Support Discs - - Stainless Steel - - Two Required

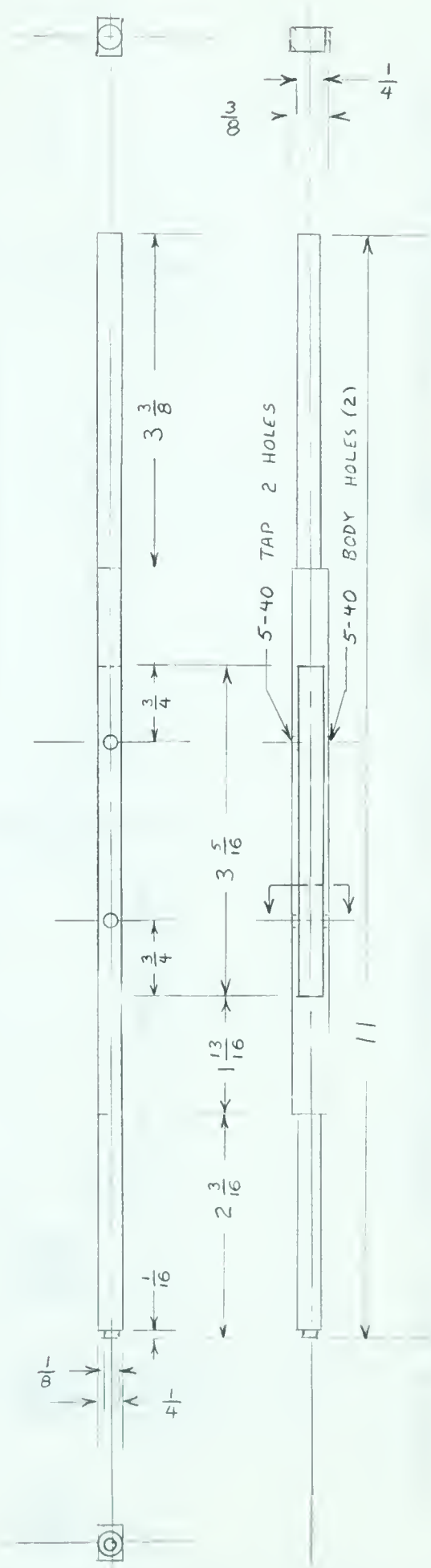


Front Center Plate - - Stainless Steel - - One Required

Figure A-6 Counter Support Discs and Front Plate
(Shown approximately half size)



Lower Horizontal Support - - Stainless Steel - - Two Required



Upper Horizontal Support - - Stainless Steel - - Two Required

Figure A-7 Horizontal Support Rods (Shown approximately half size)

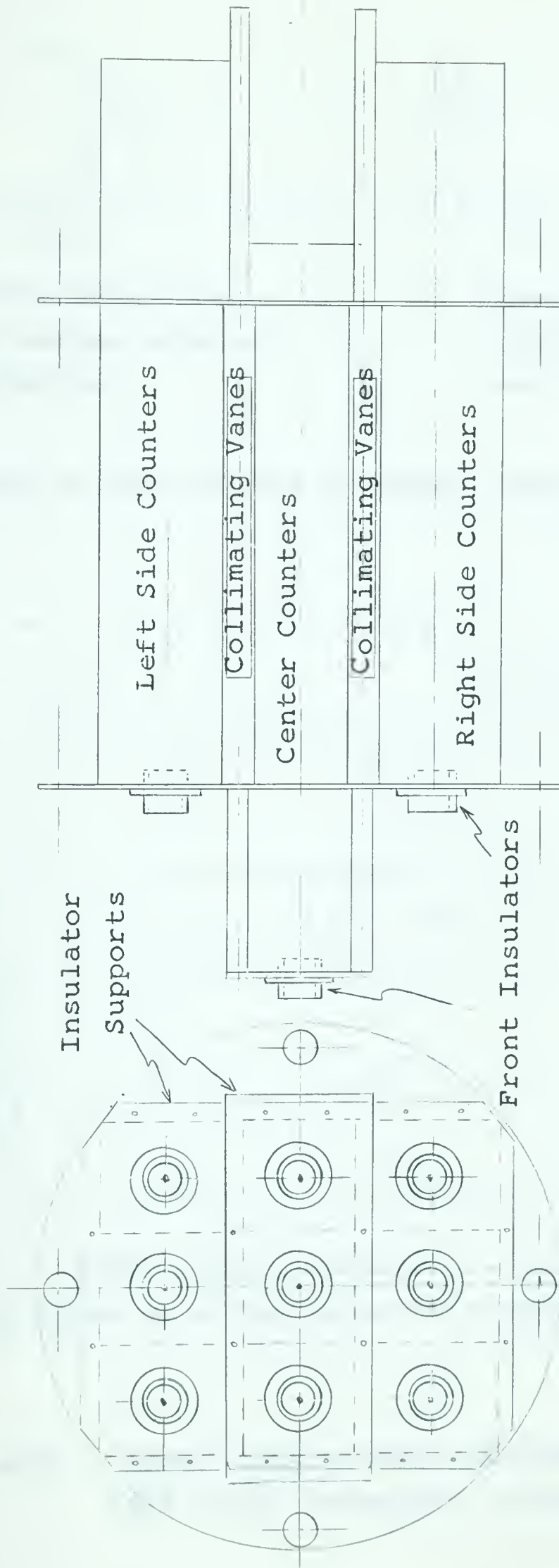
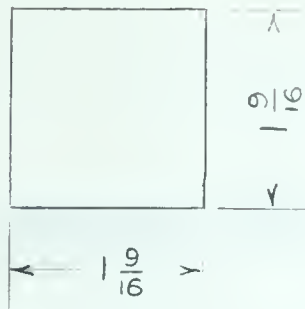
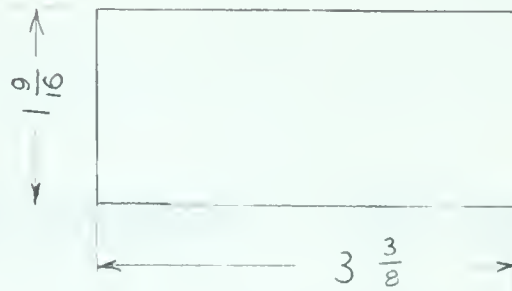


Figure A-8 Counter-in-frame Assembly (Shown approximately half size)

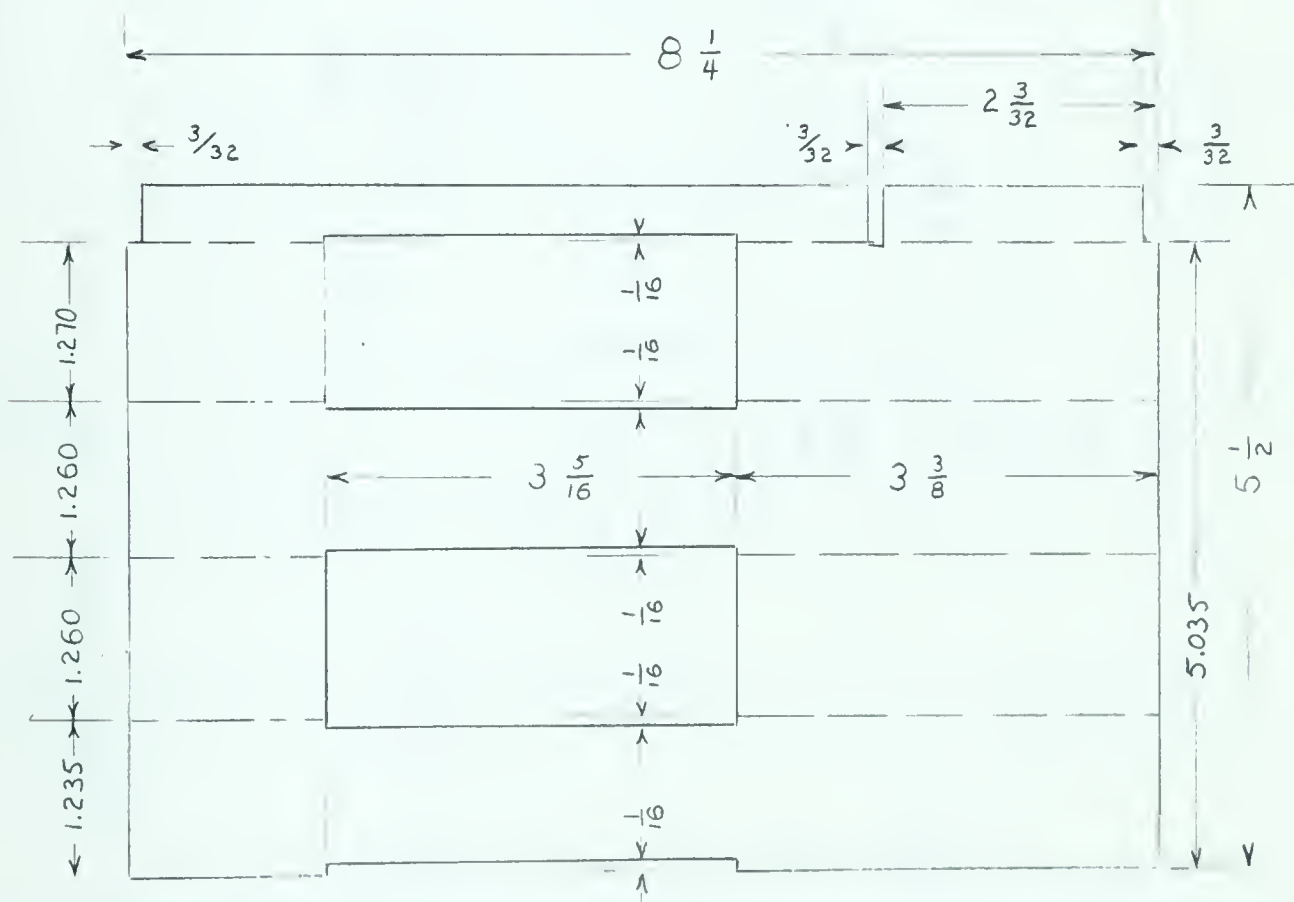


Back side walls for
middle-center counter,
two required



Front side walls for
middle-center counter,
two required

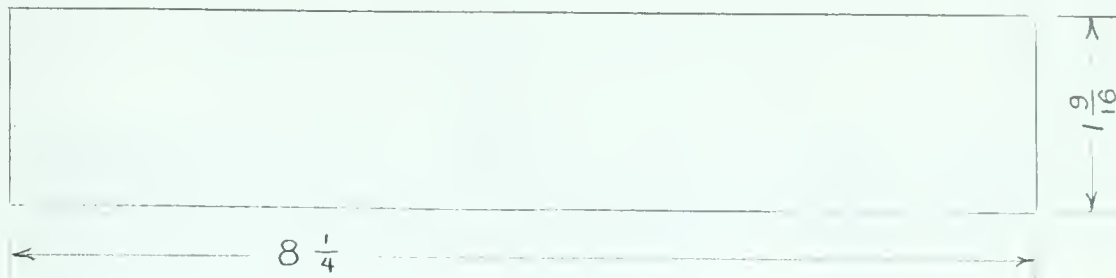
(To be spot-welded to outer central counters)



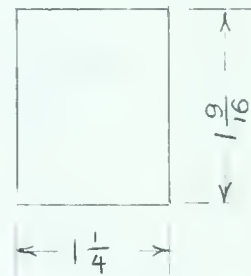
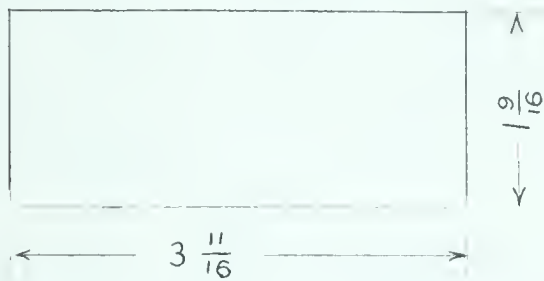
Outer cental counter - - two required

(Dashed lines show positions of required 90 degree bends)

Figure A-9 Center Counter Wall Outlines (Shown approximately half size; material: 10 mil stainless steel sheet)

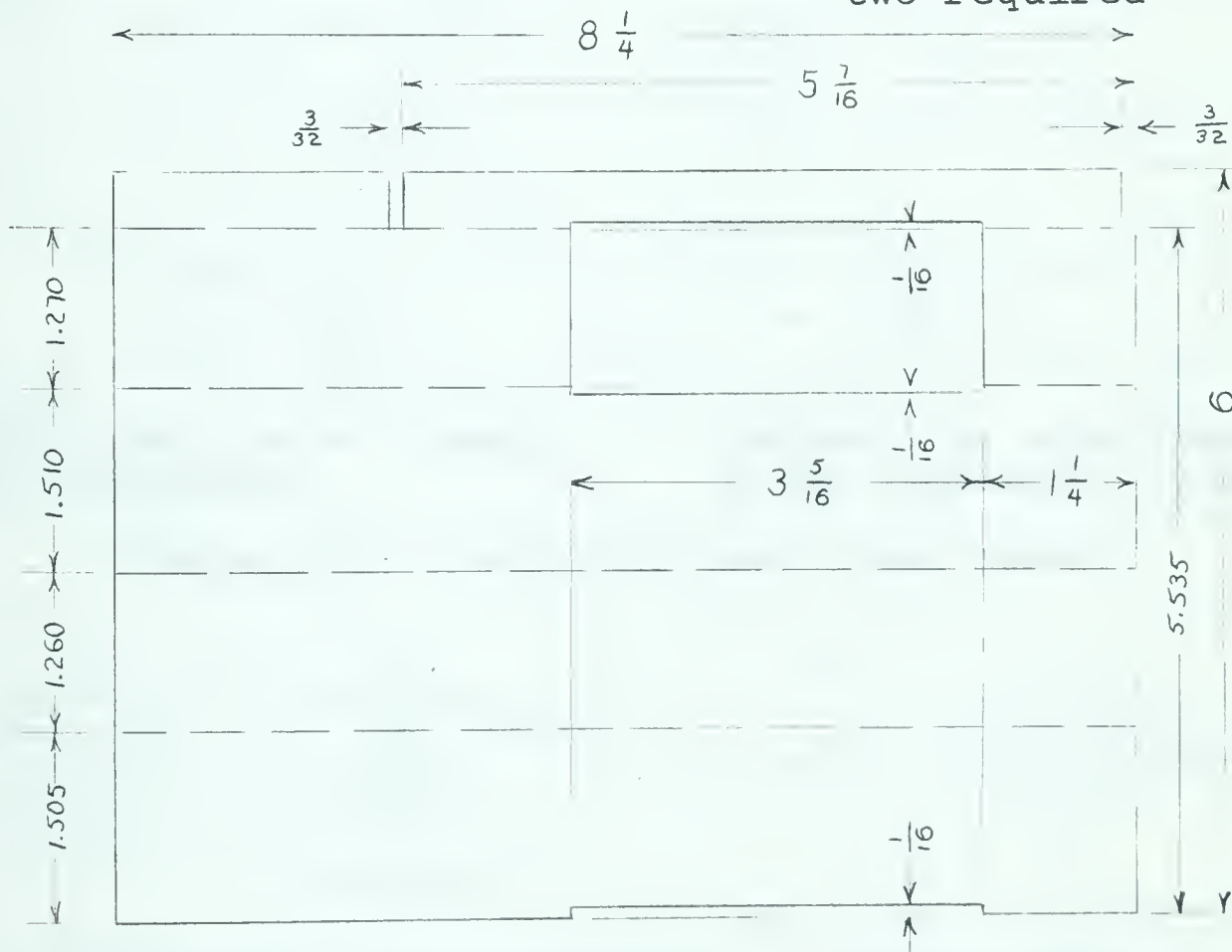


Outside wall of middle-side counters - - two required



Inside back wall of middle-side counters - - two required

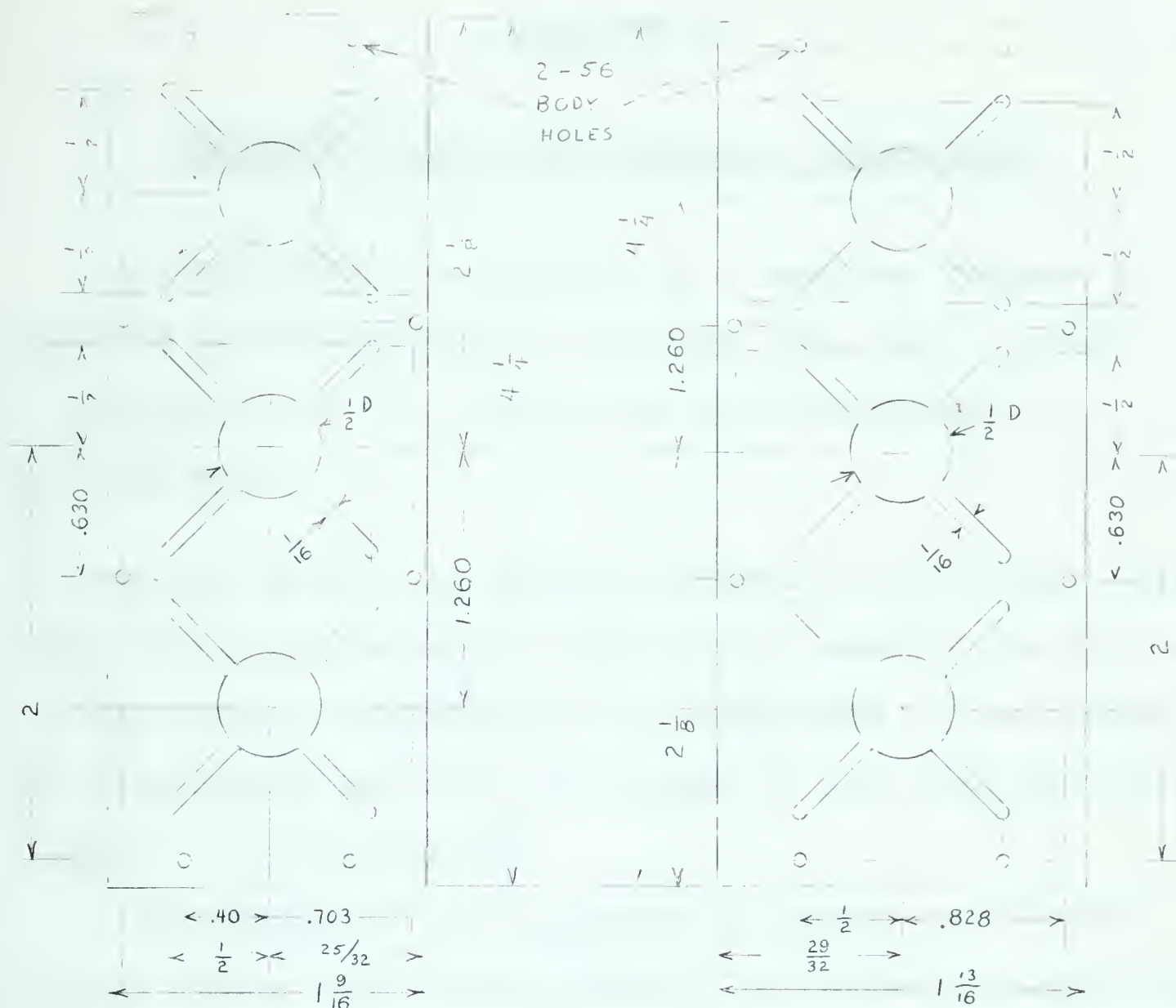
Inside front wall of middle-side counters, two required



Outer side counter outline - - - four required

(Dashed lines show positions of required 90 degree bends)

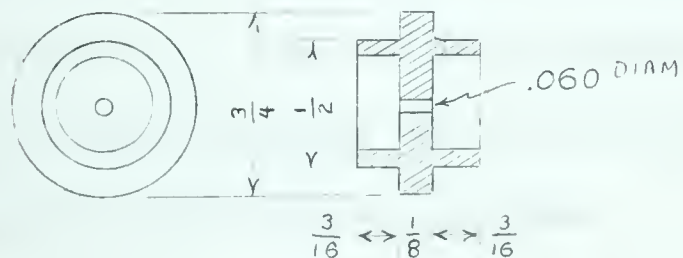
Figure A-10 Side Counter Wall Outlines (Shown approximately half size; material: 10 mil stainless steel sheet)



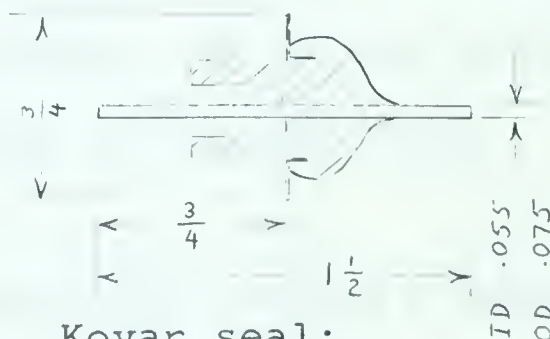
Support for center counter front insulators

Support for side counter front insulators; two required

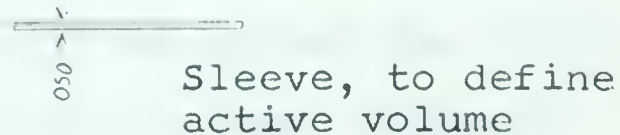
(Material: 2 mil stainless steel sheet)



Front insulators; nine required; pyrex



Kovar seal; nine required



Sleeve, to define active volume

Figure A-11 Front-end Insulators and Supports, Kovar Seals, and Counter Wire

APPENDIX B

COMPUTER PROGRAM FOR GEOMETRIC CORRECTIONS

As indicated in section 6-3, a computer program is required for determining an average value for $P_2 \cdot \cos \varphi$. A description of the program and its development is included here.

It was decided to write a program for which the input data are the parameters of the initial reaction at the target and the number of divisions into which the active volume of the polarimeter and the solid angle of the alpha particle recoil are to be divided.

The variables are designated by capitalized letter groups, rather than Greek symbols, to correspond with usage in the Fortran II language for the IBM 1620 computer.

Figure B-1 shows the experimental arrangement. The polarimeter is set in the horizontal plane at an angle TP relative to the deuteron beam direction; TP is the nominal lab angle setting of the polarimeter, and is an input parameter for the program.

The central region of the polarimeter, where a neutron scattering event may take place with the recoiling alpha particle entering a side counter, will be called the active volume of the polarimeter. This active volume, although wedge shaped (see also figure 4-12), may be considered a rectangular parallelepiped of height 9.52 cm, width 2.86 cm,

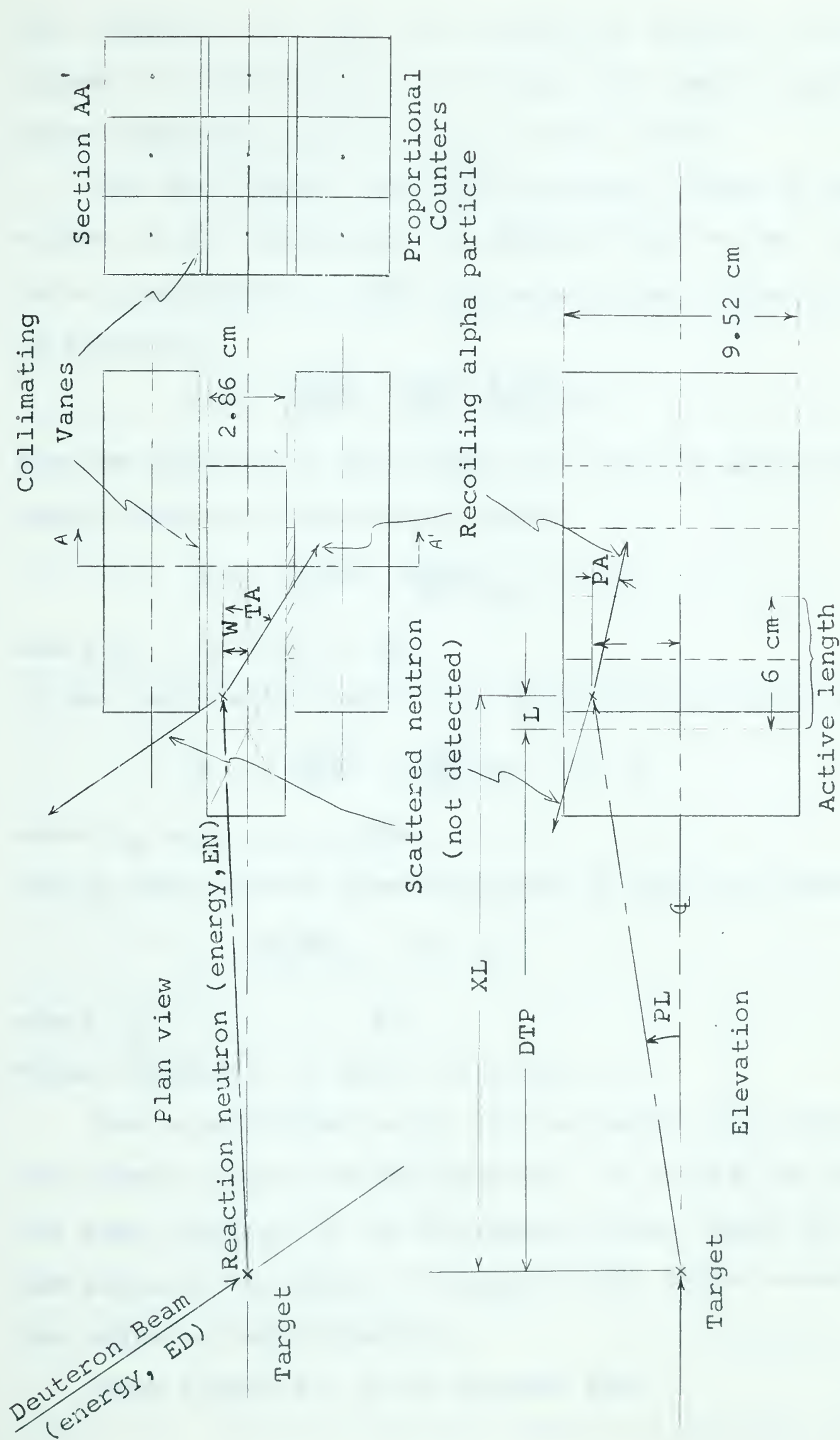


Figure B-1 Schematic Diagram of Polarimeter Showing Lab Angles and Distances

and length 6.0 cm. For the purpose of analysis, the active volume is considered to be divided into smaller rectangular parallelepipeds, which will be called cells.

Let the height, the width, and the length of the active volume of the polarimeter be divided into PH, PW, and PTL parts respectively. Then the uncorrected volume of a cell is given by

$$DVU = \frac{9.52}{PH} \cdot \frac{2.86}{PW} \cdot \frac{6.00}{PTL} \text{ cm}^3. \quad - - - \text{ B-1}$$

And the position of the center of a cell is given by the height above the horizontal plane:

$$H = - \frac{9.52}{2} + \frac{9.52}{PH} (n_H - \frac{1}{2}) \text{ cm} \quad - - - \text{ B-2}$$

where $n_H = 1, 2, \dots, PH$;

by the horizontal distance to the left of polarimeter axis:

$$W = - \frac{2.86}{2} + \frac{2.86}{PW} (n_W - \frac{1}{2}) \text{ cm} \quad - - - \text{ B-3}$$

where $n_W = 1, 2, \dots, PW$;

and by the distance from the front of the polarimeter:

$$L = \frac{6.00}{PL} (n_L - \frac{1}{2}) \text{ cm} \quad - - - \text{ B-4}$$

where $n_L = 1, 2, \dots, PL$.

These distances are shown in figure B-1.

For a particular cell, the lab angles are defined for the neutron beam from the reaction: PL is the lab angle of the beam relative to the horizontal plane, while TL is the lab angle of the beam in the horizontal plane relative to the deuteron beam direction.

From figure B-1 it is evident that

$$TL = TP \cdot \frac{\pi}{180} + \arctan \left(\frac{W}{XL} \right), \quad - - - \quad B-5$$

where $XL = DTP + L$, and TP is the nominal lab angle setting of the polarimeter, in degrees.

One also sees that $\tan PL = \frac{-H}{(XL^2 + W^2)}$ - - - B-6

Since the problem of relating angles arises several times, it is convenient at this point to outline seven different lab coordinate systems, and transformations between them. The coordinate systems are numbered; axes for a particular coordinate system will be labelled with a subscript equal to the number of the coordinate system.

1. The deuteron coordinate system has the z_1 axis horizontal and along the deuteron beam direction, the x_1 axis is horizontal and 90° to the left of z_1 , and the y_1 axis is vertical and upwards.

2. The polarimeter coordinate system is produced from coordinate system 1 by a rotation about the y_1 axis through an angle TP , the nominal lab angle setting of the polarimeter. Axis z_2 points horizontally along the axis of the polarimeter, while the y_2 axis is vertical.

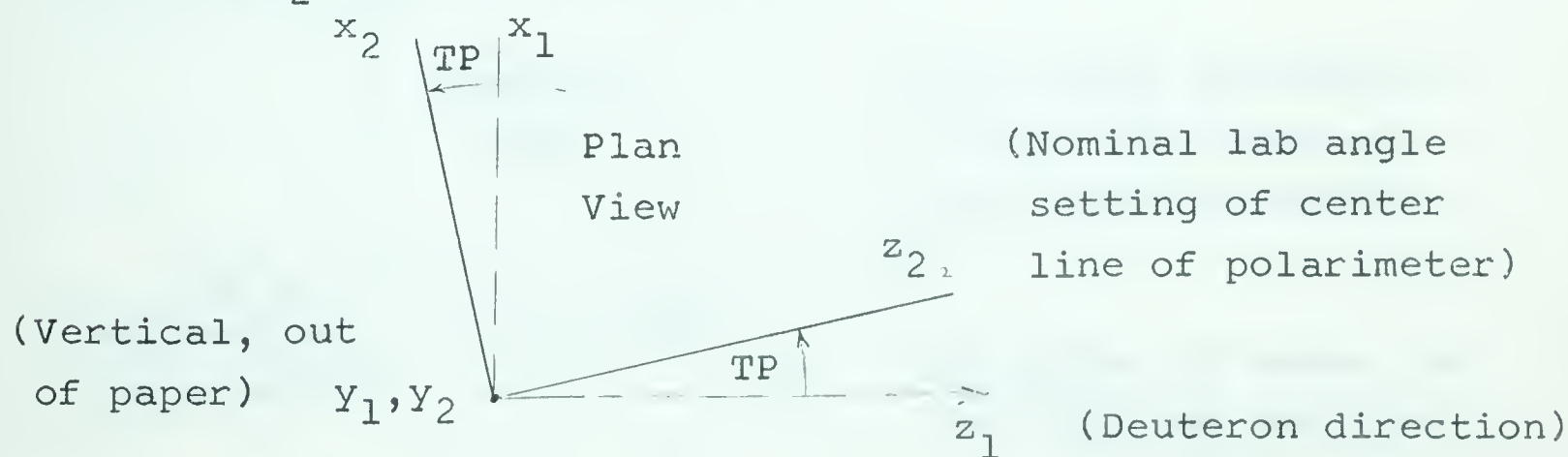


Figure B-2 Relation Between Coordinate Systems 2 and 1

3. The reaction neutron, horizontal coordinate system is produced from coordinate system 1 by a rotation about the y_1 axis through an angle TL . Axis z_3 points along the horizontal projection of the direction of the reaction neutron, while the y_3 axis is vertical.

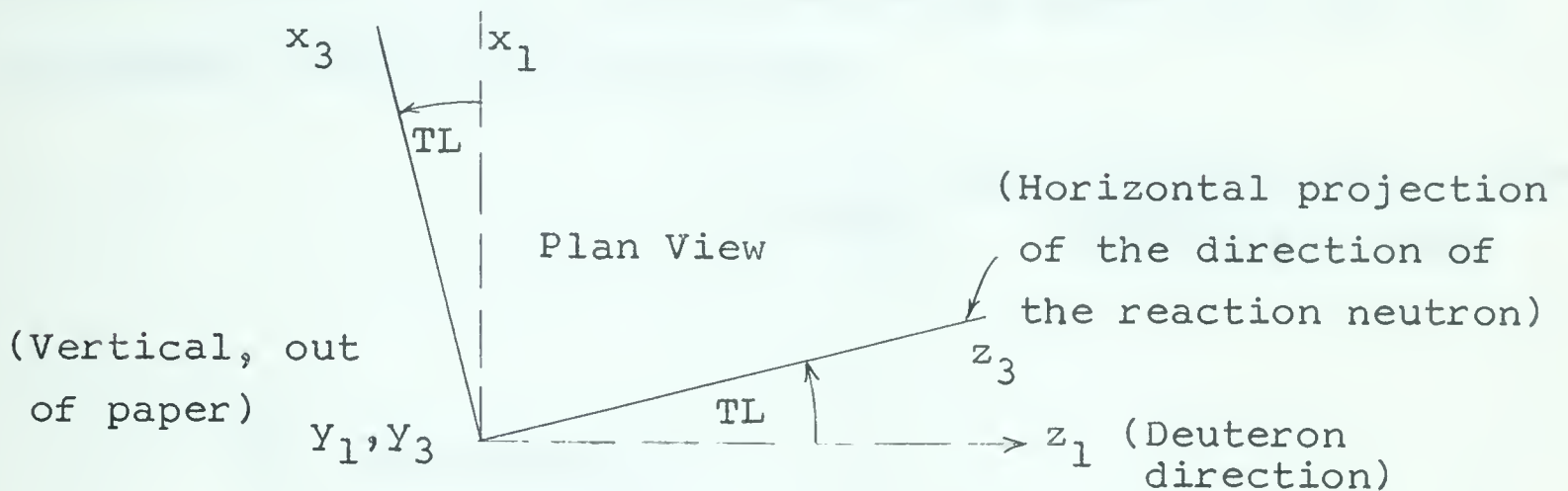


Figure B-3 Relation Between Coordinate Systems 3 and 1

4. The reaction neutron coordinate system is produced from coordinate system 3 by a rotation about the horizontal axis x_3 through an angle PL (PL is positive downwards - - see figure B-1). Axis z_4 points exactly in the direction of the reaction neutron; axis x_4 is horizontal.

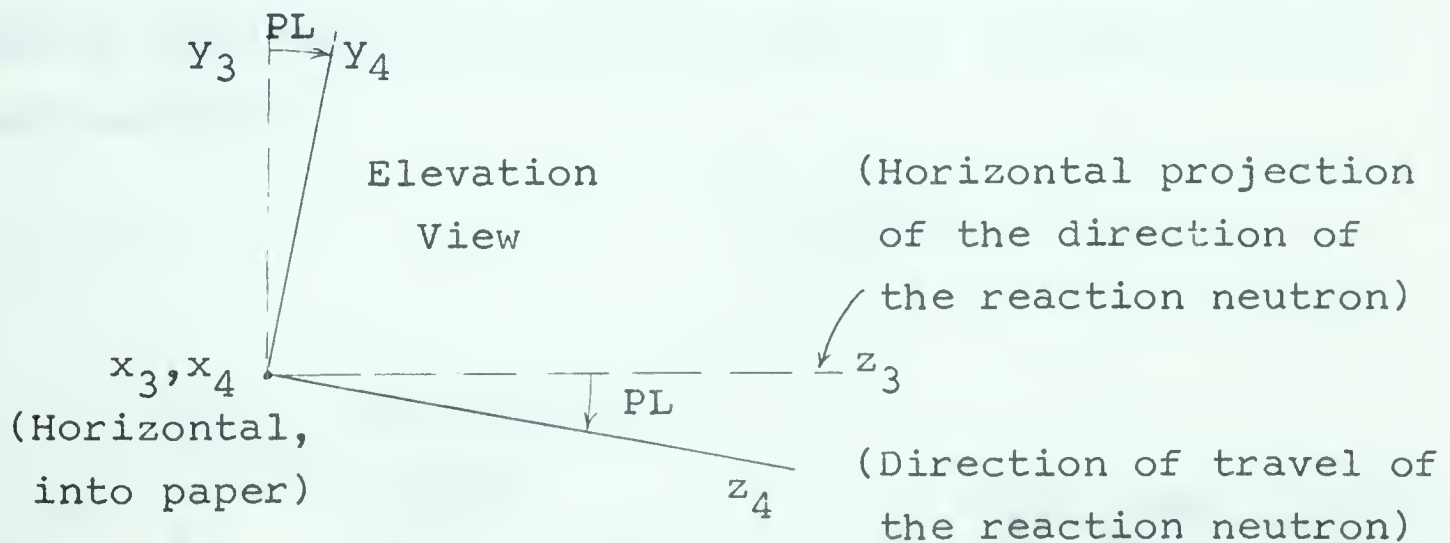


Figure B-4 Relation Between Coordinate Systems 3 and 4

5. The scattering-plane coordinate system is produced from coordinate system 4 by a rotation about the z_4 axis through an angle PAP. (PAP is the angle between the scattering plane and the x_4 - z_4 plane). Axis z_5 coincides with axis z_4 , and points in the direction of the reaction neutron; axis x_5 lies in the scattering plane, and axis y_5 is normal to the scattering plane.

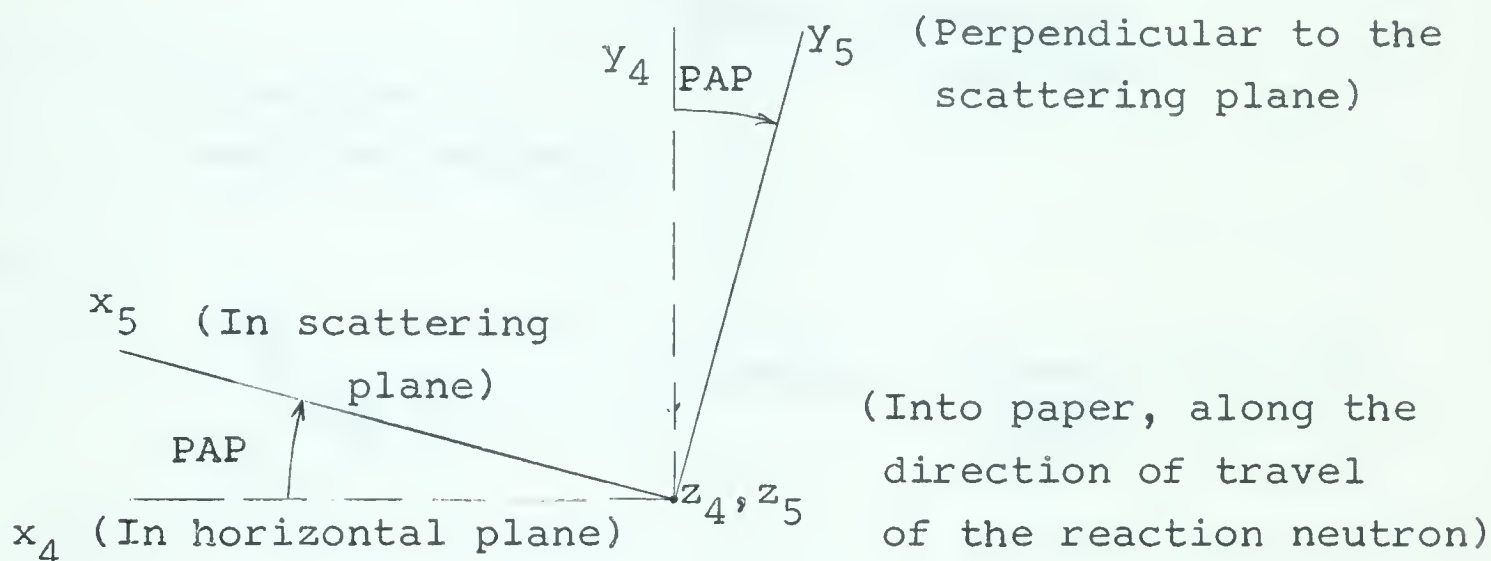


Figure B-5 Relation Between Coordinate Systems 4 and 5

6. The reaction-plane coordinate system is produced from coordinate system 1 by a rotation about the z_1 axis through an angle XI. Axis z_6 coincides with axis z_1 and lies in the deuteron direction; axis y_6 is normal to the reaction plane.

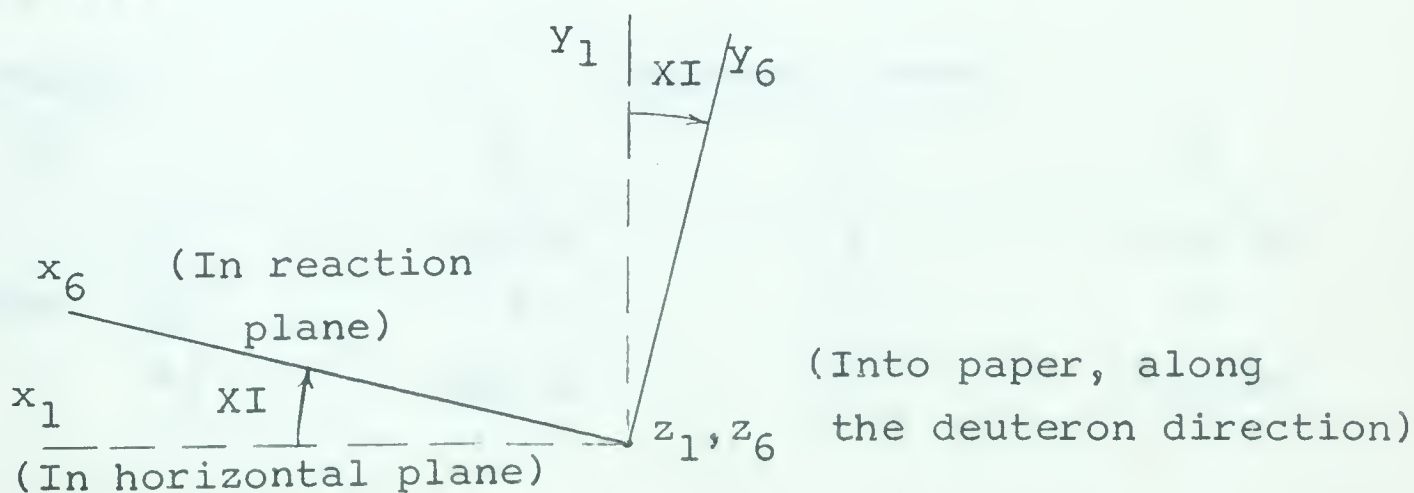


Figure B-6 Relation Between Coordinate Systems 1 and 6

7. The reaction-plane, reaction neutron coordinate system is produced from coordinate system 6 by a rotation about the y_6 axis through an angle TZZ. TZZ is the reaction neutron laboratory polar angle relative to the deuteron beam direction. Axis z_7 lies along the direction of the reaction neutron, while axis y_7 is normal to the reaction plane (and coincides with y_6).

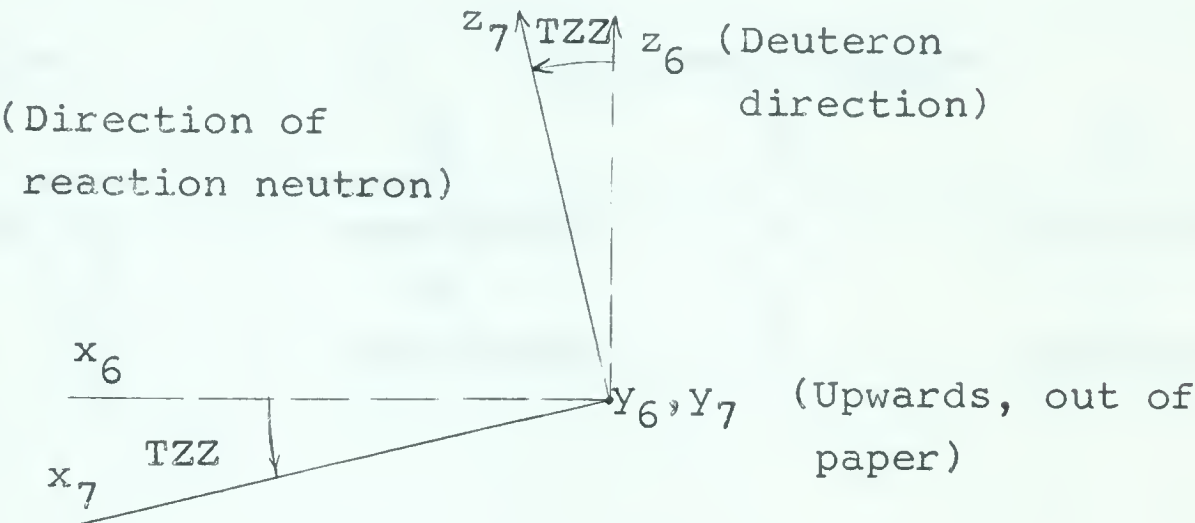


Figure B-7 Relation Between Coordinate Systems 6 and 7

Seven matrices are shown below for relating component lengths in the different coordinate systems. The items tabulated in the matrices are the direction cosines between the axes indicated by the headings.

Transformation Matrix 2-1		1. Deuteron System		
		x_1	y_1	z_1
2. Polarimeter System	x_2	$\cos TP$	0	$-\sin TP$
	y_2	0	1	0
	z_2	$\sin TP$	0	$\cos TP$

Transformation Matrix 3-1		1. Deuteron System		
		x_1	y_1	z_1
3. Reaction	x_3	$\cos TL$	0	$-\sin TL$
Neutron	y_3	0	1	0
Horizontal	z_3	$\sin TL$	0	$\cos TL$
System				
Transformation Matrix 3-2		2. Polarimeter system		
		x_2	y_2	z_2
3. Reaction	x_3	$\cos(TL-TP)$	0	$-\sin(TL-TP)$
Neutron	y_3	0	1	0
Horizontal	z_3	$\sin(TL-TP)$	0	$\cos(TL-TP)$
System				
Transformation Matrix 3-4		4. Reaction-neutron System		
		x_4	y_4	z_4
3. Reaction	x_3	1	0	0
Neutron	y_3	0	$\cos PL$	$-\sin PL$
Horizontal	z_3	0	$\sin PL$	$\cos PL$
System				
Transformation Matrix 5-4		4. Reaction-neutron System		
		x_4	y_4	z_4
5. Scattering	x_5	$\cos PAP$	$\sin PAP$	0
Plane	y_5	$-\sin PAP$	$\cos PAP$	0
System	z_5	0	0	1

Transformation Matrix 6-1		1. Deuteron System		
		x_1	y_1	z_1
6. Reaction	x_6	$\cos XI$	$\sin XI$	0
Plane	y_6	$-\sin XI$	$\cos XI$	0
System	z_6	0	0	1

Transformation Matrix 6-7		7. Reaction-plane, Reaction-neutron System		
		x_7	y_7	z_7
6. Reaction	x_6	$\cos TZZ$	0	$\sin TZZ$
Plane	y_6	0	1	0
System	z_6	$-\sin TZZ$	0	$\cos TZZ$

To determine the laboratory reaction angle for a particular cell, it is convenient first to refer to figure B-8, which illustrates the angles between the reaction neutron direction and the different coordinate axes.

Consider a given length along the z_4 (or, identical z_7) axis. The component of this length along the z_1 (or, equivalent z_6) axis has a definite value regardless of whether one goes more directly by way of the angle TZZ or in two stages, by way of PL and TL. Thus,

$$\cos TZZ = (\cos PL) (\cos TL) \quad - - - \quad B-7$$

Since the reaction process is probably not isotropic, a correction for variation in reaction cross section should normally be applied; and it is convenient to apply such a correction to the volume, DVU, of the cell. The volume,

when corrected for cross section variation, will be called DV.

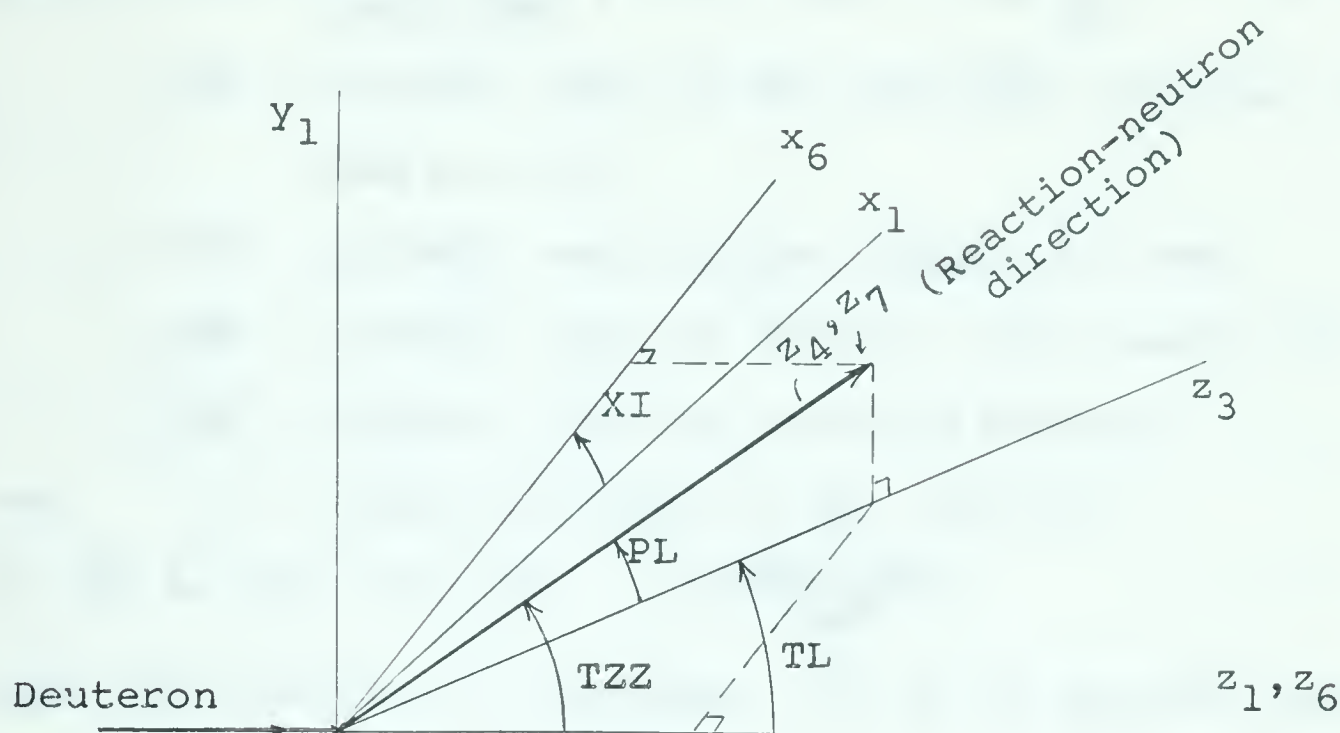


Figure B-8 Reaction-neutron Direction

An initial analytical fit must be made to cross section values, as a function of lab reaction angle TZZ. The cross section, normalized to a maximum value of one, is fitted to the expression $RCSN = A + B \cos (C(TZZ) + D)$. - - - B-8

Thus, $DV = (RCSN)DVU$. - - - B-9

Values for A, B, C and D must be put as input data for a particular computer run. For normalization, A + B must equal 1.

TZZ is the laboratory angle at which the reaction neutron emerges from the target to strike the volume cell under consideration. The neutron energy is given (Monahan, 1960) in terms of the incident deuteron energy, ED, and the reaction parameters by the equation

$$EN = ED \frac{(AMD)(AMN)}{(AMN + AMP)^2} \left[(ETA + \cos^2 TZZ) \pm \cos TZZ \right]^2 - - B-10$$

$$\text{where } \eta = \frac{AMN + AMP}{(AMD)(AMN)} \left[AMP - AMD + AMP \frac{Q}{ED} \right], \quad - - - \quad \text{B-11}$$

AMD = (atomic) mass of the incident particle, with energy, ED,

AMT = (atomic) mass of the target, at rest,

AMN = (atomic) mass of neutron, with energy EN,

AMP = (atomic) mass of reaction product,

and Q = energy released in the reaction.

$$\text{If } ED \text{ is less than } E_F = -Q \frac{AMD + AMT}{AMT}, \quad - - - \quad \text{B-12}$$

then the reaction is forbidden. If ED is greater than EF

$$\text{but less than } E_B = Q \frac{AMP}{AMD - AMP}, \quad - - - \quad \text{B-13}$$

then two distinct energy groups are obtained, one corresponding to TZZ less than 90°, and one to TZZ greater than 90°. These energy groups are determined by using either the plus or the minus sign in equation B-10.

Finally, for ED greater than EB, only a single energy group of neutrons comes from the reaction at a given lab angle; and for these the plus sign is to be used in equation B-9.

In the same way that the active volume of the polarimeter is divided into smaller parts, so also the solid angle of possible alpha recoil is divided into smaller elements for averaging. TA and PA are the laboratory polar and azimuthal recoil angles, respectively, relative to the polarimeter coordinate system 2. Let the possible azimuthal angles and polar angles of recoil be divided into PPA and PTA parts, respectively. Then the mean values for particular

segments of recoil are given by

$$TA = \frac{\pi}{180} \left[17.5 + \frac{10}{PTA} (n_{TA} - \frac{1}{2}) \right] \quad - - - \quad B-14$$

where $n_{TA} = 1, 2, \dots, PTA$,

$$\text{and by} \quad PA = \frac{\pi}{180} \left[-10 + \frac{20}{PPA} (n_{PA} - \frac{1}{2}) \right] \quad - - - \quad B-15$$

where $n_{PA} = 1, 2, \dots, PPA$.

The lab recoil angle of the helium nucleus in the scattering plane is the polar angle TAP in the scattering plane coordinate system number 5. Angle TAP must be expressed in terms of angles TA and PA, and then the center-of-mass scattering angle, T, of neutrons from the helium can be calculated from (Mather and Swan, 1958):

$$T = \pi - 2(TAP) \quad - - - \quad B-16$$

To determine the relationships between TAP and the angles TA and PA, consider a unit vector in the recoil direction. Its components along the axes x_2, y_2, z_2 , in the polarimeter system are seen from figure B-9 to be:

$$(\cos PA)(\sin TA), \sin PA, (\cos TA)(\cos PA) \quad - - - \quad B-17$$

respectively.

The recoil alpha direction may also be related to the reaction-neutron system, as shown in figure B-10. From this figure, it is evident that the components of the unit vector in the recoil alpha direction along the axes x_4, y_4 , and z_4 are $(\sin TAP)(\cos PAP)$, $(\sin TAP)(\sin PAP)$, $\cos TAP$.-- B-18

One can relate the quantities in expressions B-15 and B-16 through the transformation matrices. The following equations relate component lengths in different coordinate systems

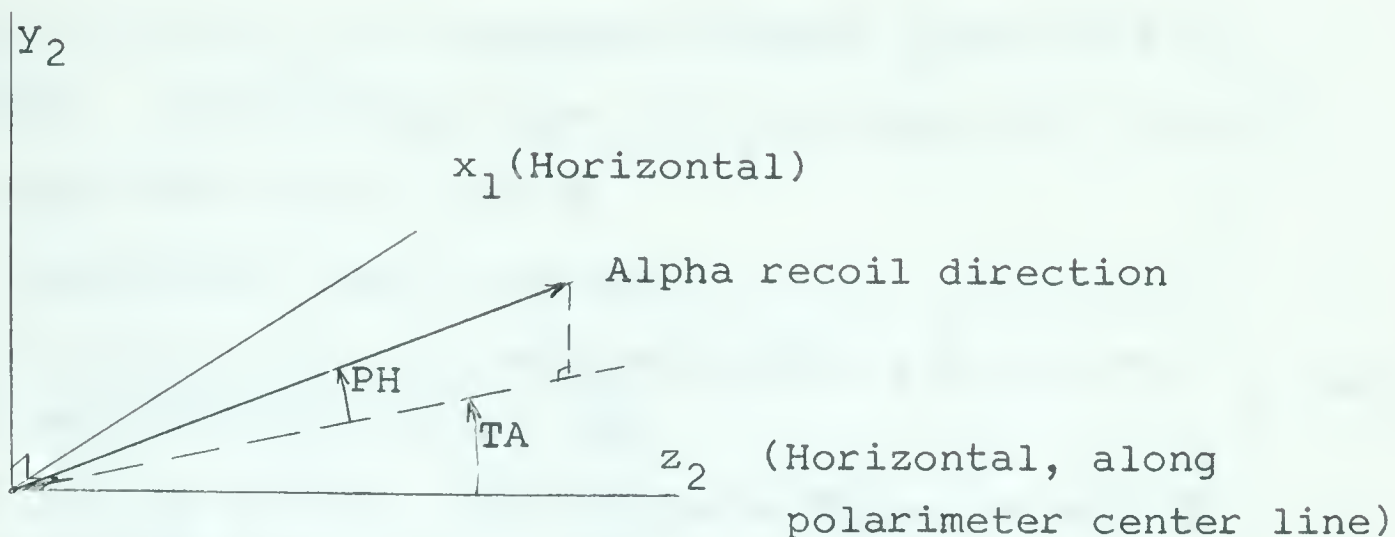


Figure B-9 Recoil Alpha Direction in the Polarimeter System, 2

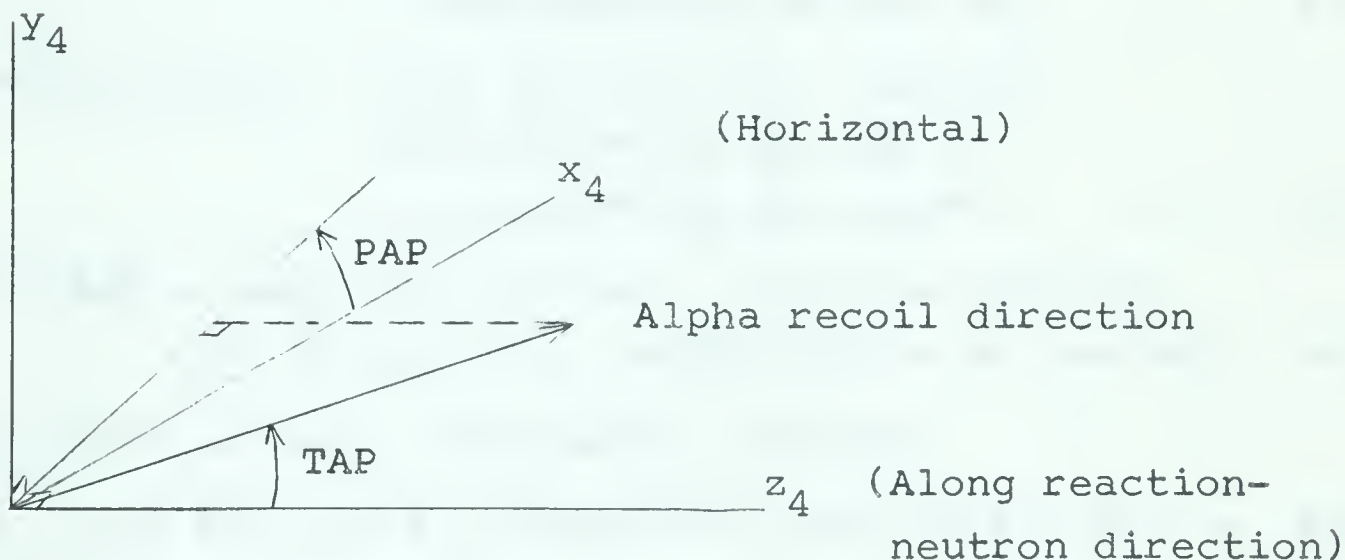


Figure B-10 Recoil Alpha Direction in the Reaction-neutron System, 4

(note that primed quantities are here used for component lengths along the corresponding axes):

$$\left. \begin{aligned} x'_4 &= x'_3 \\ y'_4 &= y'_3 (\cos PL) + z'_3 (\sin PL) \\ z'_4 &= y'_3 (-\sin PL) + z'_3 (\cos PL) \end{aligned} \right\} \text{--- B-19}$$

$$\left. \begin{aligned} \text{Also, } x'_3 &= x'_2 \cos (TL-TP) - z'_2 \sin (TL-TP) \\ y'_3 &= y'_2 \\ z'_3 &= x'_2 \sin (TL-TP) + z'_2 \cos (TL-TP) \end{aligned} \right\} \text{--- B-20}$$

But x_2' , y_2' , and z_2' are component lengths given by B-17.

Therefore, substituting first B-20 and then B-17 in B-19:

$$\left. \begin{aligned} x_4' &= \cos(TL-TP) \cos PA \sin TA \\ &\quad - \sin(TL-TP) \cos PA \cos TA \\ y_4' &= \cos PL \sin PA + \sin PL [\sin(TL-TP) \cos PA \sin TA \\ &\quad + \cos(TL-TP) \cos PA \cos TA] \\ z_4' &= -\sin PL \sin PA + \cos PL [\sin(TL-TP) \cos PA \sin TA \\ &\quad + \cos(TL-TP) \cos PA \cos TA] \end{aligned} \right\} \text{---B-21}$$

Comparing expressions B-18 with equations B-21, then:

$$\begin{aligned} (\sin TAP)(\cos PAP) &= \cos(TL-TP) \cos PA \sin TA \\ &\quad - \sin(TL-TP) \cos PA \cos TA \quad \text{--- B-22} \end{aligned}$$

$$\begin{aligned} (\sin TAP)(\sin PAP) &= (\cos PL)(\sin PA) + (\sin PL) \cdot \\ &\quad \cdot [\sin(TL-TP) \cos PA \sin TA + \\ &\quad \cos(TL-TP) \cos PA \cos TA] \quad \text{--- B-23} \end{aligned}$$

$$\begin{aligned} \text{and, } \cos TAP &= (-\sin PL)(\sin PA) + \cos PL [\sin(TL-TP) \cdot \\ &\quad \cdot \cos PA \sin TA + \cos(TL-TP) \cos PA \cos TA] \text{--- B-24} \end{aligned}$$

Equation B-24 is more conveniently written

$$\cos TAP = \cos PL \cos PA \cos(TA+TP-TL) - \sin PL \sin PA \quad \text{--- B-25}$$

from which TAP can be determined.

One can also solve equations B-22 and B-23 for PAP:

$$\tan PAP = \frac{\cos PL \sin PA + \sin PL \cos PA \cos(TA+TP-TL)}{\cos PA \sin(TA+TP-TL)} \text{--- B-26}$$

Having determined the lab recoil angle TAP from equation B-25, one can then obtain the actual center-of-mass scattering angle, T, of the neutron from equation B-16.

It is necessary to obtain an expression for $CP \equiv \cos \phi$, where ϕ is the angle between the reaction plane and the scattering plane. The axis, y_5 , is normal to the scattering

plane, while axes y_6 and y_7 are both normal to the reaction plane. ϕ is, therefore, the angle between axes y_5 and y_6 (or y_7).

Consider a unit vector along the y_6 (or y_7) axis. The length of the component of this vector along the y_5 axis is equal to CP. Using the rotation matrices and denoting, as before, lengths by primed quantities, then:

$$y_5' = -x_4' \sin \text{PAP} + y_4' \cos \text{PAP} \quad - - - \quad \text{B-27}$$

$$= -x_3' \sin \text{PAP} + (y_3' \cos \text{PL} + z_3' \sin \text{PL}) \cos \text{PAP} \quad - - - \quad \text{B-28}$$

$$= -\sin \text{PAP}(x_1' \cos \text{TL} - z_1' \sin \text{TL}) + \cos \text{PAP} \cdot$$

$$\cdot [y_1' \cos \text{PL} + \sin \text{PL}(x_1' \sin \text{TL} + z_1' \cos \text{TL})] \quad - - - \quad \text{B-29}$$

$$= y_6' [\sin \text{XI}(\sin \text{PAP} \cos \text{TL} - \cos \text{PAP} \sin \text{PL} \sin \text{TL}) + \cos \text{XI} \cos \text{PAP} \cos \text{PL}] \quad - - - \quad \text{B-30}$$

Note that in the last step, the fact was used that both x_6' and z_6' are zero for a unit vector along y_6 .

$$\text{Thus, CP} = \sin \text{XI}(\sin \text{PAP} \cos \text{TL} - \cos \text{PAP} \sin \text{PL} \sin \text{TL}) + \cos \text{XI} \cos \text{PAP} \cos \text{PL} \quad - - - \quad \text{B-31}$$

The angle XI is expressed in terms of PL and TL in equation

$$\text{B-32:} \quad \tan \text{XI} = - \frac{\tan \text{PL}}{\sin \text{TL}} \quad - - - \quad \text{B-32}$$

This relation can be obtained using the conversion matrices or by observation from figure B-9. (Note that PL is positive downwards).

The element of solid scattering angle in the polarimeter is defined by increments in TA and PA, called DTA and DPA, respectively. The element of solid angle, DOG, in the center-of-mass system, which must be expressed in

terms of DTA and DPA, is given by

$$\text{DOG} = (\sin T) dT d\phi_{\text{cm}} \quad - - - \quad \text{B-33}$$

But $T = \pi - 2(\text{TAP})$, so that

$$dT = - 2 d(\text{TAP}) \equiv - 2 \text{DTAP} \quad - - - \quad \text{B-34}$$

Also, ϕ_{cm} for the neutron equals minus PAP, so that

$$d\phi_{\text{cm}} = - d(\text{PAP}) \equiv - \text{DPAP}. \quad - - - \quad \text{B-35}$$

$$\text{Thus, } \text{DOG} = (\sin T) 2(\text{DTAP})(\text{DPAP}) \quad - - - \quad \text{B-36}$$

TAP is expressed in terms of TA and PA in equation B-25. Taking differentials, one finds from this equation

$$\begin{aligned} \text{that } \text{DTAP} = (\sin \text{TAP})^{-1} & \left[\text{DTA} \cos \text{PL} \cos \text{PA} \sin(\text{TA} + \text{TP} - \text{TL}) \right. \\ & + \text{DPA} (\cos \text{PL} \sin \text{PA} \cos(\text{TA} + \text{TP} - \text{TL}) \\ & \left. + \sin \text{PL} \cos \text{PA}) \right] \quad - - - \quad \text{B-37} \end{aligned}$$

Similarly, by taking differentials in equation B-24, one finds that

$$\begin{aligned} \text{DPAP} = & \left[\text{DPA} \cos \text{PL} \sin(\text{TA} + \text{TP} - \text{TL}) - \text{DTA} (\cos \text{PL} \cos \text{PA} \sin \text{PA} \right. \\ & \left. \cos(\text{TA} + \text{TP} - \text{TL}) + \sin \text{PL} \cos^2 \text{PA}) \right] / \left[(1 + \tan^2 \text{PAP}) \cos^2 \right. \\ & \left. \text{PA} \sin^2(\text{TA} + \text{TP} - \text{TL}) \right] \quad - - - \quad \text{B-38} \end{aligned}$$

From the center-of-mass scattering angle, T, and the energy EN of the incoming reaction neutron, the scattering cross section, X, and polarization, P, can be calculated using known values for the phase shifts for the scattering process.

The differential scattering cross section, X, and the polarization, P, are calculated from phase shifts using formulae 2-6 and 2-7. An empirical fit to the phase shift data of Seagrave (1953) is given, within about three percent for all values, by equations B-39 to B-44 inclusive. (See

also figure 2-2).

$$-DZ = -0.49 \text{ EN} + 26.5 (\text{EN})^{\frac{1}{2}} \quad - - - \text{ B-39}$$

$$-DTM = 0.30 \text{ EN} + 0.40 (\text{EN})^2 \quad - - - \text{ B-40}$$

For EN less than or equal to 4 Mev:

$$DOP = 94.0 + 17.0 - 2.5 (\text{EN})^2 \quad - - - \text{ B-41}$$

$$DOM = 7.0 \text{ EN} + 0.5 (\text{EN})^2. \quad - - - \text{ B-42}$$

For EN greater than 4 Mev but less than 20 Mev:

$$DOP = 132.7 - 2.95 \text{ EN} \quad - - - \text{ B-43}$$

$$DOM = 36.0 + 2.75 \text{ EN} - 0.1528 (\text{EN})^2. \quad - - - \text{ B-44}$$

Using these phase shifts, equations 2-8 and 2-9 may be written more explicitly as

$$g = \frac{1}{k} \left\{ \sin \delta_0^+ e^{i\delta_0^+} + \cos T \left[2 \sin \delta_1^+ e^{i\delta_1^+} + \sin \delta_1^- e^{i\delta_1^-} \right] + (3 \cos^2 T - 1) \sin \delta_2^- e^{i\delta_2^-} \right\} \quad - - - \text{ B-45}$$

$$\text{and } h = \frac{1}{k} \left\{ \sin T \left[\sin \delta_1^+ e^{i\delta_1^+} - \sin \delta_1^- e^{i\delta_1^-} \right] + 3 \sin^2 T \sin \delta_2^- e^{i\delta_2^-} \right\}. \quad - - - \text{ B-46}$$

For computation one must consider separately the real and imaginary parts of g and h. The real part of g is designated

$$\text{GR: } GR = (GR0) + (GR1) \cos T + (GR2) \cos^2 T \quad - - - \text{ B-47}$$

$$\text{where } GR0 = k^{-1} (\sin \delta_0^+ \cos \delta_0^+ - \sin \delta_1^- \cos \delta_1^-)$$

$$GR1 = k^{-1} (2 \sin \delta_1^+ \cos \delta_1^+ + \sin \delta_1^- \cos \delta_1^-)$$

$$GR2 = k^{-1} (3 \sin \delta_2^- \cos \delta_2^-).$$

The imaginary part of g is designated GI:

$$GI = (GI0) + (GI1) \cos T + (GI2) \cos^2 T \quad - - - \text{ B-48}$$

$$\text{where } GI0 = k^{-1} (\sin^2 \delta_0^+ - \sin^2 \delta_2^-)$$

$$GI1 = k^{-1} (2 \sin^2 \delta_1^+ + \sin^2 \delta_1^-)$$

$$GI2 = k^{-1} (3 \sin^2 \delta_2^-).$$

The real part of h is designated HR:

$$HR = (HR1) \sin T + (HR2) \sin^2 T \quad - - - \quad B-49$$

where $HR1 = k^{-1} (\sin \delta_1^+ \cos \delta_1^+ - \sin \delta_1^- \cos \delta_1^-)$

$$HR2 = k^{-1} (3 \sin \delta_2^- \cos \delta_2^-) \equiv GR2.$$

And finally, the imaginary part of h is denoted by HI:

$$HI = (HI1) \sin T + (HI2) \sin^2 T \quad - - - \quad B-50$$

where $HI1 = k^{-1} (\sin^2 \delta_1^+ - \sin^2 \delta_1^-)$

$$HI2 = (3 \sin^2 \delta_2^-) \equiv GI 2.$$

The differential scattering cross section is then given by

$$X = |g|^2 + |h|^2 = (GR)^2 + (GI)^2 + (HR)^2 + (HI)^2 \quad - - - \quad B-51$$

while the polarization is given by

$$P = \frac{-2 \operatorname{Im} (g^* h)}{|g|^2 + |h|^2} = 2 X^{-1} [(GR)(HI) - (GI)(HR)] \quad - - - \quad B-52$$

The average value of $P_2 \cos \varphi$ will be denoted by EDP, and is given by equation B-53:

$$EDP \equiv \overline{P \cos \varphi} = \frac{\int X \cdot P \cos \varphi}{\int X} \equiv \frac{SSXP}{SSX} \quad - - - \quad B-53$$

where $SSX = \int X$ is an integral of the cross section over volume elements and over elements of solid angle recoil, and $SSXP = \int X \cdot P \cos \varphi$ is a corresponding integral over the same elements.

A flow diagram for the program is shown as figure B-11.

An alphabetical list of definitions of symbols used in the program is given as table B-1, while the Fortran II statements are given as table B-2.

Three input cards are required for a particular reaction. On the first card, columns 7 to 21 are used for alphameric identification of the reaction; as, for example, B11(D,N)Cl2. Then, four groups of seven columns each are allotted to AMD, AMT, AMN and AMP, respectively, in atomic mass units to five decimal places. Finally, six columns are used for the Q of the reaction, in Mev, to four decimal places.

The data and format required for the second and third input cards are similar, and are apparent from the Fortran II statements given.

All four of the sense switches available on an IBM 1620 computer are used in this program, and should be in the 'OFF' position unless the particular function indicated below is desired.

With sense switch 1 in the 'ON' position, if EN is double-valued, then asymmetry factors are computed for the 'abnormal' values of EN (i.e., values of EN obtained when the negative sign is used in equation B-10).

With sense switch 2 in the 'ON' position, data is typed out by the machine for individual values of TA and PA for each cell. Except for testing purposes, this data output is unnecessary and normally would consume too much computer running time.

With sense switch 3 in the 'ON' position, data is typed out for individual 'layers' of active volume cells.

With sense switch 4 in the 'ON' position the polarimeter

is considered in three layers, and asymmetry factors computed separately for the central one-third layer, and for the combination of the two outer one-third layers. This is to allow for the possibility of electronic failure in the part of the polarimeter but where complete data is still available for one of the two segregated portions of the polarimeter. Sense switch 4 should only be 'ON' if PH equals 3, or higher multiples of 3.

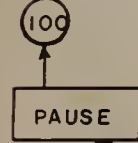
Shortly after the program has started, a general heading 'Helium Neutron Polarimeter Asymmetry Calculation' will be typed out and then all the input data is typed out for reference and identification.

Identifying information is typed out with each line of results. How much data is typed out depends upon the positions of the sense switches.

After completing calculations for the input data, the machine will pause until given further instructions; at this time another set of input cards can be fed into the machine for processing.

A FORTRAN II DIGITAL COMPUTER PROGRAM
FOR ANALYSIS OF NEUTRON POLARIZATION DATA

Encircled numbers refer to statement numbers.
Bracketed numbers refer to equations given under "Analysis"



The flowchart describes the logic for calculating the solid angle. It begins with a loop for calculating the solid angle for each element of the rectangular area (loop PA). The process involves calculating the distance (BN, EN), determining the type of element (EN has two values or is single valued), and calculating the solid angle (DZ, DTM, DOP, DOM, SDZ, CDZ, SDTM, CDTM, SDOP, CDOP, SDOM, CDOM, HK, GRI, GR, GIO, GII, GI2, HRI, HR2, HI1, HI2). The solid angle is then added to the total solid angle (PA). The process continues until all elements are processed (loop PA ends). The final solid angle (PA) is then used to calculate the total solid angle (TA) for the entire rectangular area (loop TA). The process ends with the calculation of the solid angle (SPA, CPA) and the output of the results.

May 1964 G.R.M.

Table B-1 Alphabetical List of Definitions and Symbols

AMD	mass of incoming particle (deuteron), in amu
AMN	mass of neutron, in amu
AMP	mass of product nucleus from the reaction, in amu
AMT	mass of target nucleus, in amu
BN	negative factor in computation of reaction neutron energy
BP	positive factor in computation of the reaction neutron energy
CDOM	cosine of phase shift angle DOM
CDOP	cosine of phase shift angle DOP
CDTM	cosine of phase shift angle DTM
CDZ	cosine of phase shift angle DZ
CP	cosine of angle between reaction and scattering planes
CPA	cosine of angle PA
CPAP	cosine of angle PAP
CPL	cosine of angle PL
CT	cosine of angle T
CTA	cosine of angle TA
CTAP	cosine of angle TAP
CTAPL	cosine of angle (TA+TP-TL)
CTL	cosine of angle TL
CTZZ	cosine of angle TZZ
CXI	cosine of angle XI
DH	incremental height of volume cell, in cm
DL	incremental length of volume cell, in cm
DOG	element of solid angle of scattering in steradians
DOM	neutron-alpha scattering phase shift, delta one minus
DOP	neutron-alpha scattering phase shift, delta one plus
DPA	increment in recoil angle PA
DPAP	increment in angle PAP
DSSPXP	increment in double sum of PXP
DSSV	increment in double sum of cell volumes
DSSX	increment in double sum of cross section, X
DTA	increment in recoil angle, TA
DTAP	increment in angle TAP
DTM	neutron-alpha scattering phase shift, delta two minus
DTP	distance from target to active volume
DV	cell volume, normalized for cross section, in cc
DVU	cell volume, or increment to active volume, in cc
DW	incremental width of volume cell, in cm
DZ	neutron-alpha scattering phase shift, delta zero
EB	a limiting value for the incoming particle energy, Mev
ED	energy, in Mev, of incoming particle in lab
EDD	increment in energy of incoming particle, in Mev
EDI	initial lab energy of incoming particle, in Mev
EDF	final lab energy of incoming particle, in Mev
EDP	average value of $P \cos \phi$
EDPC	average value of $P \cos \phi$ for central counters only
EDPTB	average value of $P \cos \phi$ for top plus bottom counters

EF	limiting value for the incoming particle energy, below which no reaction can occur
EN	calculated energy of reaction neutron, in Mev
ETA	a factor in the calculation of EN
F	a constant factor, for a particular reaction, in the calculation of EN
GI	imaginary part of g
GI0	coefficient of zeroth-power terms in calculation of GI
GI1	coefficient of first-power terms in calculation of GI
GI2	coefficient of second-power terms in calculation of GI
GR	real part of g
GR0	coefficient of zeroth-power terms in calculation of GR
GR1	coefficient of first-power terms in calculation of GR
GR2	coefficient of second-power terms in calculation of GR
H	average height of volume cell above the horizontal plane, in cm
HI	imaginary part of h
HI1	coefficient of first-power terms in calculation of HI
HI2	coefficient of second-power terms in calculation of HI
HR	real part of h
HR1	coefficient of first-power terms in calculation of HR
HR2	coefficient of second-power terms in calculation of HR
HK	momentum of incoming reaction neutron, in cm^{-1}
K	stepping constant in evaluation of EN
P	polarization for a particular scattering angle
PA	phi-alpha ... the nominal recoil angle of the alpha particles relative to the horizontal plane
PAP	phi-alpha-prime ... the azimuthal angle of recoil in the reaction neutron coordinate system
PH	number of parts into which the height of the active volume is considered divided
PL	vertical angle between volume cell and horizontal plane at the target position
PPA	number of parts into which PA is divided
PTA	number of parts into which TA is divided
PTK	number of parts into which the length of the active volume is divided
PXP	product of cross section, polarization, and CP
PXPC	product of cross section, polarization, and CP for center counters only
PXPTB	product of cross section, polarization, and CP for combined top and bottom counters
PW	number of parts into which the width of the active volume is divided
Q	the amount of energy released, in Mev, during the reaction
REACT	reaction being studied; e.g., B11(D,N)C12
RCSN	normalized reaction cross section
SDOM	sine of phase shift angle DOM
SDOP	sine of phase shift angle DOP
SDTM	sine of phase shift angle DTM
SDZ	sine of phase shift angle DZ
SPA	sine of recoil angle PA
SPAP	sine of angle PAP

SPL	sine of angle PL
SPXP	sum of PXP over elements of solid angle, for a particular cell
SSPXP	sum of SPXP over volume elements (cells)
SSPXP1	intermediate sum of PXP used in segregating contributions to center layer, and to top and bottom layers
SSPXP2	intermediate double sum of PXP, over solid angles and volume cells
SSPXPB	sum of SPXP over volume elements for bottom layers
SSPXPC	sum of SPXP over volume elements for center layers
SSV	sum of SV over volumes
SSV1	intermediate double sum of volumes
SSVB	sum SSV for bottom layer cells
SSVC	sum SSV for center layer cells
SSVTB	sum SSV for top-plus-bottom layer cells
SSX	integral of scattering cross section
SSX1	intermediate sum of cross sections
SSXB	integral of scattering cross section for bottom counter
SSXC	integral of scattering cross section for central counter
SSXTB	integral of scattering cross section for top and bottom counters
ST	sine of angle T
STA	sine of angle TA
STAP	sine of angle TAP
STAPL	sine of angle (TA+TP-TL)
STL	sine of angle TL
SV	integral over solid angle for a given volume element
SX	integral of cross section over solid angle
SXI	sine of angle XI
T	center-of-mass scattering angle of neutrons on helium
TA	polar, lab recoil angle of alpha particles relative to vertical axial plane through polarimeter
TAP	polar, lab recoil angle of alpha particles in the scattering plane coordinate system 5
TL	lab angle in horizontal plane to volume cell
TP	nominal lab angle setting of polarimeter
TPAP	tangent of PAP
TPD	increment value for TP
TPF	maximum value for TP
TPI	initial value for TP
TZZ	theta zero, the angle between the reaction neutron direction and the deuteron beam direction
U	factor of $(\pi/180) = .0174533$, for conversion of angles in degrees to angles in radians
W	horizontal distance of volume cell from central plane of polarimeter
X	center-of-mass cross section for neutron helium scattering
XC	total scattering cross section for center counters
XI	angle between the reaction plane and the horizontal plane
XL	distance from target to volume cell, in cm
XTB	total scattering cross section for top-plus-bottom counters

Table B-2 Fortran II Statements for Program to Determine the Geometric Average Values of the Analyzing Power, $P_2 \cos \phi$, for the Neutron Polarimeter

```

C      SENSE SWITCH 4 OFF UNLESS PH=3OR MORE
      DIMENSION REACT(5)
100 READ 1, REACT ,AMD,AMT,AMN,AMP,Q
      1 FORMAT (5A3 ,F7.5,F7.5,F7.5,F7.5,F6.4)
      READ 2, DTP,TPI,TPF,TPD,EDI,EDF,EDD,PTA,PPA,PTL,PW,PH
      2 FORMAT (F4.1,F5.1,F5.1,F4.1,F4.2,F4.2,F4.2,F3.0,F3.0,
                F3.0,F3.0,F3.
      10)
      READ 43,A,B,C,D
43  Format (F7.5,F7.5,F7.4,F7.3)
      TYPE4,REACT ,Q
      4 FORMAT (49H HELIUM NEUTRON POLARIMETER ASYMMETRY CALC
                ULATION,
      15A3 ,3H Q ,F8.4)
      TYPE 61,AMD,AMT,AMN,AMP,DTP,TPI,TPF,TPD,EDI,EDF,EDD,P
                TA PPA,PTL,PW
      1,PH,A,B,C,D
61  FORMAT(5H AMD ,F8.5,5H AMT ,F9.5,5H AMN ,F8.5,5H AMP
                ,F9.5/5H DTP
      1,F5.1,5H TPI ,F6.1,5H TPF ,F6.1,5H TPD ,F5.1/5H EDI
                ,F5.2,5H EDF ,
      2F5.2,5H EDD ,F5.2/5H PTA ,F4.0,5H PPA ,F4.0,5H PTL ,F
                4.0,5H PW ,F
      34.0,5H PH ,F4.0/4H A ,F8.5,4H B ,F8.5,4H C ,F8.4,
                4H D ,F8.3/)

C      CALCULATION OF CONSTANTS
      DH=9.52/PH
      DW=2.86/PW
      DL=6.0/PTL
      DVU=DH*DW*DL
      U=0.0174533
      DPA=U*20.0/PPA
      DTA=U*10.0/PTA
      F=(AMD)*(AMN)/((AMN+AMP)*(AMN+AMP))
      EF=-Q*(AMD+AMT)/AMT
      EB=Q*AMP/(AMD-AMP)
      ED=EDI
      5  ETA=((AMN+AMP)/(AMD*AMN))*(AMP-AMD+(AMP*Q/ED))
      IF(ED-EF)7,7,8
      8  TP=TPI
      6  SSV=0.0
      SSX=0.0
      SSPXP=0.0
      SSV1=0.0
      SSX1=0.0
      SSPXP1=0.0
      H=(DH/2.0)-4.76
      K=1

```



```

25 W=(DW/2.0)-1.43
23 XL=DTP+(DL/2.0)
21 SX=0.0
    SV=0.0
    SPXP=0.0
44 TL=(TP)*U+(W/XL)
    TPMTL=-W/XL
    PL=ATANF(H/SQRTF((XL*(XL)+(W*W))))
    STL=SINF(TL)
    CTL=COSF(TL)
    SPL=SINF(PL)
    CPL=COSF(PL)
    IF (ABSF(STL)-1.0E-6)47,47,46
47 IF(ABSF(PL)-1.0E-6)49,49,50
49 XI=0.0
    GO TO 51
50 IF(PL) 52,7,55
52 XI=+1.5707964
    GO TO 51
55 XI=-1.5707964
    GO TO 51
46 XI=ATANF(-SPL/(CPL*STL))
51 CXI=COSF(XI)
    SXI=SINF(XI)
48 CTZZ=CPL*CTL
    TZZ=ATANF(SQRTF(1.0/(CTZZ*CTZZ)-1.0))
    RCSN=A+B*COSF(C*TZZ+D)
    DV=RCSN*DVU
C   IF SENSE SWITCH 1 IS ON, CALC NEG EN , ... IF OFF, CA
    LC POS EN.

    IF(ED-EB)9,11,11
    9 IF(SENSE SWITCH 1)10,56
10 BN=(-CTZZ+SQRTF(ETA+((CTZZ))))
    EN=F*ED*BN*BN
    GO TO 3
11 IF (SENSE SWITCH 1)59,12
56 GO TO (57,12),K
57 TYPE 58
58 FORMAT (41H EN HAS TWO VALUES.  USE SENSE SWITCH ONE)
    K=2
12 BP=(CTZZ+SQRTF(ETA+((CTZZ)*(CTZZ))))
    EN=F*ED*BP*BP
C   CALCULATION OF PHASE SHIFTS
    3 DZ=U*(0.49*EN-26.5*(SQRTF(EN)))
    DTM=-U*(0.30*EN+0.040*EN*EN)
    IF(EN-4.0)14,14,15
14 DOP=U*(94.0+17.0*EN-2.5*EN*EN)
    DOM=U*(7.0*EN+0.5*EN*EN)
    GO TO 16
15 DOP=U*(132.7-2.95*EN)
    DOM=U*(36.0+2.75*EN-0.1528*EN*EN)
16 SDZ=SINF(DZ)
    CDZ=COSF(DZ)
    SDTM=SINF(DTM)

```



```

CDTM=COSE(DTM)
SDOP=SINF(DOP)
CDOP=COSE(DOP)
SDOM=SINF(DOM)
CDOM=COSE(DOM)
HK=(1.54617E+12)*(SQRTF(2.0*AMN*EN))
HK=1.0/HK
GRO=HKI*(SDZ*CDZ-SDTM*CDTM)
GR1=HKI*(2.0*SDOP*CDOP+SDOM*CDOM)
GR2=HKI*3.0*SDTM*CDTM
GI0=HKI*(SDZ*SDZ-SDTM*SDTM)
GI1=HKI*(2.0*SDOP*SDOP+SDOM*SDOM)
GI2=HKI*3.0*SDTM*SDTM
HR1=HKI*(SDOP*CDOP-SDOM*CDOM)
HR2=GR2
HI1=HKI*(1.0-CDOP*CDOP-SDOM*SDOM)
HI2=GI2
PA=-0.174533+DPA/2.0
13 TA=DTA/2.0+0.30543275
CPA=COSE(PA)
SPA=SINF(PA)
18 CTA=COSE(TA)
STA=SINF(TA)
STAPL=SINF(TA+TPMTL)
CTAPL=COSE(TA+TPMTL)
CTAP=CPL*CPA*CTAPL-SPL*SPA
TPAP=(CPL*SPA+SPL*CPA*CTAPL)/(CPA*STAPL)
TAP=ATANF(SQRTF(1.0/(CTAP*CTAP)-1.0))
STAP=SINF(TAP)
T=3.14159-2.0*TAP
CT=COSE(T)
ST=SINF(T)
PAP=ATANF(TPAP)
CPAP=COSE(PAP)
SPAP=SINF(PAP)
CP=SXI*(SPAP*CTL-CPAP*SPL*STL)+CXI*CPAP*CPL
GI=GI0+GI1*CT+GI2*CT*CT
GR=GRO+GR1*CT+GR2*CT*CT
HI=HI1*ST+HI2*ST*ST
HR=HR1*ST+HR2*ST*ST
X=GI*GI+GR*GR+HI*HI+HR*HR
P=2.0*(GR*HI-GI*HR)/X
DTAP=(DTA*CPL*CPA*STAPL+DPA*(CPL*SPA*CTAPL+SPL*CPA))/
(STAP)
DPAP=(DPA*CPL*STAPL-DTA*(CPL*CPA*SPA*CTAPL-SPL*CPA*CP
A))/((1.0+TPA
1P*TPAP)*CPA*CPA*STAPL*STAPL)
DOG=ST*2.0*DTAP*DPAP
SV=SV+DOG
SX=SX+X*DOG
SPXP=SPXP+X*P*CP*DOG
IF(SENSE SWITCH 2)27,28
27 TYPE 29,H,W,XL,TA,PA,T,CP,X,P,SV,SX,SPXP

```



```

29 FORMAT(3H H ,F6.2,3H W ,F6.2,4H XL ,F7.2,4H TA ,F6.3,
          4H PA ,F6.3,3
          1H T ,F6.3,4H CP ,F7.4/3H X ,E10.3,3H P ,F7.4,4H SV ,E
          10.3,4H SX ,E
          110.3,6H SPXP ,E10.3
28 TA=TA+DTA
   IF(0.47996575-TA)17,17,18
17 PA=PA+DPA
   IF(0.174533-PA)19,19,13
19 SSV=SSV+SV*DV
   SSX=SSX+SX*DV
   SSPXP=SSPXP+SPXP*DV
   IF(SENSE SWITCH 3)30,31
30 TYPE32,H,W,XL,TL,PL,XI,EN,SSV,SSX,SSPXP
32 FORMAT(3H H ,F6.2,3H W ,F6.2,4H XL ,F7.2,4H TL ,F6.3,
          4H PL ,F6.3,4
          1H XI ,F7.4,4H EN ,F7.3/5H SSV ,E10.3,5H SSX ,E10.3,7H
          SSPXP ,E10.3
          1)
31 XL=XL+DL
   IF(DTP+6.0-XL)20,20,21
20 W=W+DW
   IF(1.43-W)22,22,23
22 IF(SENSE SWITCH 4)34,33
34 DSSV=SSV-SSV1
   DSSX=SSX-SSX1
   DSSPXP=SSPXP-SSPXP1
   TYPE 36,H,DSSV,DSSX,DSSPXP
36 FORMAT(3H H ,F6.3,6H DSSV ,E10.2,6H DSSX ,E10.2,8H DS
          SPXP ,E10.2)
   SSV1=SSV
   SSX1=SSX
   SSPXP1=SSPXP
   IF(H+1.587)35,7,37
35 SSVB=SSV
   SSXB=SSX
   SSPXPB=SSPXP
   GO TO 33
37 IF(H-1.587)38,7,39
38 SSVc=SSV-SSVB
   SSXC=SSX-SSXB
   SSPXPc=SSPXP-SSPXPB
   GO TO 33
39 SSVTB=SSV-SSVC
   SSXTB=SSX-SSXC
   SSPXP2 =SSPXP-SSPXPc
33 H=H+DH
   IF(4.76-H)24,24,25
24 X=SSX/SSV
   PXP=SSPXP/SSV
   EDP=SSPXP/SSX
   TYPE 26,ED,TP,CP,SSV,X,PXP,EDP
26 FORMAT(4H ED ,F5.1,4H TP ,F6.1,4H CP ,F7.4,5H SSV ,E1
          0.3/3H X ,E10

```



```
1.3,5H PXP ,E10.3,5H EDP ,E10.3/)
  IF(SENSE SWITCH 4)40,53
40 XC=SSXC/SSVC
  PXPC=SSPXPC/SSVC
  EDPC=SSPXPC/SSXC
  XTB=SSXTB/SSVTB
  PXPTB=SSXP2 /SSVTB
  EDPTB=SSXP2 /SSXTB
  TYPE 41,ED,TP,SSVC,XC,PXPC,EDPC
41 FORMAT(4H ED ,F5.1,4H TP ,F6.1,6H SSVC ,E10.3,4H XC ,
          E10.3/6H PXPC
          1 ,E10.3,6H EDPC ,E10.3)
  TYPE42,ED,TP,SSVTB,XTB,PXPTB,EDPTB
42 FORMAT(4H ED ,F5.1,4H TP ,F6.1,7H SSVTB ,E10.3,5H XTB
          ,E10.3/7H PX
          1PTB ,E10.3,7H EDPTB ,10.3/)
53 TP=TP+TPD
  IF(TPF-TP)54,6,6
54 ED=ED+EDD
  IF(EDF-ED)7,5,5
59 TYPE 60
60 FORMAT (47H EN IS SINGLE VALUED. TURN SENSE SWITCH ON
          E OFF)

7 PAUSE
  GO TO 100
  END
```


B29826